

**Investigation of the role of SIRT6 in the molecular  
mechanisms of the gene expression regulation,  
metabolism and aging**

*Doctoral Thesis*

by

Dmitrii Smirnov

Doctoral Program in Life Sciences

Supervisor

Assistant Professor Ekaterina Khrameeva, Skolkovo Institute of  
Science and Technology, Russia

Supervisor

Associate Professor Debra Toiber, Ben-Gurion University of the Negev,  
Israel

Moscow - 2023

© Dmitrii Smirnov 2023

I hereby declare that the work presented in this thesis was carried out by myself at Skolkovo Institute of Science and Technology, Moscow, and Ben-Gurion University of the Negev, Be'er Sheva, except where due acknowledgment is made, and has not been submitted for any other degree.

Dmitrii Smirnov (Candidate)

Prof. Ekaterina Khrameeva (Supervisor)

Prof. Debra Toiber (Supervisor)

## Abstract

The NAD<sup>+</sup>-dependent histone deacetylase SIRT6 is implicated in many intracellular pathways and has critical roles in the brain from its development to neurodegeneration. In this project, we focused on studying SIRT6's roles in cellular homeostasis in the mammalian brain using multi-omics approaches. First, we established a methodology for untargeted liquid chromatography coupled with mass spectrometry (LC-MS) data analysis and created an R pipeline comprising all data analysis steps, starting from raw spectral data processing to the analysis of differentially abundant metabolites. Next, we combined our method with differential expression analysis to bioinformatically define metabolomic and transcriptomic signatures of brain-specific SIRT6 knockout mice. Our multilayer analysis revealed a detrimental effect of the SIRT6 deficiency on mitochondrial functions, specifically targeting oxidative phosphorylation and tricarboxylic acid cycle (TCA) pathways. We showed that SIRT6 may cooperate with YY1 (Yin Yang 1) and two other mitochondria-residing sirtuins (SIRT3 and SIRT4) to facilitate the transcription of the mitochondria-related genes. Furthermore, we demonstrated that mitochondrial decline caused by SIRT6 deficiency can contribute to aging and neurodegenerative disease manifestation. Finally, we studied the role of SIRT6's co-binding partner YY1 in pathological brain aging. We found that YY1 can enhance tumor prognostic marker *TP73-AS1* expression levels in an age-related manner, thereby linking brain cancer and aging. Together, these findings shed light on the multilayer regulatory activity of SIRT6 in the mammalian brain.

## Publications

1. **Dmitrii Smirnov**, Pavel Mazin, Maria Osetrova, Elena Stekolshchikova, and Ekaterina Khrameeva. The Hitchhiker’s Guide to Untargeted Lipidomics Analysis: Practical Guidelines. *Metabolites*, 11(11):713, October 2021. ISSN 2218-1989. [doi:10.3390/metabo11110713](https://doi.org/10.3390/metabo11110713)  
IF = 5.581 (year 2023)
2. **Dmitrii Smirnov**, Ekaterina Eremenko, Daniel Stein, Shai Kaluski, Weronika Jasinska, Claudia Cosentino, Barbara Martinez-Pastor, Yariv Brotman, Raul Mostoslavsky, Ekaterina Khrameeva, and Debra Toiber. SIRT6 is a key regulator of mitochondrial function in the brain. *Cell Death & Disease*, 14(1):35, January 2023. ISSN 2041-4889. [doi:10.1038/s41419-022-05542-w](https://doi.org/10.1038/s41419-022-05542-w)  
IF = 9.696 (year 2023)
3. Gal Mazor, **Dmitri Smirnov**, Hila Ben David, Ekaterina Khrameeva, Debra Toiber, and Barak Rotblat. TP73-AS1 is induced by YY1 during TMZ treatment and highly expressed in the aging brain. *Aging*, 13(11):14843–14861, June 2021. ISSN 1945-4589. [doi:10.18632/aging.203182](https://doi.org/10.18632/aging.203182)  
IF = 5.955 (year 2023)

## Conference presentations

1. **Smirnov DN**, Khrameeva EE “Topologically Associating Domain optimal set prediction using Armatus software” – Oral presentation at ITASb, online conference, April 2020
2. **Dmitrii Smirnov**, Ekaterina Khrameeva, “optimalTAD: a novel algorithm for Topologically Associating Domain optimal set prediction” – poster presentation at Moscow Conference on Computational Molecular Biology (MC-CMB’21), 2021
3. **Dmitrii Smirnov**, Ekaterina Eremenko, Daniel Stein, Shai Kaluski, Weronika Jasinska, Ekaterina Khrameeva, Debra Toiber, “The role of SIRT6 in the reg-

ulation of mitochondrial functions” – poster presentation at Aging and Epigenetics meeting-II, Ramat Gan, Israel, 2022.

4. **D Smirnov**, E Eremenko, D Stein, S Kaluski, W Jasinska, E Khrameeva, D Toiber. “The emerging role of SIRT6 in the mitochondrial regulation” – poster presentation at Bioinformatics of Genome Regulation and Structure/Systems Biology (BGRS/SB-2022), Novosibirsk, Russia, 2022.

## Acknowledgments

First, I would like to thank my scientific advisors, Prof. Ekaterina Khrameeva and Prof. Debra Toiber. First of all, I am grateful for their trust in me at each stage of my PhD studies, especially in its early years. I came to the field with a different background, having almost no prior experience in molecular biology and bioinformatics, therefore their guidance and wholehearted support throughout the years helped me a lot and made this thesis possible. I admire their endless supply of scientific optimism and their ability to find unexpected solutions even in the most dead-end situations. I am also grateful to Ekaterina and Debra for granting me freedom in choosing research topics and for the opportunity to combine work on projects in both laboratories.

I am deeply thankful to Prof. Khrameeva's lab colleagues for the invaluable scientific discussions and motivation. I am also very grateful to the former lab members, Anastasia Golova and Artemiy Shumskiy, with whom we have been working together on the SIRT6-related projects since the laboratory's founding. I would like to express my gratitude to the colleagues from Prof. Toiber lab. Many thanks to my long-time collaborators Dr. Shai Kaluski, Daniel Stein, Yuval Rabuah and especially to Dr. Ekaterina Eremenko who experimentally validated my bioinformatics findings. I am also thankful to Adam Zaretsky, who introduced me to the lab and immensely helped me on my first visit to Beer Sheva. I wish to thank Dr. Alfredo Garcia-Venzor and Dr. Miguel Portillo, to whom I am grateful for the friendship and the wonderful time spent inside and outside the laboratory.

I am also grateful to my individual PhD committee members, Prof. Mikhail Gelfand, Prof. Dan Mishmar, Prof. Ramon Birnbaum and Dr. Ilya Kurochkin, for their comments and suggestions regarding my work.

Finally, I would like to thank my family, especially my beloved wife Hanna, for their emotional support and for being there along the way.

# Contents

<b>Abstract</b>	<b>3</b>
<b>Publications</b>	<b>4</b>
<b>Conference presentations</b>	<b>4</b>
<b>Acknowledgments</b>	<b>6</b>
<b>Contents</b>	<b>7</b>
<b>List of Figures</b>	<b>10</b>
<b>List of Tables</b>	<b>11</b>
<b>List of Symbols, Abbreviations</b>	<b>12</b>
<b>1 Introduction</b>	<b>14</b>
1.1 Relevance and significance of the work . . . . .	14
1.2 Research objectives . . . . .	14
1.3 Thesis structure . . . . .	15
1.4 Author contribution . . . . .	16
<b>2 Review of the Literature</b>	<b>18</b>
2.1 Aging . . . . .	18
2.1.1 Mitochondrial dysfunction as a hallmark of aging . . . . .	18
2.2 Cellular functions of SIRT6 . . . . .	20
2.2.1 Sirtuins and lipid metabolism . . . . .	22
2.2.2 Sirtuins and mitochondrial activity . . . . .	24
2.2.3 Role of SIRT6 in brain aging and neurodegeneration . . . . .	25
2.2.4 Cooperation between SIRT6 and YY1 . . . . .	26
2.3 Associations between glioblastoma and brain aging . . . . .	27
<b>3 A novel pipeline for the untargeted lipidomics data analysis</b>	<b>30</b>
3.1 Workflow . . . . .	31
3.1.1 Measurements of Lipidome Composition . . . . .	31
3.1.2 Study Design Considerations . . . . .	32
3.1.3 Materials . . . . .	33
3.1.4 Equipment . . . . .	33

3.1.5	Data Conversion . . . . .	34
3.1.6	Data Import . . . . .	35
3.1.7	Peak Picking . . . . .	36
3.1.8	Peak Alignment . . . . .	36
3.1.9	Peak Grouping . . . . .	37
3.1.10	Selection of Parameters for Peak Picking, Alignment, and Grouping . . . . .	37
3.1.11	Imputation of Missing Values . . . . .	38
3.1.12	Data Export . . . . .	39
3.1.13	Filtering of Peaks . . . . .	39
3.1.14	Normalization . . . . .	40
3.1.15	Annotation . . . . .	41
3.1.16	Visualization of LC-MS Data . . . . .	42
3.2	Results . . . . .	44
3.2.1	Analysis of brSIRT6-KO lipidomics profiles . . . . .	44
3.3	Discussion . . . . .	46
3.3.1	Future Challenges . . . . .	46
<b>4</b>	<b>Effect of SIRT6 deficiency on transcriptome and metabolome levels during normal and pathological aging.</b>	<b>49</b>
4.1	Methods . . . . .	50
4.1.1	Generation of brain-specific SIRT6-KO mice and cells . . . . .	50
4.1.2	RNA preparation and quality control . . . . .	50
4.1.3	Full-length poly-A RNA sequencing . . . . .	50
4.1.4	RNA-seq data processing . . . . .	51
4.1.5	Differential expression analysis . . . . .	51
4.1.6	Functional analysis of genes . . . . .	51
4.1.7	Analysis of mitochondria-related genes . . . . .	52
4.1.8	Differential abundance analysis . . . . .	52
4.1.9	Analysis of public brain RNA-seq data . . . . .	53
4.1.10	Analysis of YY1 and SIRT6 ChIP-seq data . . . . .	53
4.1.11	Analysis of public aging brain datasets . . . . .	54
4.2	Results . . . . .	54
4.2.1	Lack of SIRT6 alters gene expression levels in the mouse brain . . . . .	54
4.2.2	SIRT6 regulates mitochondrial metabolism . . . . .	56
4.2.3	SIRT6 deficiency leads to impaired oxidative phosphorylation . . . . .	58
4.2.4	Lack of SIRT6 results in a reduction of mtDNA gene expression and mitochondrial content . . . . .	62
4.2.5	SIRT6-SIRT3,4 and SIRT6-YY1 axes promote OXPHOS in the brain . . . . .	62
4.2.6	Neuropathological role of SIRT6 through the prism of mitochondrial deregulation . . . . .	65
4.3	Discussion . . . . .	68

<b>5</b>	<b>The role of SIRT6' co-partner YY1 in aging and brain tumors</b>	<b>72</b>
5.1	Methods . . . . .	73
5.1.1	Primers . . . . .	73
5.1.2	Luciferase activity assay . . . . .	73
5.1.3	Data analysis . . . . .	73
5.2	Results . . . . .	74
5.2.1	<i>TP73-AS1</i> is highly expressed in the aging brain . . . . .	74
5.3	Discussion . . . . .	77
<b>6</b>	<b>Conclusion</b>	<b>78</b>
	<b>Bibliography</b>	<b>80</b>
	<b>Supplementary materials for Chapter 3: A novel pipeline for untargeted lipidomics data analysis</b>	<b>99</b>
	Supplementary tables . . . . .	99
	<b>Supplementary materials for Chapter 4: Effect of SIRT6 deficiency on transcriptome and metabolome levels during normal and pathological aging</b>	<b>105</b>
	Supplementary figures . . . . .	105
	<b>Supplementary materials for Chapter 5: The role of SIRT6' co-partner YY1 in aging and brain tumors</b>	<b>111</b>
	Supplementary figures . . . . .	111

# List of Figures

2-1	Cellular localization and functions of sirtuins. . . . .	21
2-2	Lipid classes presented according to LIPIDMAPS classification. . . . .	23
2-3	Comparison between whole-body and tissue-specific SIRT6-deficient mouse models . . . . .	25
3-1	Lipidomics measurement workflow. . . . .	32
3-2	Schematic illustration of the LC-MS data analysis workflow . . . . .	34
3-3	Analysis of lipid composition in the SIRT6-KO mouse brain. . . . .	45
4-1	SIRT6 regulates gene expression levels. . . . .	55
4-2	SIRT6 deficiency triggers an abundance of energy metabolites . . . . .	57
4-3	OXPHOS impairment in SIRT6-KO. . . . .	60
4-4	SIRT6-SIRT4 and SIRT6-YY1 axes in mitochondrial regulation. . . . .	65
4-5	SIRT6 silencing triggers neurodegenerative disease pathways and normal brain aging. . . . .	67
5-1	<i>TP73-AS1</i> is highly expressed in the aging brain. . . . .	75
5-2	<i>TP73-AS1</i> is highly expressed in the pathological aging brain. . . . .	76
S-1	Analysis of WT and brSIRT6-KO gene expression data. . . . .	106
S-2	mESC metabolomics. . . . .	107
S-3	SIRT6 regulates OXPHOS-related genes. . . . .	108
S-4	Analysis of public YY1 and SIRT6 ChIP-seq datasets. . . . .	109
S-5	Full network of enriched KEGG pathways. . . . .	110
S-6	<i>TP73-AS1</i> is highly expressed in GBM tumors of aged patients. . . . .	111
S-7	<i>YY1</i> and <i>TP73-AS1</i> are co-expressed in GBM and aging brain. . . . .	112

# List of Tables

S.1	A non-comprehensive list of tools suitable for the analysis of LC-MS data . . . . .	99
-----	---	----

# List of Symbols, Abbreviations

<b>BEH</b>	Bridged Ethyl Hybrid
<b>brSIRT6-KO</b>	Brain-specific Sirtuin 6 Knockout Model
<b>CoV</b>	Coefficient of Variation
<b>DA</b>	Differential Abundance
<b>DAG</b>	Diacylglycerol
<b>DE</b>	Differential Expression
<b>FDR</b>	False Discovery Rate
<b>FPKM</b>	Fragments Per Kilobase of transcript per Million mapped reads
<b>GBM</b>	Glioblastoma Multiform
<b>GC-MS</b>	Gas Chromatography-Mass Spectrometry
<b>GO</b>	Gene Ontology
<b>IQR</b>	Interquartile Range
<b>KEGG</b>	Kyoto Encyclopedia of Genes and Genomes
<b>KNN</b>	k-Nearest Neighbors
<b>LC-MS</b>	Liquid Chromatography coupled with Mass Spectrometry
<b>LOD</b>	Limit Of Detection
<b>mESC</b>	Mouse Embryonic Stem Cells
<b>NAD<sup>+</sup></b>	Nicotinamide Adenine Dinucleotide
<b>NAM</b>	Nicotinamide
<b>OXPHOS</b>	Oxidative Phosphorylation
<b>PI</b>	Phosphatidylethanolamine
<b>PC</b>	Phosphatidylcholine
<b>PCA</b>	Principal Component Analysis
<b>PLS-DA</b>	Partial Least-Squares Discriminant Analysis

**PS** Phosphatidylserine  
**RF** Random Forest  
**RIN** RNA Integrity Number  
**ROS** Reactive Oxygen Species  
**RT** Retention Time  
**SD** Standard Deviation  
**SIRT6-KO** Sirtuin 6 Knockout model  
**SVD** Singular Value Decomposition  
**sPLS-DA** sparse Partial Least-Squares Discriminant Analysis  
**TAG** Triacylglycerides  
**TMZ** Temozolomide  
**QC** Quality Control  
**QTOF** Quadrupole Time-of-Flight  
**UPLC** Ultra Performance Liquid Chromatography  
**WT** Wild Type

# Chapter 1

## Introduction

### 1.1 Relevance and significance of the work

The mammalian sirtuin family is represented by seven NAD<sup>+</sup>-consuming enzymes (SIRT1-7) functionally implicated in multiple intracellular processes. Among the entire sirtuin family, SIRT6 is the only one that combines deacetylase and mono-ADP-ribosyltransferase activities, acting as a direct modulator of DNA repair, telomere integrity, gene expression, cellular metabolism and cancer. The absence of SIRT6 induces a particular phenotype characterized by premature aging and death by 28 days in mice, while its overexpression results in longevity. SIRT6 is especially important for the brain, where it has essential roles in the attenuation of aging and neurodegenerative disorders, including Alzheimer's disease, Parkinson's disease and multiple sclerosis. While the neuroprotective roles of SIRT6 in the brain are clear, little is known about the molecular mechanisms underlying its activity.

### 1.2 Research objectives

My work focuses on studying how changes in metabolome, lipidome and transcriptome levels affect aging phenotype, using a SIRT6-deficient mouse as a model. The primary goal of this study is to uncover the molecular aspects of SIRT6 activity on different levels of biological regulation in the mammalian brain, using bioinformatics approaches.

Specifically, the main objectives of this thesis are:

- to develop an all-in-one pipeline for the comparative analysis between WT and SIRT6-KO LC-MS lipidomics profiles
- to examine changes in the transcription and metabolism in the SIRT6-KO mouse brain
- to decipher the mechanisms behind the SIRT6-dependent regulation in the normal and pathological aging brain

### 1.3 Thesis structure

In **Chapter 3**, we focus on the improvement of existing bioinformatics methods for the analysis of the untargeted LC-MS-derived data. The developed step-by-step practical guidelines address issues related to the optimized feature signal extraction, missing value imputation methods and statistical analysis based on LC-MS lipidomics and metabolomics data. In these guidelines, we also discuss common pitfalls associated with univariate and multivariate methods used for the downstream analysis of lipid relative abundance. The developed data analysis protocol is presented in the form of an R script freely available to the scientific community.

**Chapter 4** is dedicated to the investigation of functional consequences of SIRT6 deficiency in the mouse brain. Here, we analyze mouse brain-specific SIRT6-KO RNA-seq profiles to study how the lack of SIRT6 affects gene expression levels. Our results suggest that SIRT6 functions are required for normal mitochondrial activity, and its deficiency results in widespread down-regulation of mitochondria-related genes, primarily associated with electron transport chain complexes. Applying the data analysis workflow presented in Chapter 3 to the metabolomics profiles of SIRT6<sup>-/-</sup> mES cells, we characterize abundance alterations of compounds from several functional groups, including those related to TCA cycle, Oxidative phosphorylation and carbohydrate metabolism. Furthermore, we investigate mechanisms of SIRT6-dependent mitochondrial regulation and propose two possible axes (SIRT6-YY1 and SIRT6-SIRT3/4) through which SIRT6 can regulate the transcription of

the mitochondria-related genes. Finally, we show that mitochondrial decline caused by SIRT6 deficiency can contribute to aging and neurodegenerative phenotype.

In **Chapter 5**, we continue the investigation of the SIRT6-YY1 axis but focus mainly on YY1 targets and its role in pathological brain aging. We discover that YY1 may regulate the activity of the *TP73-AS1* gene, which is positively correlated with the progression of both pediatric (medulloblastoma) and adult (glioblastoma) brain cancers. Our analysis of human brain profiles reveals an age-related increase in the expression level of *TP73-AS1* in glioblastoma patients, as well as in the brains of AD donors compared to healthy donors. These results may partially explain why glioblastoma is more aggressive in older patients.

## 1.4 Author contribution

In **Chapter 3**: developed the computational approach (together with Ekaterina Khrameeva, Pavel Mazin and Maria Osetrova), wrote the R markdown for LC-MS lipidomics data analysis (together with Pavel Mazin and Ekaterina Khrameeva), prepared Figure 3-2e, contributed to the description of multivariate methods (sections about PCA and PLS-DA), description of untargeted LC-MS lipidomics application and missing value imputation techniques. Also, I prepared a review of the existing LC-MS data analysis tools. Elena Stekolshchikova collected experimental data for computational approach demonstration. Weronika Jasinska and Shai Kaluski conducted sample extraction and MS-based quantification of lipid abundances for the analysis of lipid composition in SIRT6-KO mouse brains.

In **Chapter 4**: performed all the bioinformatics analyses, prepared all the figures except Figure 4-3f and S-3a, collected and analyzed all the publicly available data. Shai Kaluski and Daniel Stein did the generation of SIRT6-KO mice and RNA-seq library preparation. Experimental data for Figure 4-3i,f,g,i and Figure 4-4c was collected by Ekaterina Eremenko.

In **Chapter 5**: collected the public data of expression profiles in normal and pathological brain aging as well as data from GBM patients, conducted the statistical analysis and prepared all the figures presented (except Figure 5-1b and Supple-

mentary Figures S-7a,c,d).

# Chapter 2

## Review of the Literature

### 2.1 Aging

Aging is a consequence of the dysregulation of various self-maintenance mechanisms of a living system. Aging at the cellular level is accompanied by genomic instability, telomere shortening, loss of proteostasis, and mitochondrial dysfunction, together with a decrease in the efficiency of the DNA repair mechanism (López-Otín et al., 2013; Hernandez-Segura et al., 2018; Mattson and Arumugam, 2018). Moreover, these factors are interconnected. For example, the shortening of telomeres can lead to mitochondrial dysfunction (Sahin and DePinho, 2012), that, in turn, may contribute to epigenetic alterations and inflammation (Chatterjee et al., 2022). Aging involves significant changes in brain structure and functional capabilities (Raz et al., 2005; Peters, 2006; Mattson and Arumugam, 2018; Blinkouskaya et al., 2021). Cognitive decline occurs naturally during aging, but in some cases, it can become pathological, such as in neurodegenerative diseases. Notably, about 95% of neurodegenerative cases are age-related with no known genetic mutation. Therefore, a better understanding of the aging process in disease development is needed.

#### 2.1.1 Mitochondrial dysfunction as a hallmark of aging

One of the hallmarks of aging that has also been implicated in neurodegeneration is the impairment of mitochondrial activity. Mitochondria are vital cell organelles

with many functions, including adenosine triphosphate (ATP) synthesis, calcium homeostasis handling, and lipid metabolism. ATP production occurs on the inner mitochondrial membrane, which incorporates five specific protein complexes (complexes I-V), forming the electron transport chain. The mammalian mitochondrial protein biosynthesis system involves genes from both nuclear and mitochondrial genomes. While mtDNA encodes only a small fraction of mitochondrial genes compared to nuclear DNA (1%), they are all necessary for synthesizing the respiratory complex proteins. To generate energy, electrons are transported through complexes I-IV moving across an electrochemical gradient to the ultimate acceptor, oxygen. This process is called oxidative phosphorylation (OXPHOS). As part of ATP production, various metabolites are formed in the mitochondria, such as Acetyl-CoA, Citric Acid, Oxoglutaric acid, Succinic Acid, Malate, and Fumarate. These metabolites control mitochondrial bioenergetics, and their altered levels might result in the deregulation of several aging-related pathways (e.g., mTOR, AMPK), implicating mitochondrial bioenergetic defects in aging (Mecocci et al., 1993; Wallace, 2005; Park and Larsson, 2011). During oxidative phosphorylation, the mitochondria also generate reactive oxygen species (ROS) molecules as a byproduct of ATP synthesis (Harman, 1956). These molecules induce damage, which accumulates throughout the organismal lifespan and becomes harmful at high concentrations, inducing oxidative stress, DNA damage, and lipid peroxidation (Chakrabarti et al., 2011). Since mtDNA is located near the ROS production sites, it might be more sensitive to oxidative damage and prone to possible mutations. The brain is particularly vulnerable to age-related mitochondrial damage because of its high energy demand (Raichle and Gusnard, 2002). Age-related accumulation of mitochondrial abnormalities disrupts synaptic transmission and neuronal metabolism, leading to neurodegeneration (Motori et al., 2020; Storozhuk et al., 2005). However, despite the clear role of mitochondrial dysfunction as a key marker of aging and neurodegenerative diseases, the exact mechanisms initiating this dysfunction are still poorly understood.

## 2.2 Cellular functions of SIRT6

Sirtuins are a family of evolutionary conserved proteins that have mono-ADP ribosyltransferase or deacetylase activity (Rine et al., 1979; Tanner et al., 2000; Raz et al., 2005). The founding member of the sirtuin family, Sir2, was initially characterized in *Saccharomyces cerevisiae* and derived its name due to the ability to silence transcription and establish heterochromatin structure (Klar et al., 1979). Next, three additional yeast sirtuin family members (Sir1, Sir3, Sir4), also involved in chromatin silencing at HML and HMR loci, were identified (Chang et al., 2020). Sir homologs were further characterized in many other eukaryotic and prokaryotic organisms, including nematodes, flies and mice, where they retain their roles in epigenetic regulation. Interestingly, prokaryotic species have one or two sirtuins, while eukaryotic genomes typically contain at least four sirtuin orthologs (Viswanathan and Tissenbaum, 2013). In mammals, this family consists of seven members named SIRT1 to SIRT7, presented in most tissues and cell types (Thul et al., 2017) and participating in the regulation of many housekeeping cellular pathways, such as DNA repair and metabolism (Chang et al., 2020). Mammalian sirtuins are localized in different cellular compartments (Figure 2-1a). SIRT1 and SIRT2 are found in the nucleus and cytoplasm, SIRT3-SIRT5 are functioning in mitochondria, SIRT6 is a nuclear protein while SIRT7 is located in the nucleoli. Sirtuins consume NAD<sup>+</sup> to perform their main intracellular function – transcriptional inactivation through histone deacetylation activity. Furthermore, SIRT4 and SIRT6 were shown to affect their target proteins via mono-ADP-ribosylation modifications (Figure 2-1b), which is the most prominent function of SIRT4 since its deacetylase activity is weak. SIRT1 remains the most extensively studied, while much less is known about the other family members.

As one of the most notable proteins of this family, SIRT6 is implicated in genomic stability (Mostoslavsky et al., 2006; Toiber et al., 2013; Van Meter et al., 2014; Onn et al., 2020), DNA repair (Mao et al., 2011; Onn et al., 2020), telomere maintenance (Michishita et al., 2008) and cellular metabolism (Roichman et al., 2021). SIRT6 enzymatic activity is directly associated with chromatin regulation. Acting as a

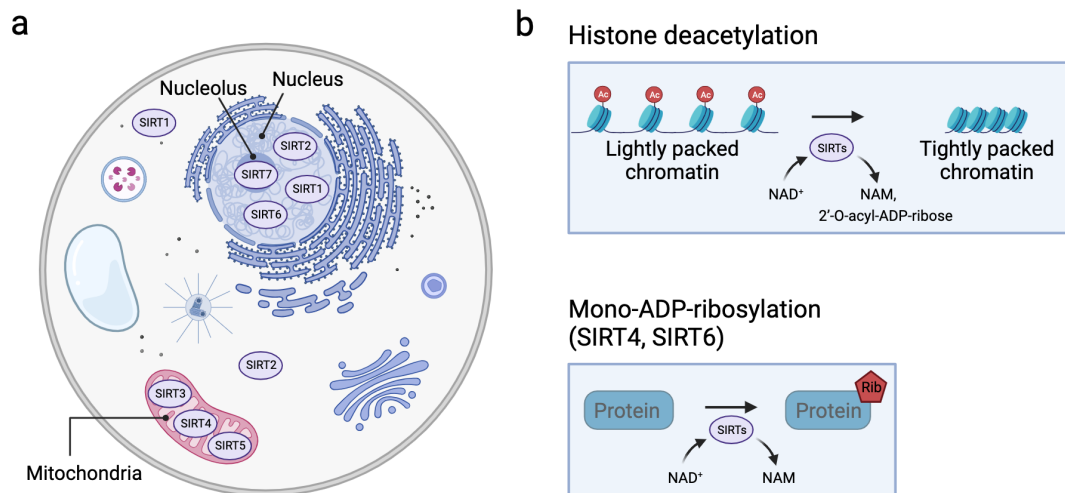


Figure 2-1: Cellular localization (a) and functions (b) of sirtuins. Panel (b) is adapted from Chang et al. (Chang et al., 2020), with modifications. Figure was prepared using BioRender website.

histone deacetylase, it removes acetyl groups from the H3K9, H3K18 and H3K56 sites leading to chromatin compactization (Zhong et al., 2010; Jiang et al., 2013; Tasselli et al., 2016). Through deacetylation, SIRT6 can repress the transcriptional activity of histone and non-histone target genes. In particular, SIRT6 may directly deacetylate *TRF2* gene at TRFH domain promoting telomere integrity (Rizzo et al., 2017). Lack of SIRT6 causes derepression of subtelomeric chromatin as well as genome-wide activation of LINE1 transposable elements and centromeric satellites (Simon et al., 2019). Importantly, SIRT6 can act as a co-regulation partner of Lamin A/C (LMNA) protein to maintain tight packing of retrotransposons and lamina-associated domains (LADs) (Korotkov et al., 2021).

Another crucial cellular function of SIRT6 is related to the facilitation of base excision repair (BER) and double-strand break (DSB) repairs. It was shown that SIRT6 acts as a sensor of DNA damage, recruiting to a break site and engaging repair factors, such as 53BP1 and RPA, via deacetylation of H3K56 and H3K9 sites (Xu et al., 2015). However, the functions of SIRT6 in DNA repair assistance are not limited to deacetylation. Several studies suggested that SIRT6 is required to activate PARP1 through ADP-ribosylation at lysine 521, thereby promoting both BER and DSB (Chou et al., 2010; Mao et al., 2011; Liszczak et al., 2018).

It is worth mentioning the remarkable role of SIRT6 in regulating cellular metabolism.

Cells lacking SIRT6 undergo a metabolic switch from mitochondrial respiration to aerobic glycolysis, promoting tumorigenic phenotype (Zhong et al., 2010; Sebastian et al., 2012). Several studies also reported the involvement of SIRT6 in gluconeogenesis modulation, though its role remains controversial. Earlier studies suggested the repressive functions of SIRT6 regarding gluconeogenesis. Dominy et al. claimed that SIRT6 downregulates hepatic gluconeogenesis via the enhanced activity of transcriptional coactivator PGC-1 $\alpha$  (Dominy et al., 2012). Another study put SIRT6 as an intermediate actor in the p53-FoxO1 axis responsible for gluconeogenesis suppression in the liver (Zhang et al., 2014a). However, a more recent work reported a positive association between SIRT6 and hepatic gluconeogenesis, explained by an increased rate of triglycerides conversion into glycerol and free fatty acids in liver-specific SIRT6-overexpressing mice, also implicating SIRT6 in fat metabolism regulation (Roichman et al., 2021).

### 2.2.1 Sirtuins and lipid metabolism

Lipids represent the hydrophobic fraction of small biological molecules with a molecular weight below 1500 Da, known as metabolites (Simons and Toomre, 2000). Lipids play a crucial role in the cell, tissue, and organ physiology, acting not only as structural components of the membranes but also as signaling molecules and active members of various protein complexes. The significance of lipids is highlighted by a large number of studies and diseases involving the disruption of lipid metabolic enzymes and pathways, including neurological disorders, such as Alzheimer's or Parkinson's diseases, as well as diabetes and cancer (Han et al., 2002; Adibhatla et al., 2006; Colsch et al., 2008). High-performance liquid chromatography (HPLC) covers many lipid classes, including sterols, glycerolipids, glycerophospholipids, sphingolipids, fatty acyls, and lipid headgroup derivatives (Figure 2-2a,b).

The lipid composition of the myelin sheath is distinctive, made of a high amount of cholesterol and enriched in glycolipids, in the ratio of 40:40:20 (cholesterol, phospholipids, and glycolipids, respectively) compared to most biological membranes (25:65:10). In addition, some glycerophospholipids, i.e., phosphatidylinositols, can play the role of membrane-derived second messengers. Glycerolipids, including

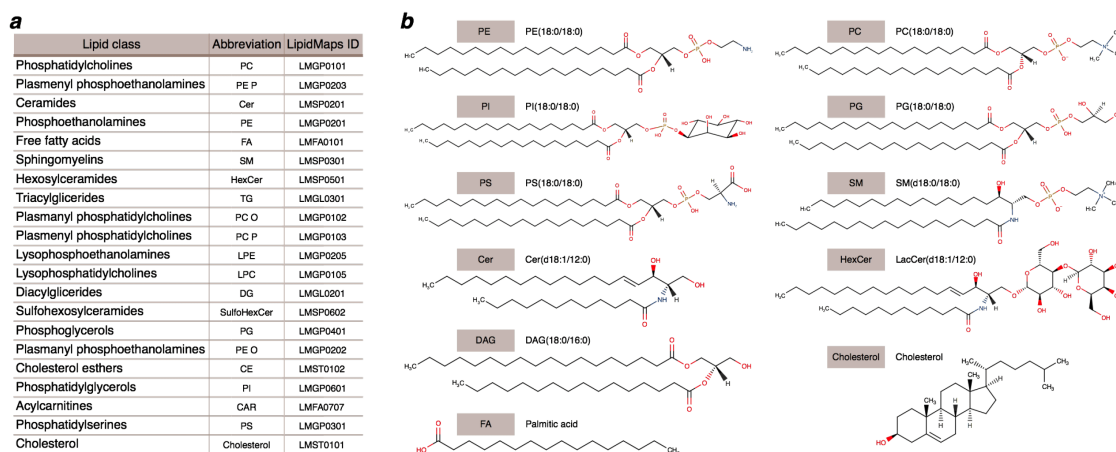


Figure 2-2: Lipid classes presented according to LIPIDMAPS classification. (a) Abbreviations and LIPIDMAPS identifications of lipid classes. (b) Examples of prominent representatives of lipid subclasses.

mono-, di-, and tri-substituted glycerols, function as an energy store and comprise the fat in animal tissues. Sphingolipids, containing a long-chain base as their core structure, represent another essential component of cellular membranes and include ceramides, sphingomyelins, and glycosphingolipids, which play important roles in signal transduction and cell recognition, especially in neural tissues. Moreover, the human brain has a different lipidome composition compared to other non-neural tissues, with 25% lipids presented exclusively in the brain (Bozek et al., 2015). Thus, studying lipidome organization is crucial to understanding the mechanisms behind brain physiology and neurological diseases.

Sirtuins play important roles in the regulation of lipid metabolism. SIRT1 enhances the oxidation of fatty acids in the liver and skeletal muscle, promotes cholesterol metabolism in the liver, and mobilizes lipids in white adipose tissue (Lomb et al., 2010). In addition, small-molecule activators of SIRT1 can partially protect mice from the detrimental consequences of a high-fat diet. Another important regulator of lipid metabolism is SIRT6. It was shown to control the production of hepatic triglycerides and fat metabolism in a negative manner, targeting promoters of several genes involved in lipid biosynthesis, including *FAS*, *ELOVL6*, *ACC1* and *SCD1* (Kim et al., 2010). Elhanati et al. discovered that SIRT6 also inhibits the activity of lipogenic transcription factors SREBP1/2, followed by a reduction in cellular cholesterol levels (Elhanati et al., 2013). While the above results are relevant

mainly for the liver or adipose tissue, the regulatory roles of sirtuins in brain lipid homeostasis are still poorly understood.

### 2.2.2 Sirtuins and mitochondrial activity

Maintenance of mitochondrial activity remains an essential task of sirtuins, linking them with pro-longevity regulatory pathways. SIRT3, SIRT4 and SIRT5 reside mainly in the mitochondrial matrix and therefore considered as the most influencing mitochondrial functions. SIRT3 is reported to be a key deacetylase in the mitochondria, targeting OXPHOS and mitochondrial dynamics (Ansari et al., 2017). Because of these abilities, SIRT3 can contribute to the protection against oxidative stress, preventing neuronal cell death (Dai et al., 2014). SIRT4 has very limited histone deacetylation activity compared to SIRT3 and utilizes ADP-ribosylation activity to accomplish its interactions with other mitochondrial proteins. It was found to mediate fatty acid  $\beta$ -oxidation via the downregulation of malonyl CoA decarboxylase (MCD) (Laurent et al., 2013) and enhance ROS levels by disrupting interactions between SOD2 and SIRT3 (Luo et al., 2016). Interestingly, both SIRT3 and SIRT4 have been shown to regulate glutamate dehydrogenase (GDH)-dependent amino acid metabolism and TCA cycle (van de Ven et al., 2017). SIRT5 drives lysine desuccinylation of many mitochondrial proteins, affecting fatty acid  $\beta$ -oxidation and ketone body synthesis pathways. Thus, all the mitochondrial sirtuins are implicated in age-related pathways, also having neuroprotective roles in the brain (Shih et al., 2014; Lee et al., 2018).

Non-mitochondrial sirtuins also participate in mitochondrial biology. SIRT1 deacetylates PGC-1 $\alpha$  (Cantó and Auwerx, 2009; Fanibunda et al., 2019) to maintain mitochondrial biogenesis and prevent ROS accumulation in cortical neurons. SIRT2 regulates mitochondrial fission in a DPR1-dependent manner and mediates OXPHOS by deacetylation of AKT1 leading to suppression of DPR1 activity (Cha et al., 2021). SIRT7 deficiency is linked with decreased expression of mitochondrial ribosomal proteins in hematopoietic cells (Ryu et al., 2014) and increased mitochondrial respiration in brown adipose tissue (Yoshizawa et al., 2022), but does not cause significant differences in mitochondrial content. Much less is known about the role

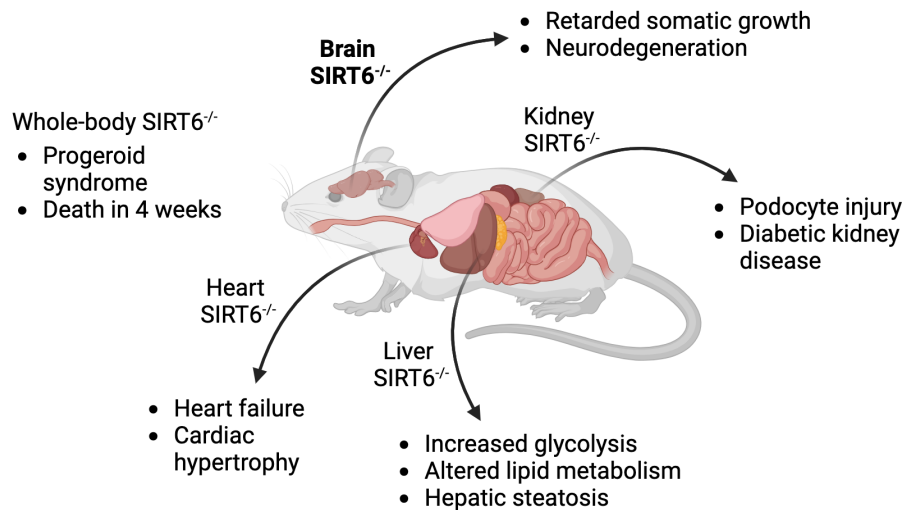


Figure 2-3: Comparison between conventional (whole-body) and tissue-specific SIRT6-deficient mouse models. The figure was prepared using the BioRender website.

of SIRT6 in mitochondrial processes. Several studies reported its involvement in mitochondrial biogenesis in heart and skeletal muscles (Cheng et al., 2016; Pillai et al., 2021), but it is still unclear if SIRT6 can orchestrate mitochondrial regulation in the brain and whether it has the ability to counteract brain aging and neurodegenerative diseases through these functions.

### 2.2.3 Role of SIRT6 in brain aging and neurodegeneration

SIRT6 has critical roles in the protection against aging-associated diseases (Kaluski et al., 2017; Khan et al., 2018; Li et al., 2021). Conventional SIRT6-deficient mice have a progeroid (“premature aging-like”) syndrome with low body weight and a very short lifespan of  $\sim$  four weeks compared to normal mice (Figure 2-3) (Mostoslavsky et al., 2006). Heart-specific SIRT6 ablation results in heart failure and premature cardiomyocyte senescence (Pillai et al., 2021). Mice with liver-specific ablation of SIRT6 are vulnerable to hepatic steatosis (Kim et al., 2010) and to metabolic alterations associated with defective mitochondrial respiration (Zhong et al., 2010), as discussed previously. SIRT6 attenuates podocyte inflammation and diabetic kidney disease in mouse (Yang et al., 2021). Being widely expressed in mammalian brain tissues, SIRT6 plays a neuroprotective role, protecting against DNA damage accu-

mulation and during ischemic brain injury (Figure 2-3) (Lee et al., 2013; Kaluski et al., 2017). The lack of SIRT6, specifically in the brain, results in learning and memory impairments, increased DNA damage, and the promotion of cortical apoptotic cells, partially through the hyperphosphorylation and hyperacetylation of Tau (Kaluski et al., 2017; Portillo et al., 2021). In addition, through the changes in gene expression in these brains, Stein et al. identified signatures of pathological aging, particularly relevant for AD and PD, that could be partially reversed by calorie restriction (Stein et al., 2021). Importantly, SIRT6 levels are decreased in the aging brains (Kaluski et al., 2017) and even more pronounced in Alzheimer's patients (Portillo et al., 2021), suggesting its involvement in age-related neurodegeneration and making it a good model to find the molecular mechanism of pathological aging in the brain.

#### 2.2.4 Cooperation between SIRT6 and YY1

SIRT6 often colocalizes with other proteins to regulate the transcriptional activity of its target genes. One example of such a partner is the YY1 transcription factor, that was previously shown to share many cellular functions with SIRT6, including those related to aging and neurodegeneration (Stein et al., 2021). YY1 can positively regulate SIRT6 transcriptional activity through direct association with its promoter (Stein et al., 2021). Interestingly, YY1-SIRT6 axis was observed not only in vertebrates, but also in tunicates, suggesting a conservative nature of this interaction in chordates. In *Polyandrocarpa misakiensis*, YY1 and SIRT6 form a complex with YAF2 to promote more effective SIRT6-induced deacetylation of H3K9 lysine residue (Kawamura et al., 2021).

In addition to SIRT6, YY1 can interact with both histone deacetylases (HDAC1-HDAC3) and histone acetyltransferases (p300 and CREB), serving as a context-specific regulator of chromatin remodeling (Verheul et al., 2020). This versatility implicates YY1 in key transcriptional mechanisms within the cell, while its depletion leads to a reduction in enhancer-promoter interactions and global gene expression alterations (Weintraub et al., 2017). In particular, YY1 is implicated in the regulation of mitochondria-related genes (Cunningham et al., 2007), protection from

ROS accumulation and mitochondrial dysfunction (Song et al., 2020). The latter is achieved through the interaction with NRF2 transcription factor that is a master regulator of antioxidant defense machinery (Liu et al., 2018).

YY1 is known to be a part of the transcriptional program of aging and age-related diseases (Stein et al., 2021). YY1 mRNA levels are increased in the aging (Verheul et al., 2020) and AD brains (Aubry et al., 2015), but not in PD, where its down-regulation was observed in microglia profiles of patients (Pal et al., 2016). Computational analysis of transcriptional network in AD cortical neurons revealed YY1 as one of the most prominent signatures of the disease progression (Pal et al., 2016). However, YY1 has two-faced roles in cancers, acting as a tumor suppressor or promoter depending on the context. YY1 is highly active in brain tumors, including glioblastoma and medulloblastoma, and its elevated levels are associated with disease aggressiveness (Sarvagalla et al., 2019; Zhang et al., 2020a). More specifically, YY1 is known to contribute to temozolomide (TMZ) resistance by promoting the expression of DNA repair genes (Jia et al., 2019). While the implication of YY1 in brain pathology mechanisms is clear, the interplay between its enzymatic activity and affected molecular pathways is far from being fully investigated.

## 2.3 Associations between glioblastoma and brain aging

Glioblastoma multiform (GBM) is a cancer of the brain with a dismal outcome and a five-year survival rate of  $< 10\%$  (Reifenberger et al., 2017). Its location in the brain, recurrence, and tendency to infiltrate areas adjacent to the primary tumor are some of the major features contributing to its aggressiveness. Current treatments rely on surgical resection, radiotherapy and TMZ administration (Stupp et al., 2005), which extends patient survival. However, therapy resistance in tumor cells is a major limiting factor in therapeutic success (Lee, 2016; Wheeler et al., 2021). It is therefore important to advance our understanding of resistance mechanisms for the development of new much needed therapies. Aging contributes to cancer (de Magalhães, 2013; Ben-Zion Berliner et al., 2021) and is a factor associated with poor survival

in GBM animal models (Ladomersky et al., 2016) and patients (Chaichana et al., 2011; Ladomersky et al., 2019). In particular, epigenetic changes affecting gene expression strongly correlated with age in low-grade glioma (Chatsirisupachai et al., 2021). The molecular mechanisms linking aging and GBM are still vague and were proposed to be related to the gain of function of tumor-associated fibroblasts and the functional decline of the immune system (Ladomersky et al., 2016). Nevertheless, the molecular details linking aging to GBM aggressiveness are still vague.

Long noncoding RNA (lncRNA) are regulatory RNA molecules known to play important roles in cancer such as promoting resistance to therapy (Bester et al., 2018; Zottel et al., 2020). The lncRNA *TP73-AS1* is a gene neighbor of the transcription factor (TF) p73, a member of the p53 TF family (Amelio and Melino, 2018) known to play important roles in aging (Rufini et al., 2012; Agostini et al., 2014; Lopriore et al., 2018), cancer (Flores et al., 2005; Tomasini et al., 2008; Du et al., 2013) and brain development (Yang et al., 2000; Agostini et al., 2011; Amelio et al., 2020) by regulating gene expression at the transcriptional and translational levels (Marini et al., 2018; Rotblat et al., 2018). LncRNA function by diverse mechanisms including by regulating gene expression in cis (Toiber et al., 2017); however, *TP73-AS1* does not regulate *p73* in GBM stem cells (Mazor et al., 2019) and was not found to regulate *p73* in other biological scenarios.

*TP73-AS1* is a negative prognostic factor in several tumor types (Zhang et al., 2020a). In glioma, the expression of *TP73-AS1* was shown to be associated with poor patient outcome and, importantly, with aging (Zhang et al., 2021). In GBM cancer stem cells, *TP73-AS1* was found to promote TMZ resistance by facilitating the expression of the TMZ detoxifying enzyme, *ALDH1A1* (Mazor et al., 2019). In accordance, *TP73-AS1* is clinically relevant in GBM and its high expression in GBM tumors is associated with poor patient outcome. Furthermore, *TP73-AS1* is highly expressed in the more aggressive IDH WT and EGFR amplified GBM tumors (Mazor et al., 2019). Interestingly, *TP73-AS1* is relevant and functional in other brain tumors including medulloblastoma (Varon et al., 2019) and astrocytoma (Marine et al., 2020; Pang et al., 2010). Nevertheless, how the expression of *TP73-AS1* is regulated in the context of TMZ treatment is not known, nor is it known if

the expression of *TP73-AS1* is associated with aging in the brain.

# Chapter 3

## A novel pipeline for the untargeted lipidomics data analysis

In this chapter we focus on the LC-MS method, which has become the analytical tool of choice for untargeted lipidomics because of its high sensitivity, convenient sample preparation, and broad coverage of lipid species. However, computational analysis of LC-MS-derived lipidomics profiles is still associated with several challenges, including the choice of the correct normalization strategy, selection of internal parameters for peak peaking and alignment algorithms or false positive annotation of lipidomics species. Additionally, most of the existing lipidomics-oriented tools cover only a specific part of the analysis, such as raw spectral data processing (*xcms*) or downstream analysis (*lipidr* (Mohamed et al., 2020), *lipidSig* (Lin et al., 2021)). A well-known example of a step-by-step lipidomics analysis tool is *MetaboAnalyst* (Pang et al., 2021). However, it has no stable implementation for the latest versions of R. Moreover, its website has limitations regarding the number and size of the manual uploading of input files, which makes it unsuitable for large datasets. Therefore, the analysis of large datasets remains challenging, underscoring the necessity for the development of a comprehensive pipeline that spans all stages of data analysis.

Here, we present a detailed LC-MS data analysis workflow designed for untargeted lipidomics but also applicable to metabolomics data analysis. To overcome the pitfalls discussed above, we combine all the essential steps of lipidomics data

analysis from the raw spectra loading to statistical testing into one R pipeline, additionally supplementing it with an implementation of advanced methods, such as manually verified m/z-RT 'grid'-based lipid annotation approach and peak peaking parameter optimization. Finally, we demonstrate an application of this tool for the identification of lipidomics changes in the SIRT6-KO mouse brain.

## 3.1 Workflow

### 3.1.1 Measurements of Lipidome Composition

LC-MS experimental workflow (Figure 3-1a) starts with sample preparation: homogenization of tissue samples or aliquoting samples of biological liquids. After this step, it is essential to add the isotope-labeled internal standards to the samples as early as possible to enable normalization for multiple potential sources of experimental biases at the data analysis stage.

Therefore, the extraction buffer is spiked with internal standards. The choice of standards depends on the lipids of interest and is selected according to the lipid class characteristic of the studied samples. After stratified randomization, lipid extraction is performed in batches of 48-96 samples. After every 23rd sample, a blank extraction sample is inserted, consisting of an empty tube without a tissue sample. These blank samples are essential for the analysis of the obtained LC-MS data because they serve as a baseline for filtering out peaks resulting from the extraction or other technical contamination. To achieve separation of the organic and aqueous phases, the samples are centrifuged, and the lipid fraction is selected.

To prepare quality control (QC) samples, an aliquot of each sample is additionally collected into a pooled sample. The mass spectra are then acquired for all samples processed in one sequence without interruption in positive and negative modes using an LC-MS system. QC samples are injected several times before initiating the run in order to condition the column, several times after each batch of samples, and after the completion of the run. QC samples are also injected after every ten samples to assess the instrument stability and analyte reproducibility. In addition, several blank samples are injected at the very beginning of the run and the very end of the

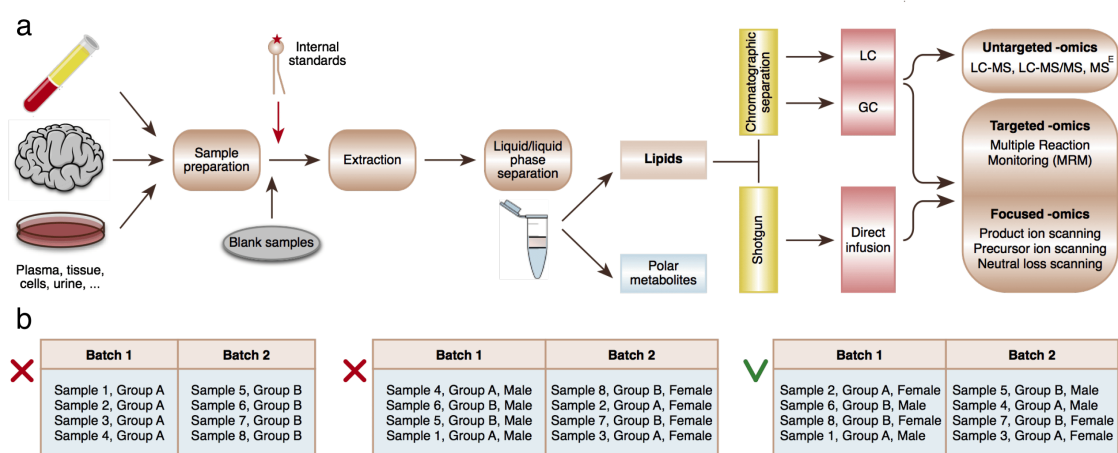


Figure 3-1: Lipidomics measurement workflow. (a) Experimental approaches that can be applied in lipidomics research. LC-MS and GC-MS are based on the separation of different lipid categories using extraction and chromatographic separation prior to mass analysis. Shotgun lipidomics omits chromatographic separation and analyzes all lipid classes together, directly infusing them into the mass spectrometer. (b) Balancing confounding factors between batches is an essential step of study design.

run.

### 3.1.2 Study Design Considerations

The main limitation of LC-MS experiments is the small batch sizes compared to the total number of samples in large study cohorts. Typically, a batch of samples for LC-MS measurements includes 48–96 samples. At the same time, advanced studies tend to measure lipidome composition in thousands of samples because of the relatively small effect sizes compared to the technical and inter-individual variability associated with the confounding factors, such as sex, age, postmortem interval (PMI), smoking status, and others.

Moreover, despite adding internal standards and QC samples, the batch effect might still be visible even after thorough normalization. Thus, it is crucial to distribute samples among batches in a way that enables comparisons between groups of interest within the batch and, most importantly, to avoid mixing the factor of interest with the batch covariate, as well as with the measurement order, because both of these confounding covariates might persist in the data after all normalizations

and corrections. In addition, it is essential to balance confounding factors between samples and controls and to randomize samples and controls in batches (Figure 3-1b). Technical replicates might be helpful for solving batch effect issues, but their use is not always practical in the case of large sample cohorts. Even without technical replicates, LC-MS runs can take several months as chromatographic separation takes about 30 min per sample, which, multiplied by 10000 samples, results in 208 days.

### 3.1.3 Materials

This workflow is demonstrated on a test dataset obtained with a Reversed-Phase Bridged Ethyl Hybrid (BEH) C8 column reverse coupled to a Vanguard precolumn, using a Waters Acquity UPLC system and a heated electrospray ionization source in combination with a Bruker Impact II QTOF (quadrupole-Time-of-Flight) mass spectrometer. This untargeted lipidome LC-MS dataset consists of two sample groups (two samples per group) and a blank sample, thus containing five samples in total.

### 3.1.4 Equipment

While many tools can be employed for LC-MS data analysis (Smith et al., 2006; Tautenhahn et al., 2008; Benton et al., 2010; Fahy et al., 2019) (Supplementary table S.1), this workflow is demonstrated with this suitable software combination:

- *ProteoWizard* cross-platform tool (Kessner et al., 2008; Chambers et al., 2012).
- *xcms* Bioconductor package (version 3.12.0) in the R environment (Smith et al., 2006; Tautenhahn et al., 2008; Benton et al., 2010).
- *IPO* Bioconductor R package (version 1.16.0) (Libiseller et al., 2015; Albóniga et al., 2020).
- *mixOmics* Bioconductor R package (version 6.14.1) (Rohart et al., 2017).

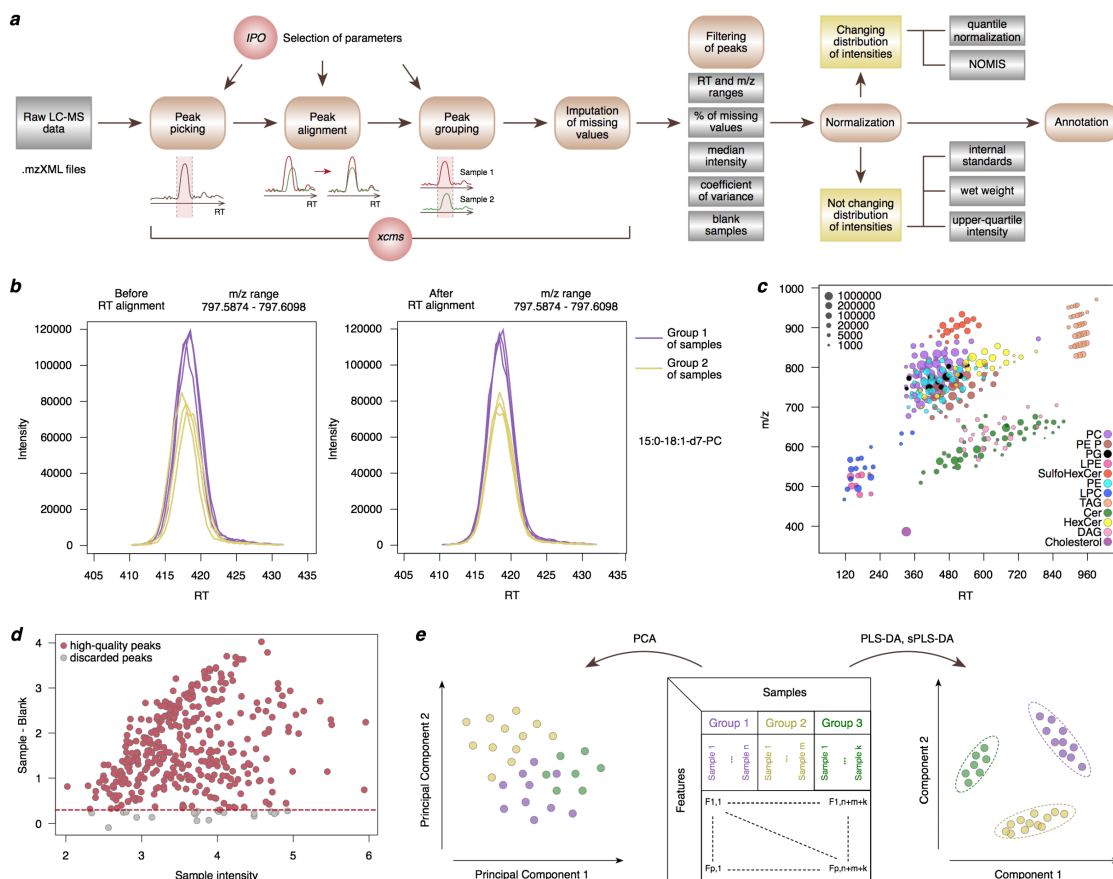


Figure 3-2: Schematic illustration of the LC-MS data analysis workflow. (a) Peak picking, alignment, and grouping are followed by the imputation of missing values, filtering, normalization, and annotation of lipid features. IPO and NOMIS abbreviations in the figure correspond to *IPO* and *NOMIS* tools, respectively. (b) An example of the peak alignment procedure for a deuterium-labeled lipid PC(15:0/18:1). (c) Mass and retention time of lipids with manually verified annotation based on a visually distinguishable 'grid' on this scatterplot. (d) A mean-difference plot visualizing the relationship of lipid intensities between biological samples and blank samples. For each peak, the median  $\log_{10}$  intensities are calculated among biological samples and among blank samples. Each circle represents the sample intensity and the difference between the sample and blank intensities for a peak. The dashed red line shows the threshold of a two-fold difference between the sample and blank intensities used for peak filtering. (e) An illustrative example of Principal Component Analysis (PCA), Partial Least Squares-Discriminant Analysis (PLS-DA) and sparse PLS-DA score plots. Each data point on both plots corresponds to the coordinates of a single sample in a low-dimensional space.

### 3.1.5 Data Conversion

The LC-MS procedure results in an abundance of thousands of lipid species, measured as ion counts for a specific mass-to-charge ratio ( $m/z$ ) and retention time (RT).

While it is possible to store signals obtained by the MS instrument for all discrete  $m/z$  and RT values in the 'profile data' mode, the resulting files can be as large as 5 Gb per sample. To reduce this massive amount of data, MS instruments can export files in an alternative 'centroid data' mode, storing a single representative signal per peak and producing much smaller files, up to 400 Mb, without losing information relevant for further analysis. Centroid data can be stored in multiple formats, depending on the MS instrument type. However, for further processing (Figure 3-2a), the files should be converted into a conventional mzXML format supported by most data analysis software, using the cross-platform *ProteoWizard* tool (Kessner et al., 2008; Chambers et al., 2012) or MS instrument vendor software.

### 3.1.6 Data Import

To give practical guidance, we illustrate the further steps of LC-MS data processing based on the *xcms* Bioconductor package (version 3.12.0) in the R environment, which is probably the most widely used solution among a multitude of available tools for MS data analysis.

However, before mzXML files can be imported into the R environment, they should be organized into a folder structure reasonable for the study design because *xcms* will guess the grouping of samples based on the subfolder structure and will align peaks between samples according to the folder hierarchy. Thus, the folder structure affects the grouping of peaks; the procedure matches MS peaks with similar  $m/z$  and RT across samples. mzXML files corresponding to samples that are expected to be most similar to each other (e.g., technical replicates) should be placed into a subfolder.

These subfolders should, in turn, be organized into higher-order hierarchies according to the study design and expectations about lipidome composition similarities between samples. Then, the data import can be performed with the 'readMSData' command. In a detailed R notebook available at [https://github.com/Khrameeva-Lab/lipidomics\\_analysis\\_2021](https://github.com/Khrameeva-Lab/lipidomics_analysis_2021) (accessed on 22 November 2023), we provide an example of the code that creates the list of files in the working directory, parses folder names to extract group labels for samples (i.e., mzXML files) stored in the folders,

creates a metadata data frame, and finally, reads and imports all mzXML files.

### 3.1.7 Peak Picking

Untargeted LC-MS experiments aim to identify the abundances of individual lipid species characterized by unique  $m/z$  and RT values. To distinguish such peaks from background noise, a procedure of peak picking (i.e., MS peak detection) should be performed for all samples, with the 'CentWaveParam' command setting the parameters for the peak picking procedure and 'findChromPeaks' command performing peak picking for all samples. One of the most important parameters for these commands is peakwidth that defines the minimum and maximum possible MS peak width in RT dimension and can be adjusted based on ion chromatograms for internal standards, which can be extracted from the dataset using the chromatogram function. Another critical parameter is ppm, which defines the width of the region in the  $m/z$  dimension where all consecutive data points are combined before the peak detection procedure. It can be adjusted according to the mass accuracy of the employed LC-MS system.

### 3.1.8 Peak Alignment

Next, peaks identified at the previous step in each sample separately should be matched between samples. This is not a trivial task, as chromatography can be affected by multiple factors leading to shifts in RT between measurement runs. Thus, the alignment procedure should be applied to adjust for these RT shifts from sample to sample (Figure 3-2b), with the 'ObiwrapParam' command setting the parameters for the alignment procedure and 'adjustRtime' command performing this procedure.

Of note, in this example, we use the Obiwrap algorithm (Patti et al., 2012), which is considered to be optimal for the untargeted LC-MS data. It is based on the dynamic time warping, which aims to make two samples as similar as possible via finding the best stretching of the time dimension (Prince and Marcotte, 2006). The default parameters define the reference sample for the alignment as the one contain-

ing the largest number of peaks. The two most important parameters, 'gapInit' and 'gapExtend', control the penalties in the warping optimization algorithm.

### 3.1.9 Peak Grouping

Finally, aligned peaks corresponding to the same lipid species should be grouped across samples. We illustrate this step using the PeakDensity algorithm (Smith et al., 2006), which iterates through the slices of  $m/z$  values and groups peaks according to the RT, as peaks representing the same lipid species are expected to cluster at the RT axis. Peak grouping can be performed using the 'PeakDensity-Param' command that sets the parameters for the peak grouping procedure and the 'groupChromPeaks' command that performs peak grouping across all samples. The 'minFraction' parameter defines the minimum proportion of samples in which a peak has to be detected.

This is where the folder structure of mzXML files becomes important because *xcms* calculates this proportion within a group of samples (i.e., within the lowest-hierarchy subfolder). The 'minSamples' parameter works similarly, except it defines the minimum number of samples instead of the minimum proportion. The 'binsize' parameter defines the width of the bin in the  $m/z$  dimension in which peaks are grouped. The 'bw' defines the RT window used for the density function smoothing. Finally, the 'maxFeatures' parameter limits the maximum number of features defined in one bin.

### 3.1.10 Selection of Parameters for Peak Picking, Alignment, and Grouping

In this workflow, we provide parameter settings optimized for untargeted lipidome LC-MS measurements on a Reversed-Phase Bridged Ethyl Hybrid (BEH) C8 column reverse coupled to a Vanguard precolumn, using a Waters Acquity UPLC system and a heated electrospray ionization source in combination with a Bruker Impact II QTOF mass spectrometer (Bruker Daltonics, Germany). However, in addition to the MS system vendors, the choice of parameters depends on multiple experimen-

tal conditions, such as the chromatographic separation buffers and gradient, MS settings, and the ion polarity mode.

Thus, the peak picking, alignment, and grouping parameters should be customized for the employed LC-MS system. One can start with the parameters recommended in the literature for a similar LC-MS system or with the default parameters for 'findChromPeaks', 'adjustRtime', and 'groupChromPeaks' functions, and then manually adjust parameters one by one until the most appropriate settings are found. To visually inspect the outcomes of the parameter adjustment procedure, it is useful to plot a subset of well-known peaks (e.g., internal standards or known lipids) in the  $m/z$  versus RT coordinates (Figure 3-2c).

However, the manual choice of parameters is time-consuming and arbitrary. Therefore, we provide optimization of *xcms* parameters using the Bioconductor package *IPO*. First, 'getDefaultXcmsSetStartingParams' and 'getDefaultRetGroupStartingParams' commands set the range of possible parameter values for IPO to scan. Then, 'optimizeXcmsSet' and 'optimizeRetGroup' commands optimize peak picking, retention time correction, and grouping parameters within the specified ranges of possible parameter values. Finally, the 'writeRScript' command returns the result of optimization in the form of an R script, which can be directly used to process raw *mzXML* files with *xcms*.

### 3.1.11 Imputation of Missing Values

Errors in the peak picking procedure frequently result in missing values, which can be imputed by the 'fillChromPeaks' function integrating the signal that corresponds to the area of missing peak in the raw data. Of note, this procedure does not impute all missing values, while the absence of missing values is critical for downstream data analysis methods, such as Principal Component Analysis (PCA). Zero values not filled by the *xcms* imputation procedure can be further replaced using data-driven imputation techniques, such as Random Forest (RF), k-Nearest Neighbors (KNN), and Singular Value Decomposition (SVD) or simply by the limit of detection (LOD) value (Wehrens et al., 2016).

### 3.1.12 Data Export

Commands 'chromPeaks', 'featureDefinitions', and 'featureValues' extract the data matrix, where the peak intensity is defined as the integral of the area under the peak. The last command produces a peak intensity matrix containing abundances of lipid species (rows) in all samples (columns).

### 3.1.13 Filtering of Peaks

MS peaks falsely duplicated during the xcms peak grouping procedure can be defined using a 10 ppm mass threshold (calculated as  $m/z$  difference divided by  $m/z$  and multiplied by 106) and 1s retention time difference. RT and  $m/z$  thresholds should be chosen to cover lipid classes of interest, e.g., from 1 to 18 min and from 120 to 1200  $m/z$  in this example. In addition, peaks containing a high number of missing values are typically removed, as well as peaks with low median intensity and high variability in intensity calculated as the coefficient of variance (CoV), standard deviation (SD), or interquartile range (IQR).

As high-quality peaks typically have high variability among biological samples and low variability among technical replicates (e.g., pooled QC samples), CoV, SD, and IQR are usually calculated among pooled QC samples for each MS peak. A commonly used cut-off for filtering based on CoV is 25%. However, recent studies argue that CoV, SD, and IQR might be poor predictors of peak quality because they ignore biological variability (Schiffman et al., 2019). The intra-class correlation coefficient (ICC) might be used instead, as it simultaneously considers technical and biological variability. To account for possible extraction and other technical contaminations, the concentrations in extraction blanks should be compared to the sample concentrations. MS peaks with less than a two-fold difference between the sample average and extraction blank average should be discarded from the analysis. A mean-difference plot is a helpful way to visualize the relationship between the sample and extraction blank lipid abundances (Figure 3-2d) (Schiffman et al., 2019).

### 3.1.14 Normalization

Several data normalization approaches can be applied to lipidomics data. The most widely used ones operate by scaling all intensities in one sample by the same normalization factor (biomass, internal standard, mean, median, and sum intensity of features) and do not change the distribution of intensities. Typically, lipid intensities are normalized on either spiked-in internal standards representing most of the main lipid classes or the wet weight of the sample. Other normalization approaches change the distribution of intensities as each peak in each sample has its own normalization factor.

For instance, quantile normalization (Bolstad et al., 2003) stretches the distributions of all samples to make them similar, while the NOMIS approach (Sysi-Aho et al., 2007) scales intensities by multiple internal standards, applying each standard to a corresponding range of RT values. However, a general assumption for all these normalization strategies is that most lipids are not affected by the factor of interest. If this is not the case, the best option would be to look into the raw data: if the desired effect is not visible in the raw data, it might be created by the normalization procedure and is not reliable.

In a specific case of experimental design with multiple biologically different samples from the same individual, the lipid intensities may be additionally normalized by the median abundance level within each individual to reduce individual-to-individual variability. To estimate the variability, it is useful to calculate the variance explained by each known covariate (e.g., sex, age, PMI, batch, individual, and others) using the 'manova' function in R for all lipids using the following model:  $Y \sim Sex + Age + PMI + Batch + Individual$ .

If sex, age, PMI, and other known covariates account for less variance each than the individual covariate, it suggests that there might be an additional hidden source of individual-to-individual variability as the order of covariates in the model is important for the calculation of the explained variance. Thus, we can transform our model into the following one:  $Y \sim Individual + Sex + Age + PMI + Batch$ . If sex, age, RIN, and other known covariates account for a small proportion (e.g., less than 1%) of the variance in this model, while the individual covariate explains a

substantial proportion of variance, the normalization by the median lipid abundance level within each individual is necessary and sufficient.

### 3.1.15 Annotation

The easiest way to annotate MS peaks is to match each peak with lipids from a predefined database, allowing mass difference with peak  $m/z$  below the given threshold (e.g., 10 ppm). The lipid database can be downloaded from the Web (e.g., LIPIDMAPS, SwissLipids (Aimo et al., 2015)) or constructed for specific lipid classes by varying the chain lengths and number of double bonds. All possible adducts - small ions that attach to or detach from lipid molecules under the ionization step (e.g.,  $H^+$ ,  $Na^+$ , and  $NH_4^+$ ) and make them detectable by MS - should be considered.

Despite high precision, MS data frequently have a slight shift in the determined  $m/z$ -values. This shift can be found and consequently accounted for as a mode of distribution of directed annotation ppm values. For lipid classes with a sufficient number of detected members, a visually distinguishable 'grid' on the  $m/z$  versus RT scatterplot (Figure 3-2c) can be found that allows manual or semi-automatic filtering of MS peaks with RT not matching the grid-like pattern, additionally using internal standard RT as an anchor point when available. This manual filtration procedure is performed for positive and negative ionization modes depending on the lipid class. Finally, the ionization mode and adduct for which the lipid class has the highest relative intensities are used in further analysis.

Our annotation approach results in Level 3 identification ("putatively characterized compound classes") according to the Metabolomics Standards Initiative guide (Sumner et al., 2007). Namely, all lipid species are determined on a 'tentative structure' level relying on MS1 data exclusively. Proposed structures do not distinguish positional isomers (sn-attachment of fatty acids), carbon-carbon double bond positions (e.g., 18:2(n-6,n-9)) for unsaturated lipids and double bond geometry (cis- or trans-configurations). Proposed lipid annotations correspond to bulk lipid formulas (e.g., PE O-36:2) or 'bond type level' (Liebisch et al., 2013) due to the high-resolution nature of MS measurements. Discrimination between ether-linked lipids (plasmanyl- and plasmenyl-species) may be performed by elution order on

reversed-phase chromatographic systems.

### 3.1.16 Visualization of LC-MS Data

LC-MS data analysis workflow results in normalized and annotated MS peaks, which can be further visualized. Lipid features are extremely different in amplitude and demonstrate heteroscedasticity—biological and technical variance are higher for features with high intensity. Thus, centering and scaling of intensities has to be performed prior to visualization as it equalizes the contributions of features to the separation of samples in multivariate space and makes the features comparable. Lipid intensities can be scaled by the minimum and maximum values. However, this procedure is sensitive to outliers and is, thus, undesirable. Better approaches involve scaling by the standard deviation (SD) or by the root of SD (Pareto-scaling). The centering procedure is based on subtracting the mean or median intensity from all values. Finally, log transformation is typically applied because it has a scaling-like effect making features more comparable and helps to reveal multiplicative relations between features.

Principal Component Analysis (PCA) is a multivariate approach widely used to visualize lipidomics data, perform sample-level quality control, and explore differences in the lipidome profiles between sample groups (Jolliffe, 2002). The main objective of PCA is to project the original multivariate data to the low-dimensional space while preserving as much information about the original data as possible. A set of uncorrelated variables forming this new low-dimensional space is called Principal Components (PCs).

Principal components are ranked according to the proportion of variance explained in decreasing order so that PC1 always explains the most considerable variation of the original data. In the case of lipidomic data, new PCs represent vectors of the linear combination of original features. For a lipidome matrix, where features are in rows and samples are in columns, the set of PCs can be calculated using the 'prcomp' function in R. Once PCs are calculated, one can proceed to the graphic representation of the method plotting the most informative PCs against each other (Figure 3-2e).

In this PCA plot, samples with similar lipidomic profiles tend to appear close together in a new reduced space, forming clusters. Thereby, it is possible to capture sample-specific differences between experimental conditions, assess group variances, and obtain an estimation of the data quality. The ability of PCA to identify outlier samples makes its application essential for the correct interpretation of conducted experiments prior to statistical analysis. Some noteworthy implementations of the PCA method in lipidomics studies include analyses of lipid profiles in drug-resistant prostate cancer, early Alzheimer's disease (Xicota et al., 2019; Zhang et al., 2020b), and coronary heart disease (Harshfield et al., 2019).

Partial Least-Squares Discriminant Analysis (PLS-DA) is a calibration algorithm that has become incredibly popular in the field of lipidomics (Wu et al., 2016; Lee et al., 2018). In contrast with the classic PCA technique, PLS-DA can be considered as a "supervised" method and might be especially useful when dealing with a dataset for which a class membership for each sample is known. The general idea of PLS-DA is to project predictor variables and response variables to new low-dimensional space while preserving, in the first PLS component, as much covariance between them as possible.

A PLS-DA model in its standard variant can be constructed and subsequently visualized using 'plsda' and 'plotIndiv' functions from the *mixOmics* R package (Rohart et al., 2017). Lipid names, along with their scores of contribution into the first component, might be extracted from the model using the 'selectVar' command. Of note, there is a sparse version of the PLS-DA method (sPLS-DA) that performs variable selection on a subset of all possible covariances (Lê Cao et al., 2011; Ruiz-Perez et al., 2020).

While PLS-DA is widely accessible and may be helpful in many cases, it also has several drawbacks, e.g., the problem of overfitting or dependence on the distribution within sample classes (Brereton and Lloyd, 2014; Gromski et al., 2014, 2015; Kjeldahl and Bro, 2010; Ruiz-Perez et al., 2020). Gromski et al. have investigated the efficiency of PLS-DA for the classification and feature selection problems and concluded that it has a rather low prediction accuracy for a small number of predictor variables compared to LDA, SVM, and RF-based approaches (Gromski

et al., 2014). Therefore, one should be especially cautious when applying PLS-DA for mass-spectrometry data analysis.

## 3.2 Results

### 3.2.1 Analysis of brSIRT6-KO lipidomics profiles

LC-MS pipeline presented above was applied to the lipidomics profiles derived from WT ( $n = 3$ ) and brSIRT6-KO ( $n = 3$ ) mouse brains. Nestin-Cre SIRT6-KO mice were generated based on the protocol from Kaluski et al. (Kaluski et al., 2017). Lipidomic samples were extracted according to a previously published protocol (Lapidot-Cohen et al., 2020) and then lipid compounds were quantified with ultra-performance liquid chromatography on a C8 reverse-phase column coupled with mass spectrometer (Q-Exactive Thermo Fisher Scientific, H-ESI) in both positive and negative modes. Overall, we measured and annotated 44 TAGs, 20 PCs, 14 PCs, 5 PEs, 1 DAGs and 1 PIs (Figure 3-3a).

Before the statistical analysis, missing abundances were imputed with a Random Forest-based imputation algorithm and then raw abundances were sample-wise normalized using the median normalization method. Hierarchical clustering of the processed and normalized profiles revealed no condition-specific clusters (Figure 3-3b). Furthermore, statistical analysis revealed no significantly changed lipid compounds between WT and SIRT6-KO groups ( $t$ -test, FDR  $p$ -value  $< 0.05$  was used as a significance threshold). Although non-significantly changed between experimental conditions, seven TAG species (TAG(62:6), TAG(50:3), TAG(54:0), TAG(48:2), TAG(46:1), TAG(46:2), TAG(48:3)) and PI(36:4) demonstrated increased abundances in SIRT6-KO replicates ( $\log_2(\text{Fold Change}) > 0.58$ ) (Figure 3-3c), which is consistent with the results of previous studies showing the enhanced TAG production in the absence of SIRT6 (Elhanati et al., 2013; Kim et al., 2010). Of note, triglycerides function as a fatty acid storage and their elevated levels were previously associated with an increased risk of cognitive decline in both human and animal studies (Dimache et al., 2021). By contrast, only one lipid, PS(38:3), demonstrated down-regulated abundance level in the SIRT6-deficient group ( $\log_2(\text{Fold Change}) =$

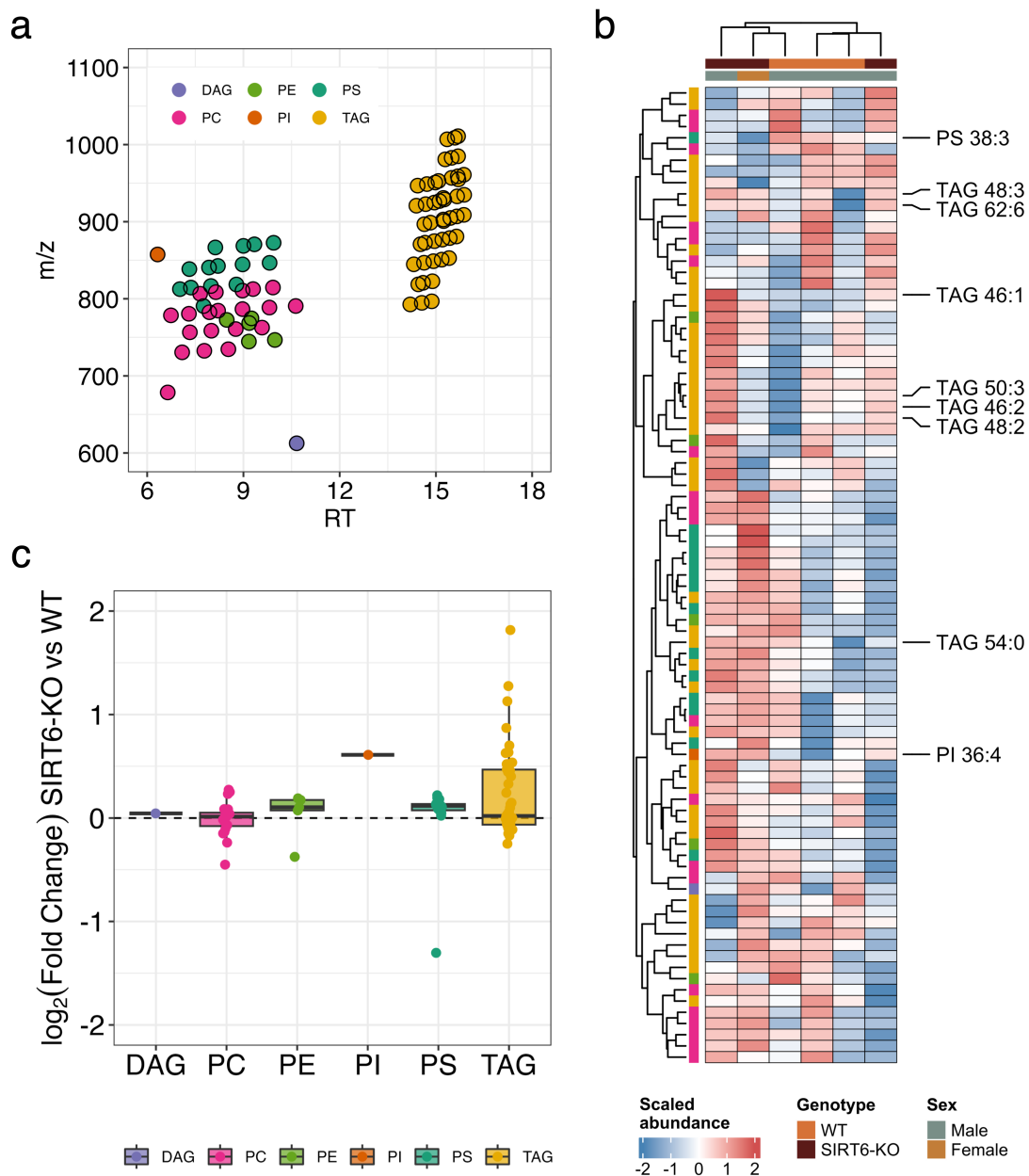


Figure 3-3: Analysis of lipid composition in the SIRT6-KO mouse brain. (a) Scatter plot showing m/z - RT relationships for measured lipids from DAG (Diacylglycerol), PE (Phosphatidylethanolamine), PS (Phosphatidylserine), PC (Phosphatidylcholine), PI (Phosphatidylinositol) and TAG (Triacylglycerides) classes. (b) Heatmap of z-score transformed lipid abundances. Lipids with  $|\log_2(\text{Fold Change})| > 0.58$  are annotated. (c) Distribution of  $\log_2(\text{Fold Change})$  values among lipid classes.

-1.3033).

One possible explanation for the insignificance of the observed abundance changes lies in the small sample sizes of the experiment, resulting in a low statistical power

of the t-test. Another possible limitation of this analysis is an unbalanced experimental design for the 'Sex' factor, appearing as an additional source of biological variability in the data. While these results are helpful for a better understanding of the abundance change direction of certain lipids under SIRT6 knockout, an additional analysis with a greater number of measured lipid species and biological samples is needed for a more detailed investigation of the SIRT6-induced alterations of the lipid composition in the brain.

## 3.3 Discussion

### 3.3.1 Future Challenges

The main benefit of untargeted LC-MS approaches lies in their ability to measure many components simultaneously in complex lipid mixtures in an unbiased way. By contrast to shotgun lipidomics, which omits the chromatography step, untargeted LC-MS offers accurate separation and detection of lipids spanning a wide range of classes. Targeted LC-MS measurements are more sensitive, accurate, and quantitative than untargeted ones. Yet, they focus on particular lipid classes or species and are poorly suitable for descriptive studies aiming to generate hypotheses due to this detection bias. Thus, untargeted LC-MS analysis is the technology of the first choice for biomarker discovery studies because of the unbiased sample preparation and lipid detection, not favoring any particular lipid class (Want, 2018). The main limitation of untargeted LC-MS measurements is their semi-quantitative nature. Absolute quantification is challenging to achieve in LC-MS experiments as it requires extensive use of internal standards. The ion response within the lipid class can depend on the fatty acid composition, creating an additional complicating factor for absolute quantification. However, the relative differences in lipid abundances are sufficient for most experimental designs. For example, studies searching for biomarkers, i.e., changes in the lipidome composition between patients and controls or between knockout and wild-type samples, would result in a list of lipids showing statistically significant differences in concentrations between two sample groups of interest.

Absolute quantification of the lipid concentration is not needed to compose such lists. It is enough to accurately measure differences between sample groups, which is a feasible and suitable task for untargeted LC-MS. Standard statistical approaches, e.g., the Wilcoxon test with multiple testing correction, can be applied to the LC-MS data to find significant lipid abundance differences and detect potential biomarkers. To cautiously apply statistical methods and avoid possible mistakes in interpreting results, it is highly recommended to involve a biostatistician, especially at the study design stage, and for the final validation of applied statistical procedures. In addition, detected candidate biomarkers and lipid composition changes can be (and should be) further validated using targeted LC-MS or MS/MS approaches.

Another limitation of untargeted LC-MS approaches is the possible suppression of ionization caused by the complexity of lipid mixtures. Thorough chromatographic separation prior to MS analysis helps to overcome this issue; however, this might not be practical for large-scale studies measuring the lipidome composition in thousands of samples because of the incredibly long time required to run the measurements.

Thus, achieving high-quality chromatographic separation in a short run time is among the critical future challenges of LC-MS technology because this affects the scalability of lipidomics studies, which tend to analyze a large number of samples. Similar to Genome-Wide Association Studies (GWAS), increasing the number of analyzed samples is necessary to achieve the power to detect significant biomarkers in lipidomics studies where the expected effect size is relatively small. To keep such studies within reasonable time frames, either the chromatographic separation time should be reduced or the number of MS machines should be increased to enable parallel runs. However, the last option dramatically increases experimental costs and introduces unwanted technical confounding factors and batch effects.

Even without parallel runs, batch effects constitute another future challenge of LC-MS technology. Small batch sizes are poorly suitable for large-scale lipidomics studies comprising thousands of samples because an accurate balancing of multiple confounding factors is difficult to achieve within a typical batch of 48–96 samples.

Apart from technological challenges, large-scale lipidomics studies introduce novel challenges at the data analysis level because they generate an extraordinary amount

of data that must be stored, processed, and analyzed efficiently. The increased resolution of novel MS systems addresses this problem as well as the need to measure the lipid composition in many technical or biological replicates to overcome technical or biological variability.

Limited databases and tools for the annotation of lipid species constitute another problem. Currently, most of them support only matching by  $m/z$  characteristic, without RT contribution, which depends on many technical factors and can only be used in in-house solutions for systems running with fixed parameters and stable environmental conditions.

The final and potentially most challenging problem resides in the lack of comprehensive curated lipid pathway databases linking lipids with proteins or genes. Multi-omics studies are in high demand but the few existing tools that are suitable for integrating different omics data types, i.e., lipidomics and transcriptomics, are mostly data-driven. Using correlations or more advanced metrics, they extract interrelationships of biomolecules from multi-omics data (Subramanian *et al.*, 2020). While such predicted links are of use for biomarker discovery, their biological interpretation is very limited, and curated biochemistry-based resources are essential for validation.

However, the Kyoto Encyclopedia of Genes and Genomes (KEGG) (Kanehisa, 2019; Kanehisa and Goto, 2000), REACTOME (Jassal *et al.*, 2020), and other widely used curated biochemical pathway databases cover only a limited set of lipid pathways, and mainly at the level of lipid classes but not individual lipid species. A detailed curated pathway database covering reactions of lipid species among all lipid classes would be an invaluable resource for the lipidomics community and future multi-omics studies.

## Chapter 4

# Effect of SIRT6 deficiency on transcriptome and metabolome levels during normal and pathological aging.

In this Chapter, we identify an essential function of SIRT6 in regulating the mitochondrial processes in the brain, including oxidative phosphorylation and aerobic respiration. By using transcriptomics and metabolomics profiles of control and brain-specific SIRT6-deficient mice, we demonstrate a reduction in the expression of OXPHOS-related genes, as well as the abundance of tricarboxylic acid cycle (TCA) metabolites. We functionally validate these findings by measuring the mitochondrial membrane potential and mitochondrial content changes. To establish the regulatory mechanisms by which SIRT6 affects mitochondria, we focus on YY1, SIRT3, and SIRT4 proteins. Finally, we link transcriptional changes of mitochondria-related genes with normal and pathological brain aging.

## 4.1 Methods

### 4.1.1 Generation of brain-specific SIRT6-KO mice and cells

SIRT6-KO mice and SH-SY5Y SIRT6-KO cells were generated by Dr. Shai Kaluski and Daniel Stein in Prof. Toiber laboratory using the protocol described in Sebastián et al. (Sebastian et al., 2012) and Kaluski et al. (Kaluski et al., 2017). Briefly, mice with loxP sites flanking exon 2 of SIRT6 gene were backcrossed for three generations and then bred with C57BL/Nestin-Cre/J transgenic mice, followed by the deletion of exon 2 by Cre/LoxP recombination. SIRT6 knockout in SH-SY5Y was achieved with two SIRT6-specific subgenomic RNAs (GCTGTCGCCGTACGCG-GACA and GCTCCACGGGAACATGTTTG) from GeCKO v2 lentiviral library (gift from Aharoni's lab).

### 4.1.2 RNA preparation and quality control

RNA was extracted from mice's left brain hemispheres, using the NucleoSpin RNA Plus kit (MACHEREY-NAGEL GmbH & Co. K.G., catalog number 740984.50), according to the manufacturer's manual. The purified RNA was then cleaned from any possible residual genomic DNA contamination using the RNeasy MinElute Cleanup Kit (QIAGEN, catalog number 74204), according to the manufacturer's manual. Using TapeStation, RNA Integrity Number (RIN) was then assessed and only samples with RIN>8.7 were in use. Dr. Shai Kaluski and Daniel Stein performed all the aforementioned procedures.

### 4.1.3 Full-length poly-A RNA sequencing

Library preparation was conducted by The Crown Genomics Institute of the Nancy and Stephen Grand Israel National Center for Personalized Medicine, Weizmann Institute of Science, Israel (G-INCPM). Briefly, the library kit used was the in-house INCPM mRNA-seq kit (G-INCPM, Weizmann Institute of Science) for full-length RNA-seq with polyA-based capturing. Sequencing was done using four lanes of NextSeq 500 High Output v2.5 Kit (75 cycles) (Illumina Inc., catalog number

20024906).

#### 4.1.4 RNA-seq data processing

Raw reads from eight *M. musculus* RNA samples were filtered and trimmed using *fastp* (Chen et al., 2018a) and then processed via version 3.0 of the *nf-core/rnaseq* pipeline (Ewels et al., 2022). In brief, trimmed reads were filtered with the *Trim Galore!* tool and mapped to the mouse GRCm39 reference genome with *STAR* (Dobin et al., 2013). Then, gene expression was quantified using the *Salmon* tool (Patro et al., 2017). The full guidelines for the pipeline are available at <https://nf-co.re/rnaseq>. Gene annotation was performed using the *AnnotationDbi* R package (Hervé Pagès, 2017) with downloaded *EnsDb.Mmusculus.v79* annotation database (Rainer, 2017) generated from Ensembl.

#### 4.1.5 Differential expression analysis

Differential expression (DE) analysis was performed in the R programming language using the *DESeq2* package (Love et al., 2014). First, we removed low-expressed genes for which the minimum expression level within any group of samples was  $< 3$ . Then, raw gene counts were normalized using DESeq2's median of ratios method, and quality control procedures were performed. The following design formula was used to evaluate expression differences between groups of samples: *design = ~ genotype*. After fitting the Negative Binomial model for each gene, we performed pairwise comparisons between groups using the Wald test. Genes were considered to be differentially expressed if FDR p-value  $< 0.05$  and  $|\log_2(\text{Fold Change})| > 1.5$ .

#### 4.1.6 Functional analysis of genes

We used *clusterProfiler* R package (Yu et al., 2012) to perform Gene Ontology (GO) enrichment analysis on both sets of down- and upregulated genes. Redundant GO categories were removed using the 'simplify' function from *clusterProfiler* package with default settings. Gene Set Enrichment Analysis (GSEA) was performed with 'gseaKEGG' function from *clusterProfiler* and pairwise similarity of significant

KEGG pathways was calculated with 'pairwise\_termsim' function from *enrichplot* package (Yu, 2018) using the Jaccard similarity measure. Then, the pathway similarity network was constructed and visualized in *Cytoscape* (Shannon et al., 2003). Next, core enrichment genes for four pathways related to neurodegenerative diseases (Parkinson's disease, Huntington's disease, Alzheimer's disease, Amyotrophic lateral sclerosis) were retrieved and classified into two groups according to their relevance to mitochondria ('mitochondrial genes' and 'others' groups). Expression level distributions for these two groups were visualized using *ggstatsplot* R package (Patil, 2021).

#### 4.1.7 Analysis of mitochondria-related genes

A list of mouse mitochondria-related genes, as well as information regarding their sub-mitochondrial localization and related mitochondrial pathways, were obtained from the MitoCarta database (Rath et al., 2021) (version 3.0). A total of 149 mitochondrial pathways were used for the enrichment analysis of DE mitochondria-related genes, performed with the 'enricher' function from the *ClusterProfiler* package. An illustration of electron transport chain complexes with associated DE genes was performed using the BioRender website (<https://biorender.com/>).

#### 4.1.8 Differential abundance analysis

Metabolite differential abundance analysis was done with the *MetaboAnalyst* platform (Pang et al., 2021). Annotated mouse ESC metabolites were normalized via the median normalization method and then were  $\log_2$  transformed. Principal components of the data were calculated using the 'prcomp' function in R and then used for the visualization of the profiles. Student's t-test was applied to define significantly changed metabolites, followed by the  $\log_2(\text{Fold Change})$  calculation. Differentially accumulated metabolites were retrieved according to  $\text{FDR} < 0.05$  and  $|\log_2(\text{Fold Change})| > 0.58$  cutoff criteria. Volcano plot visualization was done with the *EnhancedVolcano* (Blighe, 2018) package in R. Significant features were classified by their metabolic pathway identity provided by the KEGG database (Kanehisa

and Goto, 2000). *ComplexHeatmap* R package (Gu et al., 2016) was used to plot heatmaps of metabolite abundances.

#### 4.1.9 Analysis of public brain RNA-seq data

Processed and FPKM-normalized mouse brain RNA-seq profiles were downloaded from Zhang et al. (Zhang et al., 2014b). Only expression levels of SIRT6 and mitochondrial sirtuins (SIRT3, SIRT4, SIRT5) were selected, followed by the Spearman correlation calculation. Analysis of the correlation of SIRT6 with mitochondria-related genes was done using brain RNA-seq data of two human donors (H0351.2001, H0351.2002) from the Allen Brain Atlas database (Sunkin et al., 2013). Using the list of mitochondria-related genes retrieved from MitoCarta (version 3.0), Spearman's correlation coefficients of SIRT6 with OXPHOS and non-OXPHOS-related genes were calculated for both donor expression profiles. A permutation test (number of permutations = 1000000) was used to test the assumption regarding the unlikeness of distributions for OXPHOS and non-OXPHOS-related genes.

#### 4.1.10 Analysis of YY1 and SIRT6 ChIP-seq data

Processed data of two mouse YY1 ChIP-seq replicates in cortical neurons (SRX5509061 and SRX5509062 accession numbers (Boxer et al., 2020)), and SIRT6 ChIP-seq replicates in mouse embryonic stem cells (SRX873340, SRX873342, SRX873343 accession numbers (Etchegaray et al., 2015)) were downloaded from the ChIP-Atlas database (Oki et al., 2018). Called peaks with  $q < 1 \times 10^{-5}$  were annotated by their genome position using 'annotatePeak' function from *ChIPseeker* package (Yu et al., 2015) and only peaks localized at promoters of mitochondria-related genes in all replicates were selected. SIRT6 peaks called for both SIRT6-KO and WT replicates were subtracted from the analysis. The cellular component (CC) GO analysis of genes associated with the selected YY1 and SIRT6 peaks was performed using *ClusterProfiler*. Area-proportional Venn diagram for mitochondria-related DE genes, YY1- and SIRT6-regulated mitochondria-related genes was plotted using *venneuler* R package. The significance of overlap was calculated via a permutation test with

non-significant mitochondria-related genes as a specific background. ChIP-seq profiles of the selected peaks were visualized with the *karyoploteR* package (Gel and Serra, 2017).

#### 4.1.11 Analysis of public aging brain datasets

Microarray gene expression data of mouse aging neocortex (five 5-month-old and five 30-month-old, GSE13120 (Oberdoerffer et al., 2008)) and mouse aging hippocampus (three 10-days-old and three 20-month-old, GSE48911 (Wang et al., 2014)) were used for the analysis. Only WT replicates were selected from aging hippocampus datasets. Differential expression analysis was performed via *GEO2R* online tool (Barrett et al., 2013) with default parameters.

## 4.2 Results

### 4.2.1 Lack of SIRT6 alters gene expression levels in the mouse brain

Brains missing SIRT6 functionality might present changes at multiple levels of molecular organization, from gene expression to metabolism. To explore these changes, we performed transcriptome profiling (RNA-seq) in brains derived from Wild Type (WT, n=4) and brain-specific SIRT6-knockout (brSIRT6-KO, n=4) mice. In addition, we applied LC-MS techniques to quantify the abundance of metabolites in WT (n=3) and SIRT6-KO (n=3) mouse Embryonic Stem Cell (mESC) metabolomics. Then, we conducted a multilayer bioinformatics analysis of WT and SIRT6-KO transcriptomic and metabolomic profiles (Figure 4-1a).

Principal Component Analysis (PCA) of transcriptomic profiles revealed significant changes in gene expression levels between brSIRT6-KO and WT samples with a clear separation by the first principal component explaining 78% of the total variance (Figure 4-1b). At the same time, transcriptomic profiles exhibited a high level of intra-group similarity, showing Pearson's  $R > 0.9986$  for the WT group and Pearson's  $R > 0.9992$  for brSIRT6-KO replicates. In contrast, the inter-group Pearson's

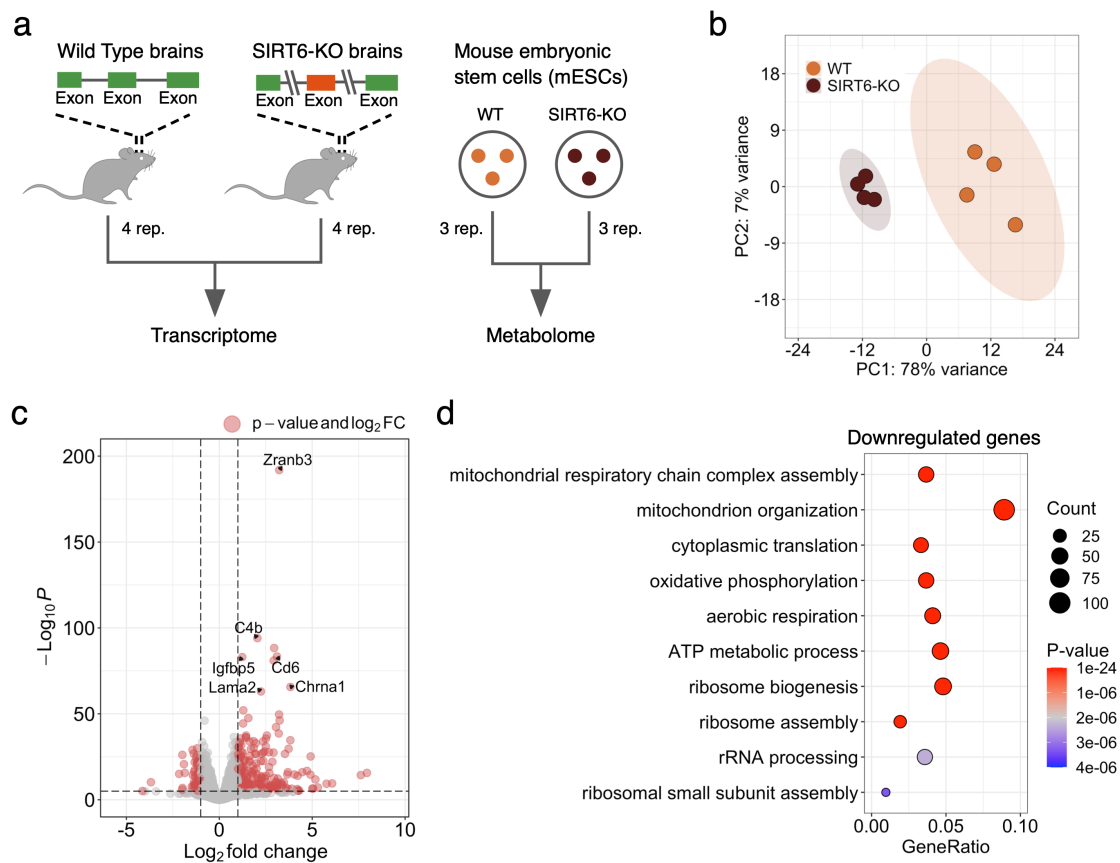


Figure 4-1: SIRT6 regulates gene expression levels. (a) Schematic illustration of the experimental design used in this study. Transcriptome profiles were collected from Wild Type (WT) and SIRT6 knockout (brSIRT6-KO) mouse brain samples. WT and brSIRT6-KO metabolomics profiles were collected from mouse embryonic stem cells (mESC). (b) Principal Component Analysis (PCA) plot showing separation between WT (orange) and brSIRT6-KO (brown) samples. Orange and brown ovals represent confidence ellipses of WT and brSIRT6-KO groups. (c) The volcano plot showing up- and down-regulated differentially expressed genes in brSIRT6-KO mice compared to WT mice. Red dots indicate significantly changed genes, and gray dots represent insignificant genes. (d) GO analysis showing the top 10 enriched biological processes for downregulated genes. Each circle corresponds to the enriched GO term and varies in size according to the number of significant genes belonging to this term. The gene ratio represents the number of DE genes belonging to the enrichment categories divided by the total number of genes per category.

R did not exceed 0.9978 (Supplementary Figure S-1a). Differential expression analysis between WT and brSIRT6-KO resulted in 2870 differentially expressed (DE) genes, 85% of which were annotated as protein-coding sequences (Supplementary Figure S-1b). Consistent with the expected impaired deacetylase activity of SIRT6 upon knockout, 1481 DE genes exhibited elevated expression levels in brSIRT6-

KO samples, while 1389 genes were downregulated (Figure 4-1c). The list of top 10 significant features was represented exclusively by upregulated genes, including *Zranb3* (FDR p-value =  $1.32 \times 10^{-192}$ ), *C4b* (FDR p-value =  $8.8 \times 10^{-95}$ ), *Cd6* (FDR p-value =  $4.18 \times 10^{-84}$ ), as well as *Chrna1* (FDR p-value =  $2.47 \times 10^{-66}$ ) and *Lama2* (FDR p-value =  $9.95 \times 10^{-64}$ ) (Supplementary Figure S-1c), which were previously found among the most significant signatures of SIRT6 deficiency in the brains of the full-body KO (Stein et al., 2021). These results collectively indicate that SIRT6 deficiency has a major effect on transcriptional regulation in the mouse brain.

We further examined the functional roles of significant DE genes. GO enrichment analysis on upregulated genes revealed enriched terms associated particularly with 'external encapsulating structure organization' (FDR p-value =  $3.7 \times 10^{-8}$ ), 'axon guidance', and 'neuron projection guidance' (FDR p-value =  $5.42 \times 10^{-8}$  for both terms) (Supplementary Figure S-1d). Conversely, the list of downregulated features in WT compared to brSIRT6-KO was significantly enriched in genes functionally related to mitochondrial processes (Figure 4-1d): 'mitochondrial respiratory chain complex assembly' (FDR p-value =  $1.21 \times 10^{-20}$ ), 'mitochondrion organization' (FDR p-value =  $9.05 \times 10^{-19}$ ), 'cytoplasmic translation' (FDR p-value =  $5.06 \times 10^{-17}$ ), and 'oxidative phosphorylation' (FDR p-value =  $6.60 \times 10^{-17}$ ). Overall, our findings show that SIRT6 deficiency provokes significant gene expression changes in the mouse brain and induces transcriptional dysregulation of mitochondria-related genes.

## 4.2.2 SIRT6 regulates mitochondrial metabolism

Based on the significant association of DE genes with essential mitochondrial processes, we wondered whether SIRT6 silencing might induce alterations in mitochondrial metabolite levels. To study the role of SIRT6 in mitochondrial metabolism, we examined the differential metabolite abundance patterns in SIRT6-KO untargeted LC-MS profiles compared to WT in the mouse embryonic stem cells data. Similar to RNA-seq results, we observed a global difference between the abundance levels of WT and SIRT6-KO metabolite profiles, underlined by their clear separation by PC1 in the PCA plot (Figure 4-2a). Differential abundance (DA) analysis re-

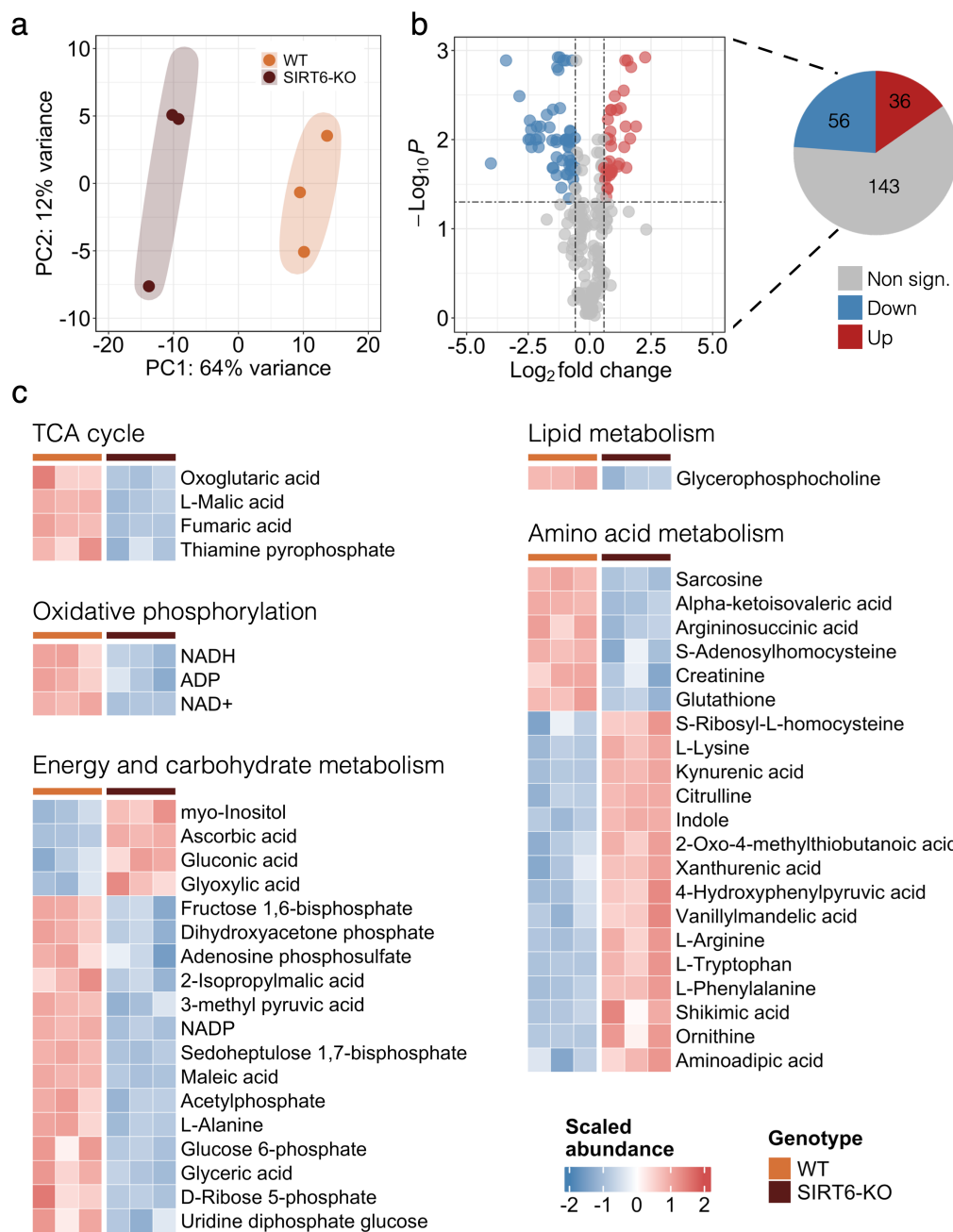
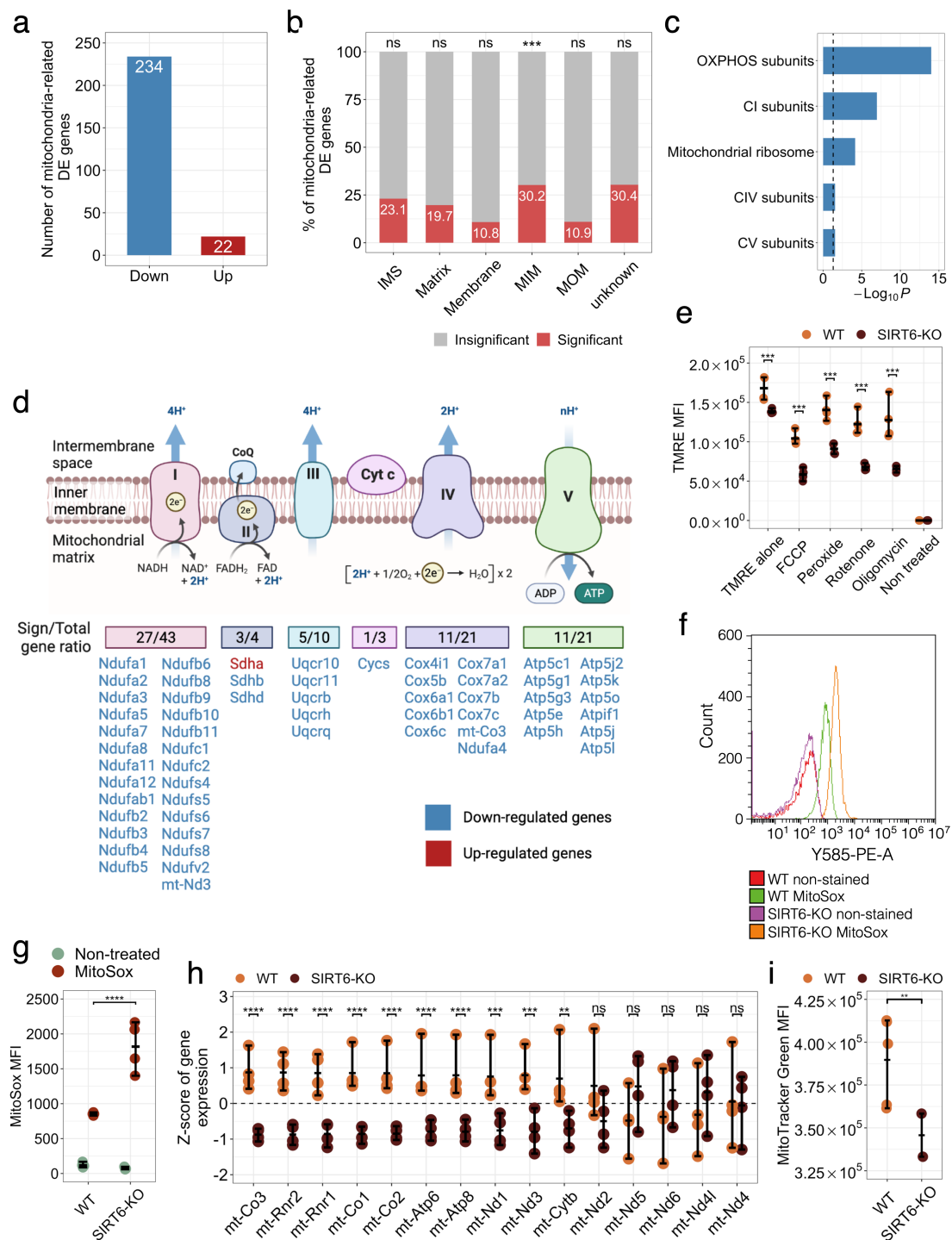


Figure 4-2: SIRT6 deficiency triggers an abundance of energy metabolites. (a) PCA plot showing separation between the WT (orange circles) and SIRT6-KO (brown circles) groups based on the mESC metabolomic profiles. Orange and brown ovals represent confidence ellipses of WT and SIRT6-KO groups. (b) The volcano plot illustrating differentially abundant metabolites detected between WT and SIRT6-KO mESC samples. Up- and downregulated metabolites are represented by red and blue circles, respectively. The pie plot (on the right) demonstrates the number of upregulated (red), downregulated (blue), and insignificant (gray) metabolites in the analysis. (c) The abundance heatmap of 68 out of 92 significant metabolites classified according to the metabolic pathways they are involved in.

vealed that 92 out of 235 metabolomic features ( $\sim 39\%$ ,  $\text{FDR} < 0.05$  and  $|\log_2(\text{Fold Change})| > 0.58$ ) changed significantly between experimental conditions (Figure 4-2b), including Ascorbic acid (upregulated), Maleic acid (downregulated), and  $\text{NAD}^+$  (downregulated) as the most significant metabolites (Supplementary Figure S-2a,b). Consistent with the transcriptome analysis, we found a number of DA features related to mitochondrial energy system pathways. Several metabolites associated with catabolic processes were more abundant in the SIRT6 WT group compared with SIRT6-KO: four metabolites (Malic acid, Fumaric acid, Oxoglutaric acid, Thiamine Pyrophosphate) associated with TCA cycle and three metabolites ( $\text{NAD}^+$ ,  $\text{NADH}$ ,  $\text{ADP}$ ) associated with OXPHOS (Figure 4-2c). The same tendency was observed for other DA metabolites related to the energy and carbohydrate metabolic pathways, of which only four metabolites were upregulated, while the remaining fourteen were decreased in SIRT6-KO. In addition to these results, we found abundant alterations of metabolomic features that constitute the Lipid and Amino Acid metabolism pathways. Thus, our results show that SIRT6 silencing alters cellular and mitochondrial metabolism.

### 4.2.3 SIRT6 deficiency leads to impaired oxidative phosphorylation

Furthermore, we focused on the significant DE mitochondrial genes that affected mitochondrial pathways. SIRT6 deficiency resulted in 256 significant DE mitochondria-related genes out of 1140 genes with confirmed mitochondrial localization according to the MitoCarta database (Figure 4-3a). Importantly, downregulated genes constituted the majority ( $>91\%$ ) of all DE mitochondria-related genes. Of note, protein levels of one of the most significantly downregulated genes (*Cyts*,  $\text{FDR p-value} = 3.00 \times 10^{-19}$ ) were consistently decreased in both male and female SIRT6-KO brains (Supplementary Figure S-3a,b). On the contrary, both expression and protein levels of *Vdac1* changed insignificantly between female WT and SIRT6-KO samples but showed a reduction in protein levels in male SIRT6-deficient brains (Supplementary Figure S-3a,b). Interestingly, we found that genes encoding mitochon-



drial proteins were overrepresented in their localization at the Mitochondrial Inner Membrane (MIM) compartment (Figure 4-3b, Supplementary Figure S-3c). Given that MIM serves as a springboard for ATP synthesis, we hypothesize that significant mitochondria-related genes should be mostly associated with electron transport chain complexes. To explore biological functions related to DE mitochondrial genes,

Figure 4-3: OXPHOS impairment in SIRT6-KO. (a) The number of significant DE genes associated with mitochondrial functions in WT compared to SIRT6-KO. Red and blue bars show the number of up- and downregulated genes. (b) Percentage of significant (red bars) and insignificant (gray bars) genes across mitochondrial compartments. 'IMS' denotes intermembrane space, 'MIM' denotes the mitochondrial inner membrane, and 'MOM' corresponds to the mitochondrial outer membrane. Black asterisks indicate the statistical significance of the enrichment ( $p$ -value =  $5.5 \times 10^{-4}$ , hypergeometric test). (c) Overrepresented mitochondrial pathways for WT compared to SIRT6-KO. A black dashed line shows the statistical significance threshold of 0.05 (hypergeometric test). (d) Schematic illustration of the ratio between the number of significant DE genes associated with Cytochrome C oxidase and I-V complexes of the electron transport chain and the total number of genes per complex. Down- and upregulated genes are marked by blue and red colors, respectively. (e) Mitochondrial membrane potential measured in SH-SY5Y WT and SIRT6-KO cells under treatment with FCCP (10 $\mu$ M), Hydrogen peroxide (800 nM), Rotenone (200 nM), Oligomycin (20  $\mu$ M), and without treatment. Asterisks indicate the level of statistical significance ( $p < 0.05$ , t-test). (f) Mitochondrial ROS detection with MitoSox assay. The histogram shows fluorescence emission distributions measured in WT and SIRT6-KO cells that were non-stained and MitoSox treated. Distribution of mean fluorescence intensity (MFI) values measured in WT and SIRT6-KO cells that were non-treated (green circles) and MitoSox-treated (red circles). Error bars are mean  $\pm$  SD, \*\*\*\* -  $p < 0.0001$  ( $n=3-5$ ). (g) Z-score transformed expression levels of mtDNA genes detected in our RNA-seq experiment. Orange and brown circles represent WT and SIRT6-KO samples, respectively. (h) Difference in mitochondrial content between WT and SIRT6-KO SH-SY5Y cells. Asterisks indicate the level of statistical significance ( $p < 0.05$ , t-test).

we performed GO enrichment analysis using information about mitochondrial pathways obtained from MitoCarta as a specific background. The top enriched categories included terms associated with mitochondrial respiratory chain complexes and mitochondrial ribosomes (Figure 4-3c). Mitochondrial Complex I turned out to be the most affected by SIRT6 depletion (FDR  $p$ -value =  $1.09 \times 10^{-7}$ ), with 27 downregulated out of 43 genes encoding this Complex. Of note, 57 out of 99 genes encoding the electron transport chain subunits were differentially expressed in our analysis. But only Succinate dehydrogenase complex flavoprotein subunit A gene (*Sdha*) demonstrated an elevated level of expression (Figure 4-3d). Also, we confirmed that these changes also occur in brain RNA-seq samples of two human donors from Allen Brain Atlas, where the correlation between the expression of SIRT6 and the expression of OXPHOS-related genes is significantly stronger ( $p$ -value = 0.000636

and p-value = 0.000002, respectively) compared to other mitochondria-related genes (Supplementary Figure S-3d).

We hypothesized that a global reduction in the expression of OXPHOS genes and electron transport chain (ETC) complex activity in SIRT6-KO models might be accompanied by the corresponding decline in mitochondrial membrane potential  $\Delta\Psi$ . In order to check this hypothesis, we first measured  $\Delta\Psi$  in WT and SIRT6-deficient SH-SY5Y cells stained with TMRE dye. Indeed, SIRT6-KO mitochondria showed a significant 1.21-fold decrease in  $\Delta\Psi$  compared to WT cells (FDR p-value = 0.0006, Tukey's multiple comparisons test, Figure 4-3e). Then, we tested  $\Delta\Psi$  in the same WT and SIRT6-KO cells but treated with an uncoupler of oxidative phosphorylation FCCP. Interestingly, supplementation of FCCP enhanced the reduction effect of  $\Delta\Psi$  upon SIRT6 deficiency, resulting in a 1.78-fold decrease of  $\Delta\Psi$  in SIRT6-KO cells (FDR p-value = 0.0001, Tukey's multiple comparisons test). Similar significant changes were observed when inhibitors of individual complexes of the ETC were added to the cells. SIRT6-KO cells with inactivated Cytochrome C complex by hydrogen peroxide showed a 1.54-fold reduction in  $\Delta\Psi$  (FDR p-value = 0.0001, Tukey's multiple comparisons test), while mitochondria with inactivated Complex I (rotenone treatment) and ATP synthase (oligomycin treatment) showed the highest level of  $\Delta\Psi$  reduction in SIRT6-KO, in 1.81 and 1.93 times, respectively (FDR p-value = 0.0001 in both cases, Tukey's multiple comparisons test), suggesting higher dependence of SIRT6 for these complexes. Then, we speculated that an elevated ROS production could also accompany observed transcriptional changes of OXPHOS-related genes and  $\Delta\Psi$  reduction upon SIRT6 knockout. Indeed, using MitoSox staining, we detected significantly increased levels of ROS in SIRT6-KO cells compared to WT (Figure 4-3f,g). All these results collectively indicate that the mitochondrial oxidative phosphorylation process is markedly impaired in SIRT6-deficient cells.

#### 4.2.4 Lack of SIRT6 results in a reduction of mtDNA gene expression and mitochondrial content

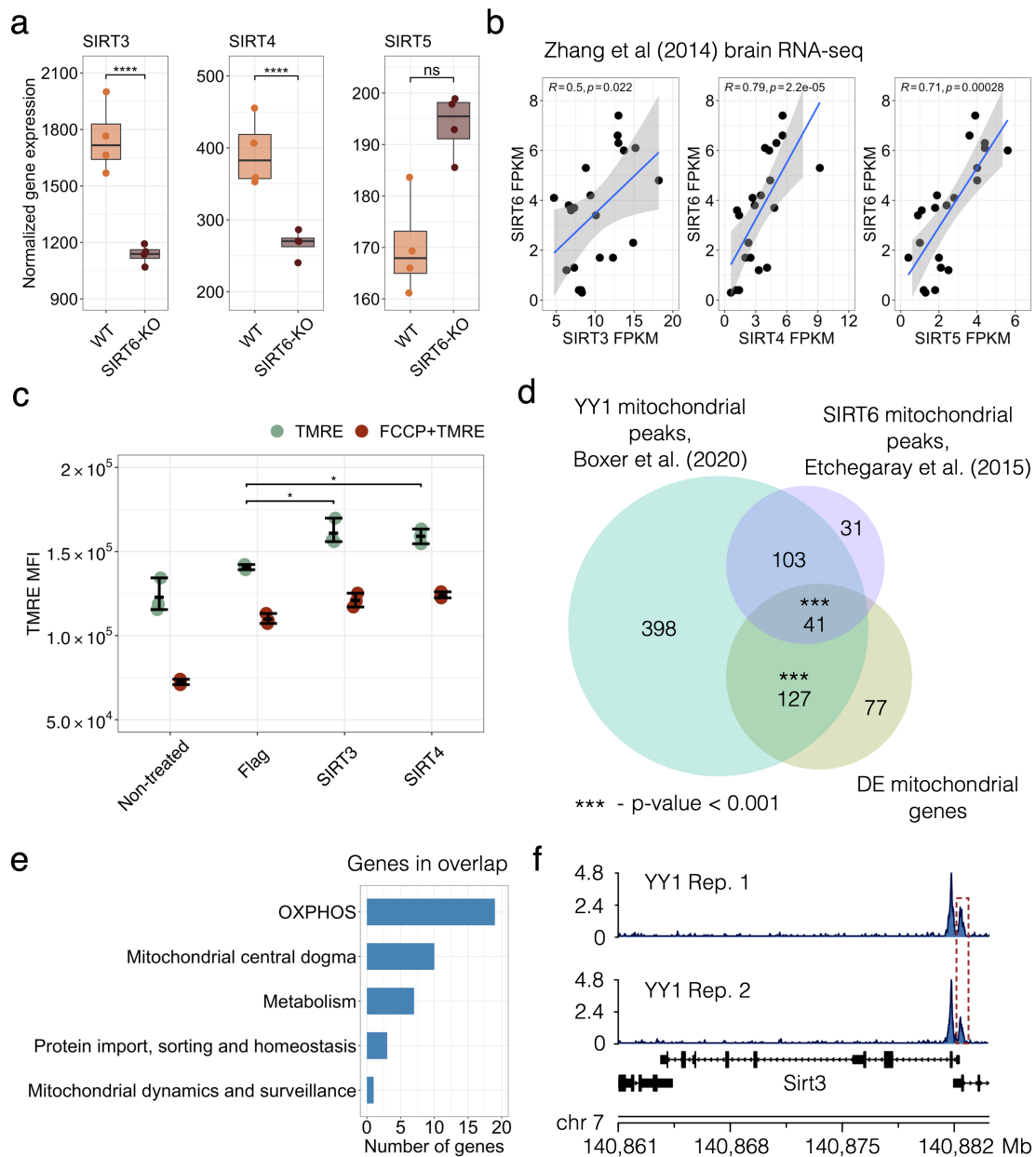
Mitochondrial activity is regulated by both nuclear and mitochondrial DNA-encoded genes. Since all mitochondrial-encoded genes are involved in oxidative phosphorylation, we studied the expression changes of these genes in SIRT6-KO brains. In particular, we extracted the expression of fifteen mtDNA genes detected in our RNA-seq data and the direction of their expression changes in WT and SIRT6-KO samples. Four out of these fifteen mtDNA genes were downregulated in SIRT6-KO mice, including statistically significant genes *mt-Co3* (FDR p-value =  $3.8 \times 10^{-18}$ ), *mt-Rnr2* (FDR p-value =  $1.1 \times 10^{-14}$ ), *mt-Rnr1* (FDR p-value =  $1.0 \times 10^{-11}$ ), *mt-Nd3* (FDR p-value =  $5.2 \times 10^{-4}$ ) (Figure 4-3h). In addition, six other mtDNA-encoded genes (*mt-Co1*, *mt-Co2*, *mt-Atp6*, *mt-Atp8*, *mt-Nd1*, *mt-Cytb*) showed a statistically significant reduction in expression (FDR < 0.05), but did not meet  $\log_2(\text{Fold Change})$  criterion for significance. Since altered mtDNA gene expression levels might indicate co-directional changes in mitochondrial content, we also measured mitochondrial mass in WT and SIRT6-KO SH-SY5Y cells using the MitoTracker Green assay. Consistent with transcriptional down-regulation patterns of mtDNA genes, mitochondrial mass was significantly lower in SIRT6-deficient cells ( $\sim 21.8\%$  decrease, t-test p-value = 0.0087) than in WT cells (Figure 4-3i), which in turn can be a marker of impaired mitochondrial biogenesis or increased degradation.

#### 4.2.5 SIRT6-SIRT3,4 and SIRT6-YY1 axes promote OXPHOS in the brain

Next, we elucidated the mechanism behind the SIRT6-dependent regulation of mitochondrial activity and the oxidative phosphorylation process. First, we explored SIRT3, SIRT4, and SIRT5 genes from the sirtuin family, which encode proteins localized in mitochondria and coordinately impact mitochondrial pathways related to redox homeostasis and cellular metabolism. To determine whether SIRT6 may transcriptionally regulate these genes, we examined their expression patterns upon SIRT6 knockout (Figure 4-4a). SIRT3 and SIRT4 were significantly reduced in

SIRT6-KO brains (FDR p-value =  $3.60 \times 10^{-12}$  and  $3.33 \times 10^{-6}$ , respectively). At the same time, the lack of SIRT6 did not substantially affect SIRT5 expression. We further confirmed the positive association between SIRT6 and SIRT3-4 by analyzing publicly available gene expression data in the mouse brain from Zhang et al. (Zhang et al., 2014b) (Figure 4-4b). SIRT6 expression levels positively correlated with the corresponding expression levels of all mitochondrial sirtuins (Pearson's R = 0.5, 0.79, 0.71 for correlations with SIRT3, SIRT4, SIRT5, respectively). Then, we focused on SIRT3 and SIRT4 genes, which most significantly changed among mitochondrial sirtuins. To experimentally validate their role in OXPHOS regulation, we assessed the changes in mitochondrial membrane potential  $\Delta\Psi$  in SIRT6-KO SH-SY5Y cells with overexpressed SIRT3 and SIRT4. We found that increased expression of SIRT3 or SIRT4 significantly rescued  $\Delta\Psi$  in SIRT6-deficient cells compared to that in WT cells, suggesting their importance for the regulation of oxidative phosphorylation when SIRT6 is absent (Figure 4-4c).

Given that SIRT6 is involved in the regulation of distinct cellular functions, we next wondered whether the transcription regulation of mitochondrial OXPHOS by SIRT6 was specified by a co-regulating transcription factor YY1. It was previously shown that SIRT6 and YY1 functionally interact by forming a complex that regulates several shared target genes (Stein et al., 2021). To examine whether they might regulate mitochondrial processes in a coordinated manner, we analyzed two publicly available YY1 ChIP-seq datasets in cortical neurons (GSE128182 GEO accession). We searched for YY1 peaks corresponding to the promoters of mitochondria-related genes. In addition, we compared these peaks with both mitochondria-related DE genes from our RNA-seq analysis as well as with SIRT6 targets involved in mitochondrial regulation derived from public mESC ChIP-seq profiles (GSE65836). As a result, we detected 669 YY1 peaks associated with promoters of mitochondrial genes, including 168 peaks that were localized within 1 kb from the promoters of mitochondrial DE genes and 144 peaks colocalized with SIRT6 binding sites in mESC (Figure 4-4d). We also identified only 11 SIRT6 binding sites in the absence of YY1 peaks at mitochondria-related gene promoters, also suggesting a smaller indirect mechanism of mitochondrial regulation by SIRT6.



Interestingly, both YY1 and SIRT6 peaks were overrepresented at the promoters of genes localized in the mitochondrial protein-containing complex (FDR p-value =  $1.01 \times 10^{-38}$  and FDR p-value =  $3.96 \times 10^{-12}$ , respectively) and the mitochondrial inner membrane (FDR p-value =  $1.82 \times 10^{-27}$  and FDR p-value =  $2.66 \times 10^{-8}$ , respectively), while YY1 target genes were also enriched for mitochondrial matrix (FDR p-value =  $3.41 \times 10^{-37}$ ) and ATPase complex (FDR p-value =  $4.34 \times 10^{-22}$ ) (Supplementary Figure S-4a,b). Our analysis revealed that the expression of more than 66% of the detected mitochondria-related genes could be regulated by either YY1 or by

Figure 4-4: SIRT6-SIRT4 and SIRT6-YY1 axes in mitochondrial regulation. (a) SIRT3-5 expression levels in transcriptomic profiles of WT and SIRT6-KO mice. Asterisks indicate the statistical significance (FDR p-value < 0.05) derived from *DESeq2* differential expression analysis. (b) Spearman's correlation coefficients of SIRT6 expression profile with expression profiles of mitochondrial sirtuins (SIRT3-5) in the brain RNA-seq data from Zhang et al. (c) Mitochondrial membrane potential measured in SH-SY5Y SIRT6-KO cells when SIRT3 or SIRT4 were exogenously overexpressed. SIRT6-KO SH-SY5Y cells were transfected with Flag-CMV, SIRT3-Flag-CMV, and SIRT4-Flag-CMV plasmids. After 48 hours, cells were collected and stained with TMRE and Life/dead viability dye and the intensity of fluorescence was measured by CytoFLEX. (d) Venn diagram showing overlaps between significant mitochondria-related genes from the RNA-seq analysis (orange), YY1 mitochondrial targets (green) and SIRT6 mitochondrial targets (purple). The statistical significance of the overlaps was calculated using the permutation test. (e) Bar plot showing biological functions along with the number of the mitochondria-related genes overlapped between all datasets presented in Figure 4-4d. (f) YY1 peaks at the SIRT3 promoter in two analyzed ChIP-seq replicates.

YY1 and SIRT6 together. Both YY1 and SIRT6 peaks were found within promoters of 41 mitochondria-related DE genes that were also over-represented (permutation test p-value =  $5.1 \times 10^{-4}$ ) in this overlap compared to non-significant mitochondria-related genes. These genes are also related to OXPHOS, mitochondrial metabolism, and protein import regulation (Figure 4-4e, Supplementary Figure S-4c). Besides its coordinated regulatory activity with SIRT6, YY1 can also independently bind to the promoters of mitochondria-related DE genes. In our analysis, it was enriched (permutation test p-value =  $1.0 \times 10^{-3}$ ) at the promoters of such 127 DE genes, including SIRT3 (Figure 4-4f), which importance for OXPHOS was shown above. Hence, our analysis suggests that SIRT6 acts as a regulator of mitochondrial functions via the SIRT6-YY1-SIRT3,4 axis.

## 4.2.6 Neuropathological role of SIRT6 through the prism of mitochondrial deregulation

Sirtuin 6 has been reported to be important in the protection against age-related and neurodegenerative diseases in the brain (Mariottini et al., 2009; Shao et al., 2016; Kaluski et al., 2017; Portillo et al., 2021). Since, in our analysis, we observed a global reduction in the transcriptional level of mitochondrial genes, we explored whether

these changes can be linked to pathways of age-associated diseases occurring in the brain. Therefore, we performed the Gene Set Enrichment Analysis (GSEA) based on all genes in our RNA-seq dataset. This analysis revealed 71 significantly affected KEGG pathways (Supplementary Figure S-5), including 'Parkinson's disease' (FDR p-value = 0.015), 'Huntington's disease' (FDR p-value = 0.0168), 'Alzheimer's disease' (FDR p-value = 0.0169), and 'Amyotrophic lateral sclerosis' (FDR p-value = 0.0168) pathways (Supplementary Figure S-5). Interestingly, these neurodegenerative disease pathways formed one distinct cluster with 'Oxidative phosphorylation' pathway in the enrichment network, showing a large number of overlapping genes between them (Figure 4-5a). To address whether the expression changes of mitochondria-related transcripts directly caused the enrichment of these pathways, we retrieved core enrichment genes from the pathways of interest. More than 67% of core enrichment genes in each selected pathway were associated with mitochondrial functions. The highest percentage was detected for Alzheimer's disease (Figure 4-5b). Moreover, the mitochondria-related core enrichment genes exhibited lower mean  $\log_2(\text{Fold Change})$  values compared to non-mitochondrial genes in each of the selected neurodegenerative disease pathways.

Since mitochondrial dysfunction is one of the most stable and crucial hallmarks of normal aging (Mecocci et al., 1993; Wallace, 2005; Park and Larsson, 2011), we then compared our downregulated mitochondria-related genes with genes that were previously reported to be signatures of mouse brain aging (Oberdoerffer et al., 2008; Wang et al., 2014). As a result, we captured ten downregulated mitochondrial genes that also showed a reduction in their expression levels in both neocortex and hippocampus aging data (Figure 4-5c). Notably, this list of commonly downregulated genes included genes related to OXPHOS complexes (*Sdhb*, *Ndufa7*, *Uqcrcq*) and mitochondrial protein import machinery (*Timm10b*). Another interesting overlapping gene was Uracil DNA Glycosylase (*Ung*), which has an important role in mitochondrial base excision repair (BER) initiation. Given the limited DNA repair mechanisms in mitochondria, one can expect that the decrease in *Ung* activity might provoke an accumulation of mutations in mtDNA. Taken together, the findings reported above suggest that the brain lacking SIRT6 expression is characterized by

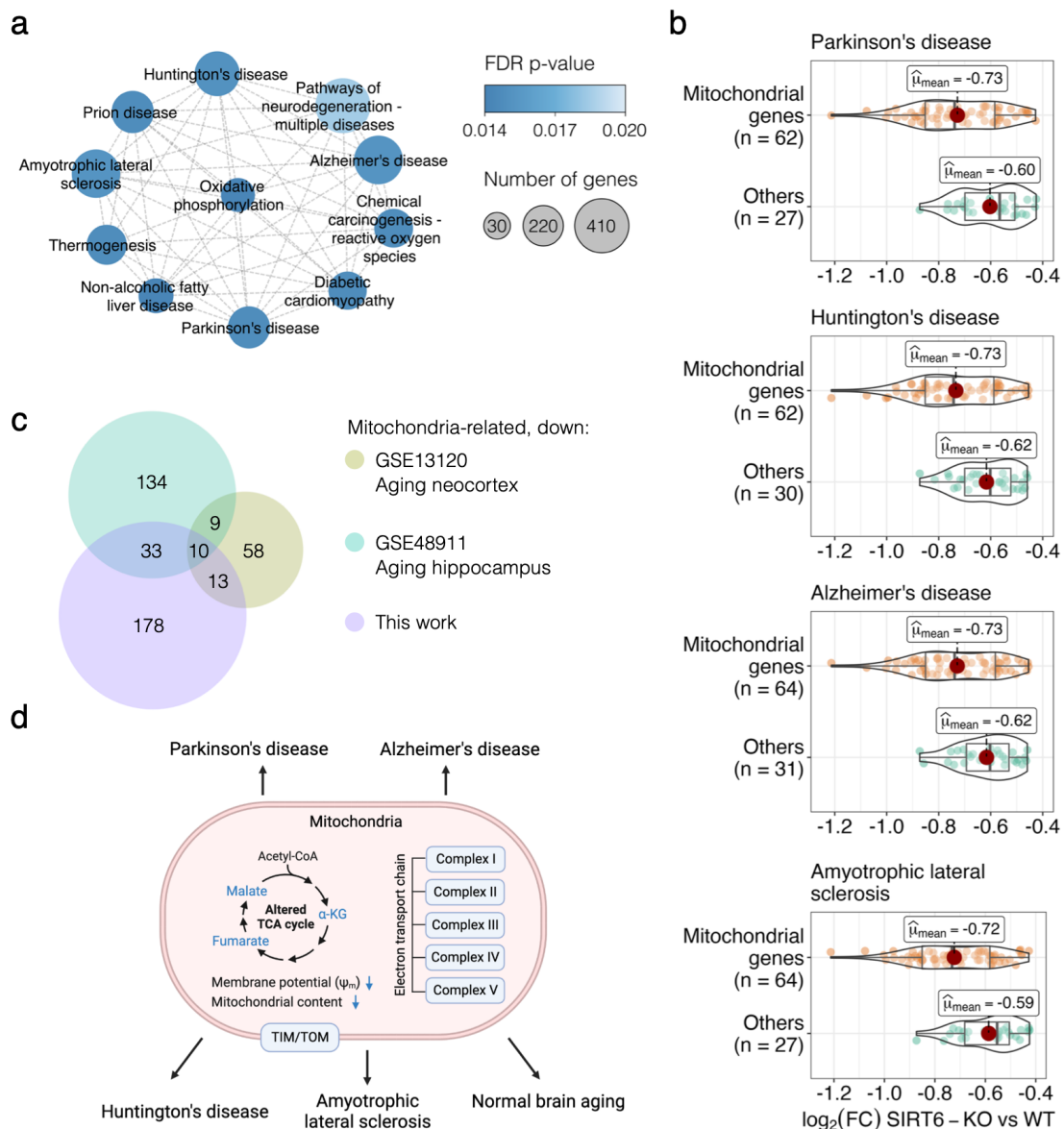


Figure 4-5: SIRT6 silencing triggers neurodegenerative disease pathways and normal brain aging. (a) A cluster of enriched KEGG pathways obtained using GSEA. Each circle represents an enriched pathway and is colored according to the FDR p-value. (b) Violin plots representing the  $\log_2(\text{Fold Change})$  expression for genes with the largest contribution to the GSEA enrichment result per neurodegenerative pathway. (c) Euler diagram showing ten common downregulated genes between publicly available aging brain gene expression datasets (GSE13120 and GSE48911 accessions in the GEO database) and significantly downregulated mitochondrial genes from this study. (d) Proposed model of the mitochondrial dysfunction caused by SIRT6 silencing and its involvement in neurodegenerative diseases and normal aging. The figure was generated using the BioRender website.

mitochondrial dysfunction (OXPHOS impairment, TCA dysregulation, reduced mitochondrial content and membrane potential) that causes a neurodegenerative-like phenotype and contributes to pathological aging of the brain (Figure 4-5d).

### 4.3 Discussion

In this study, we performed RNA-seq and LC-MS experiments to trace molecular organization changes at transcriptome and metabolome levels of SIRT6 knockout systems. We show that SIRT6 deficiency leads to a dramatic downregulation of mitochondrial genes and changes in mitochondria-related metabolite composition, suggesting that SIRT6 critically regulates mitochondrial activity in the brain.

Our analysis of gene expression levels in the SIRT6-deficient mouse brain revealed dramatic transformations upon SIRT6 knockout: almost three thousand genes changed their expression significantly, with a strong enrichment of mitochondrial functions among down-regulated ones, allowing us to conclude that SIRT6 knockout induces transcriptional dysregulation of mitochondrial genes. This result bridges the missing gap between studies demonstrating mitochondrial dysfunction in normal and pathological aging (Chabi et al., 2008; López-Otín et al., 2013) and studies proclaiming the critical role of SIRT6 in the protection against aging-associated diseases (Kaluski et al., 2017; Li et al., 2021).

Though mitochondrial dysfunction is a known marker of aging and neurodegenerative diseases, the exact mechanism behind it remains unknown. Our study suggests that the decay of SIRT6 levels during aging and in Alzheimer’s disease (Jung et al., 2016; Kaluski et al., 2017; Portillo et al., 2021) could be a key mechanism causing the deterioration of mitochondrial functions. The changes induced by the SIRT6 knockout that we observe at the metabolite level support this claim: metabolites related to mitochondrial energy system pathways (in particular, OXPHOS and TCA cycle) are significantly overrepresented among differentially abundant metabolites. In line with the discussed mitochondrial dysfunction in aging, all these metabolites are downregulated in the SIRT6-KO samples. Importantly, our metabolomics results strongly corroborate previously published findings for SIRT6-depleted ES

cells, showing the reduction of mitochondrial respiration and decreased abundances of several TCA intermediate metabolites, including Malic and Fumaric acids (Zhong et al., 2010). Another study provided evidence that SIRT6 transcriptionally controls the activity of genes involved in mitochondrial fatty acid  $\beta$ -oxidation in the mouse liver, thereby maintaining energy homeostasis of the cell (Naiman et al., 2019). Importantly, the dramatic decline of another oxidative metabolism modulator,  $\text{NAD}^+$ , was also associated with pro-senescence mechanisms in various species (Mouchiroud et al., 2013; Camacho-Pereira et al., 2016), as well as with limited neuroprotective activity of sirtuins (Imai and Guarente, 2014). Interestingly, another study reported that overexpression of SIRT6 can compensate the age-related reduction of  $\text{NAD}^+$  levels, suggesting that SIRT6 might be a promising anti-aging target (Roichman et al., 2021).

Accordingly, the vast majority of differentially expressed mitochondria-related genes were downregulated in our gene expression analysis. One possible limitation of the presented work is estimating the activity of mitochondrial and neurodegenerative pathways based on changes in transcription rates while missing information from the proteomic layer of biological regulation. Indeed, the activity of enzymes and the information about their post-translational modifications could be used as a more precise description of pathway perturbations (Hebert et al., 2013). Instead, our study utilizes changes in metabolite composition as a finite characteristic of cell state in response to perturbations in transcriptional networks caused by SIRT6 deletion. To compensate for the absence of proteomic measurements, we performed an additional experimental validation of our results, including measurements of mitochondria-related proteins *Vdac1* and Cytochrome C, to bridge the gap between initial gene expression changes and differential metabolome outcomes under SIRT6 deficiency.

Another possible limitation of this work is related to using mESC culture for the metabolomics analysis of SIRT6-KO profiles and comparing it with gene expression profiles originating from mouse brain tissues. While using SIRT6-KO stem cell models has many undeniable advantages compared to tissue-based models, including relative simplicity in producing a knockout model and the lower cost of experiments, their ability to resemble organ-based models remains an open question. First, 2D

cell culture models might not be able to replicate the complex interactions between cells and extracellular matrix (Slanzi et al., 2020). Second, ES cells can demonstrate high cell-to-cell variability, affecting the experiments' reproducibility (Chakraborty et al., 2020). Therefore, despite the promising results obtained for the transgenic mouse embryonic cell line, an additional analysis of mouse brain metabolomics is needed to confirm the observed effects in the organ-based SIRT6-KO model.

As mitochondria-related genes downregulated in our analysis were strongly enriched with mitochondrial respiratory chain complexes, we further validated our findings by measuring the mitochondrial membrane potential and mitochondrial content in SIRT6-KO cells because reduced gene expression might indicate the loss of mitochondria. Both measured characteristics were significantly decreased, validating the suggested impairment of mitochondrial oxidative phosphorylation and mitochondrial biogenesis in SIRT6-deficient brains. Interestingly, the average decrease of mtDNA gene expression ( $\sim 19.7\%$ ) in SIRT6-KO was in good agreement with the corresponding reduction of mitochondrial content (21.8%), suggesting impaired mitochondrial biogenesis as a primary cause of the observed transcriptional dysregulation in mitochondria upon SIRT6 knockout.

Concordantly, the impaired membrane potential upon SIRT6-KO can be partially rescued by restoring SIRT3 and SIRT4 levels, which were significantly downregulated in SIRT6-deficient brains. Both of them are localized in mitochondria and impact mitochondrial pathways related to redox homeostasis and cellular metabolism (van de Ven et al., 2017) and have important roles in mitochondria metabolism ROS balance and lifespan (Kincaid and Bossy-Wetzel, 2013; Min et al., 2018; Wood et al., 2018). The analysis of our and publicly available gene expression data (Zhang et al., 2014b) confirms that SIRT6 transcriptionally regulates SIRT3 and SIRT4. Our analysis further indicates that SIRT6 regulates mitochondrial gene expression through the transcription factor YY1. We have previously shown that SIRT6 and YY1 form a complex that regulates many shared target genes. Our analysis of YY1 ChIP-seq data (Boxer et al., 2020) suggests that SIRT6 and YY1 regulate mitochondrial processes coordinately.

Taken together, our results establish that SIRT6 knockout induces global molec-

ular transformations in the brain: almost three thousand genes change their expression significantly, as well as nearly half of all studied metabolites. Part of these differences are distinctly attributed to mitochondrial dysfunction, particularly in mitochondrial respiratory chain complexes, as confirmed by measurements of the mitochondrial membrane potential and mitochondrial content. Our data suggest that SIRT6 regulates mitochondrial function through YY1 and SIRT4. Lastly, we reveal that the changes driven by SIRT6 loss also occur in neurodegenerative diseases and aging brains, suggesting that age-dependent SIRT6 decay plays a causal role in neurodegenerative diseases. Preventing the reduction of SIRT6 expression or augmenting SIRT6 activity might thus provide a therapeutic opportunity to reinstate mitochondrial homeostasis in the brain and prevent neurodegenerative diseases.

## Chapter 5

# The role of SIRT6' co-partner YY1 in aging and brain tumors

A growing number of studies indicate that dysfunction of SIRT6 is associated with normal and pathological brain aging (Braidy et al., 2015; Kaluski et al., 2017; Portillo et al., 2021; Stein et al., 2021). In line with our results presented in Chapter 4, several studies reported SIRT6 protective role in the neurodegenerative brain, preventing DNA damage accumulation and impeding Tau toxicity (Kaluski et al., 2017; Portillo et al., 2021). Moreover, SIRT6 acts as a tumor suppressor in gliomas, inhibiting cell proliferation and oxidative stress via the inactivation of JAK2/STAT3 pathway (Feng et al., 2015). SIRT6 is reduced in the most common and malignant form of glioma, named glioblastoma (GBM), but its overexpression hampers cancer cell growth and downregulates the Warburg effect in GBM patients (Chen et al., 2018b; Dong et al., 2019). Given that older age is a major risk factor for glioblastoma aggressiveness, the age-related mechanisms of SIRT6 activity should be considered while studying its implication in brain tumorigenesis.

This chapter is devoted to the SIRT6' partner in transcriptional co-regulation, YY1, and its functions in pathological brain aging. Here, we found that glioblastoma marker *TP73-AS1* is highly expressed in the aging brain, and under pathological conditions its expression is increased. We discovered that the YY1 regulates *TP73-AS1* expression. Importantly, YY1 directly activates the transcription of *TP73-AS1* upon TMZ treatment. Together, these findings bring an intriguing link between

aging and cancer.

## 5.1 Methods

### 5.1.1 Primers

Based on the ENCODE TF binding data (Enc, 2012), the *TP73-AS1* promoter was divided into two regions (824 and 1124 base pair long, respectively), that were cloned into the Firefly luciferase using the TEDA method (Xia et al., 2018) between XhoI and HindIII restriction enzyme sites. The mutated YY1 binding site promoter was cloned using standard site-directed mutagenesis. YY1 overexpression vector was described in (Stein et al., 2021). The primer sequences used were as follows:

scramble/control: ACCGCGCCAAACGTGCCCTGACGG;

YY1 g#1: GGAGACCATCGAGACCACAG;

YY1 g#2: CGACACCCTCTACATCGCCA.

### 5.1.2 Luciferase activity assay

Luciferase Activity of the different *TP73-AS1* promoter parts was measured by luciferase reporter gene assay (Promega, E1500) in SHSY5Y and HEK293 cell lines. The SH-SY5Y cells were transiently transfected (Lipojet, BioConsult SL100468) with the reporter and control plasmids, and were cultured in DMEM medium with 10% fetal bovine serum. 24h later, wells were treated with DMSO for 2 days. Luciferase activity was measured and normalized by measuring co-transfected Renilla plasmid using the Dual-Luciferase Reporter Assay System, Promega.

### 5.1.3 Data analysis

Gene expression profiles from Cotman (GSE48350) (Berchtold et al., 2008) and Salomon (GSE5281) (Liang et al., 2007) datasets were downloaded from R2 database (<http://r2.amc.nl>). Expression profiles from the Cotman dataset were used to compare *TP73-AS1* expression levels between young (< 60 years old) and old (> 60 years old) donor brains in the hippocampus, entorhinal cortex, superior frontal gyrus and

post-central gyrus. Both Cotman and Salomon datasets were used to assess *TP73-AS1* expression changes between healthy and AD brains. Data from all available brain compartments in the Salomon dataset was analyzed. GTEx (Carithers et al., 2015) and ICGC GBM-US (Zhang et al., 2019) datasets were used to investigate the correlation between *TP73-AS1* and *YY1* in normal and GBM donor brains. Four brain compartments were selected for the analysis with the GTEx dataset: cerebellar, cerebellum, cortex, and frontal cortex. Wilcoxon rank test was used to determine statistical significance between groups. The statistical significance threshold was set to 0.05.

## 5.2 Results

### 5.2.1 *TP73-AS1* is highly expressed in the aging brain

To learn more about how the expression of *TP73-AS1* is regulated, and given that its expression is increased during aging in glioma (Zhang et al., 2021), we first asked if *TP73-AS1* expression is associated with natural aging in the brain and interrogated the Cotman dataset, using R2 database and 60-year-old brains as a cutoff. We found that *TP73-AS1* is highly expressed in the aged brain and this is the case in most brain regions to which data is available (Figure 5-1A). In accord, the expression of *TP73-AS1* in the brain is correlated with aging (Figure 5-1B). Together, these data suggest that *TP73-AS1* is highly expressed in the aging brain.

We next asked if *TP73-AS1* expression is also linked to pathological aging in the human brain. To this end, we interrogated the Cotman dataset and found that *TP73-AS1* is highly expressed in Alzheimer's brain and that this is the case in most tested brain regions (Figure 5-2A). We confirmed these findings using a second dataset, the Salomon dataset (Figure 5-2B) which supported our conclusion. While in the hippocampus (Cotman dataset), the median temporal and superior frontal gyrus (Salomon dataset) *TP73-AS1* expression was trending higher in Alzheimer's vs. normal brain, these differences did not reach statistical significance, possibly due to a lower number of samples as compared with the total which was obtained by pooling of all samples from different brain regions.

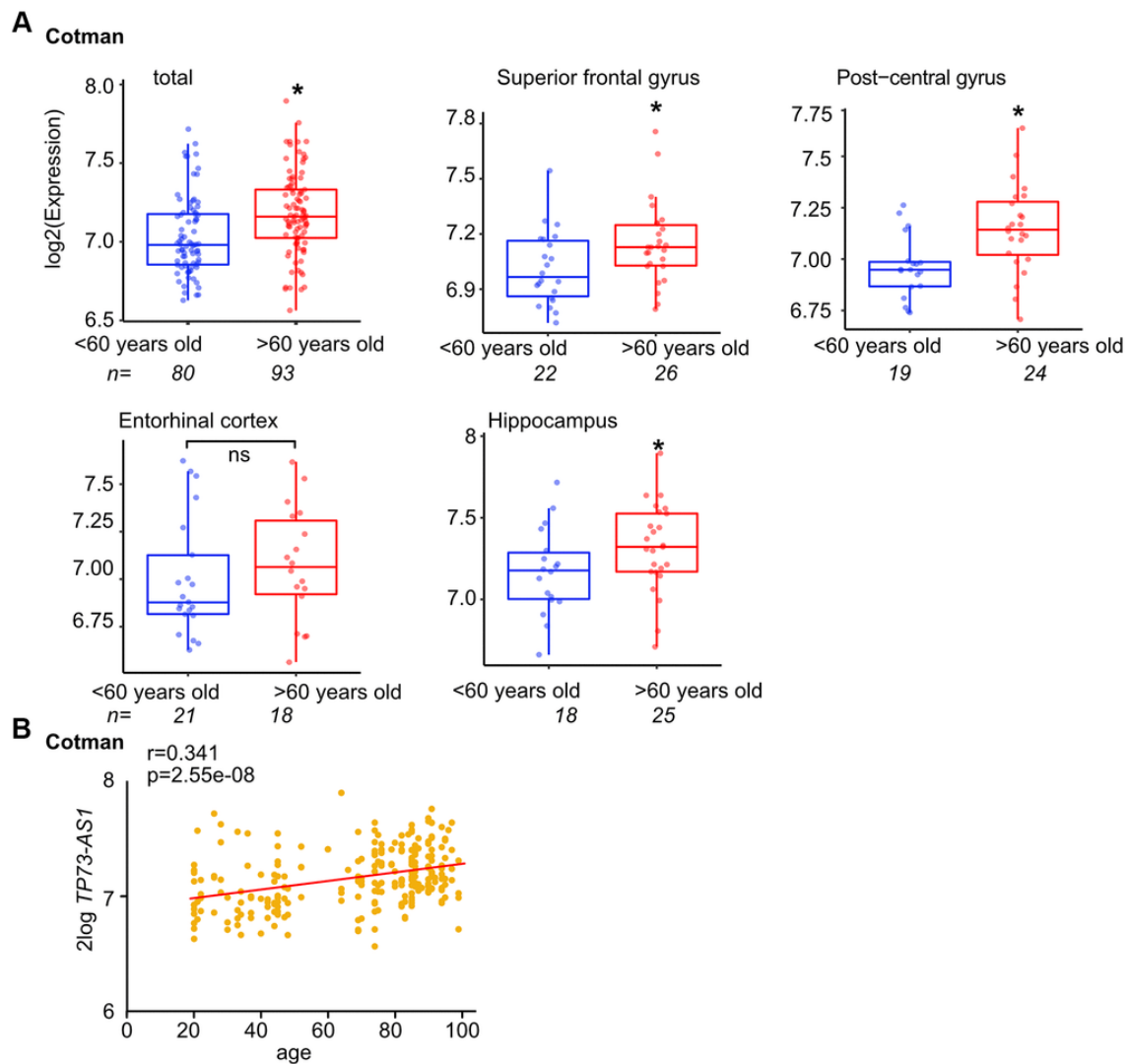


Figure 5-1: *TP73-AS1* is highly expressed in the aging brain. (A) The levels of *TP73-AS1* in the old vs. young brain are shown. Data were obtained from the R2 website and the indicated dataset (GSE48350). (B) The correlation between the expression of *TP73-AS1* and age in the brain was determined using R2 and the indicated dataset (GSE48350).

The high expression of *TP73-AS1* in the aging brain and our previous findings that *TP73-AS1* is highly expressed in GBM tumors, lead us to ask if the age of the patient is associated with *TP73-AS1* expression in GBM tumors. Therefore, we analyzed *TP73-AS1* expression in GBM tumors of old and young patients using 60-year-old as a cutoff. Indeed, *TP73-AS1* is up-regulated in GBM tumors of older patients (Supplementary Figure S-6A). In addition, we calculated the correlation between *TP73-AS1* expression and the patient's age and found that they are positively correlated (Supplementary Figure S-6B).

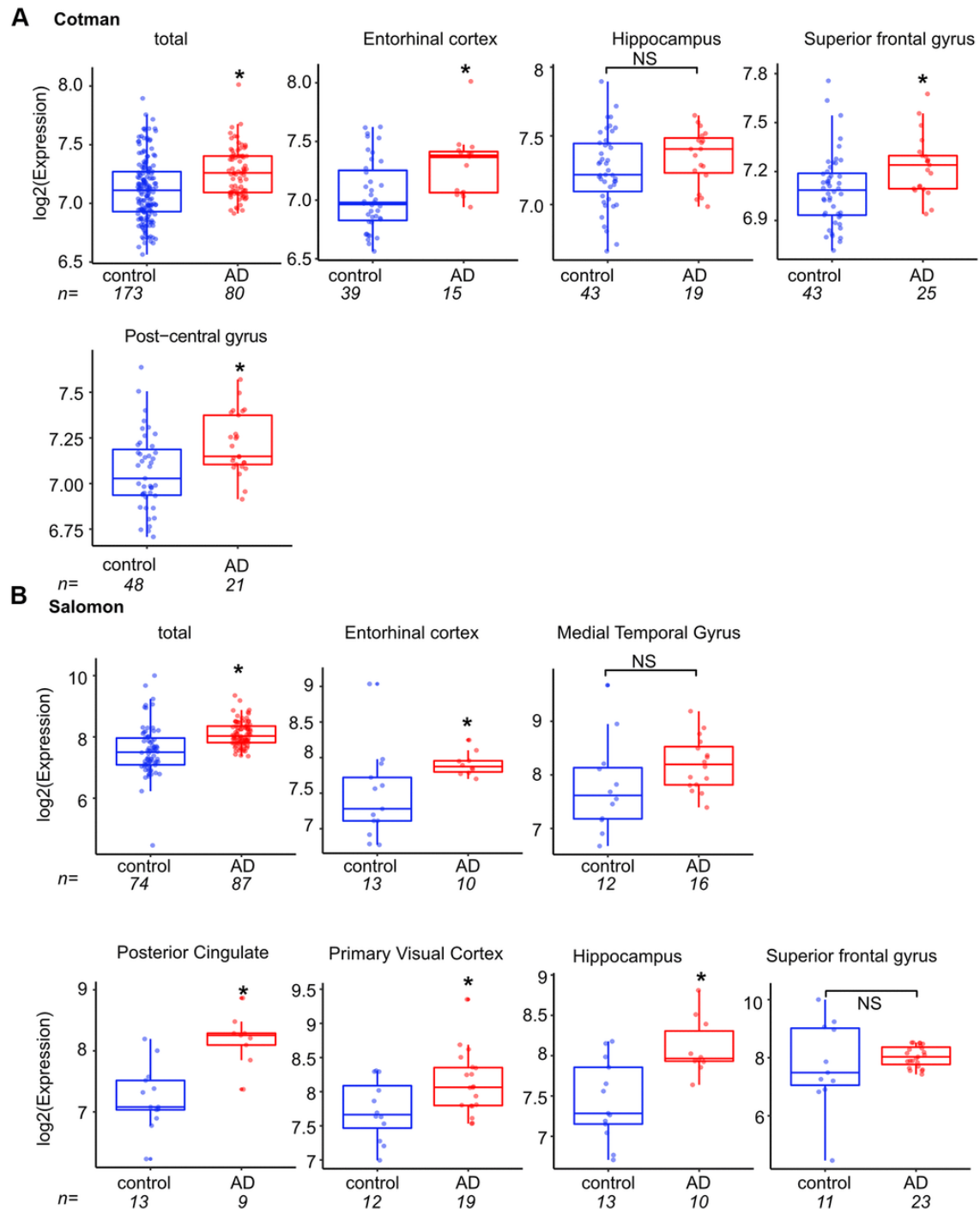


Figure 5-2: *TP73-AS1* is highly expressed in the pathological aging brain. (A) The levels of *TP73-AS1* in Alzheimer's (AD) vs. normal brain are shown. Data were obtained from R2 and the Cotman dataset (GSE48350). In both (A, B) panels, asterisks indicate statistically significant differences as calculated by the two-sample Wilcoxon test ( $*p < 0.05$ ; NS, non-significant). (B) The levels of *TP73-AS1* in Alzheimer's vs. normal brain are shown. Data were obtained from R2 and the Salomon dataset (GSE5281).

Interestingly, the TF YY1 and its gene targets are a prominent part of the pathological aging brain transcriptional program (Stein et al., 2021), therefore we asked whether YY1 could be a *TP73-AS1* TF as well. To investigate the interaction between YY1 and the promoter of *TP73-AS1*, we over-expressed YY1 and measured the 824-promoter activity using a luciferase activity assay. We found that *YY1* over-expression increased 824-promoter activity (\*p < 0.05 in the two-tailed t-test). To study the correlation of expression between *TP73-AS1* and *YY1* in normal aging we used GTEx data and found a positive correlation in the different brain regions (Supplementary Figure S-7B). In addition, the expression of *TP73-AS1* and *YY1* were correlated in both human pathological aging (AD) brain datasets (Supplementary Figure S-7C). Together, this data suggests that YY1 is an important *TP73-AS1* regulator.

### 5.3 Discussion

Aging contributes to glioma incidence and aggressiveness and interestingly, the expression pattern of *TP73-AS1* is associated with key features linked to aging and glioma aggressiveness. These include high expression of *TP73-AS1* in EGFR amplified and IDH-wild type tumors (Chatsirisupachai et al., 2021). These associations are in line with our findings that *TP73-AS1* expression correlates with aging and aggressiveness providing a possible molecular link explaining how aging contributes to GBM aggressiveness.

Aberrant YY1 function in the aging brain was recently reported and attributed to reduced expression of its binding partner, SIRT6. Reduced SIRT6 expression, occurring during aging, leads to changes in the expression of genes which are regulated by YY1, many of which are involved in pathological aging. It is therefore possible that *TP73-AS1* is a YY1 target in the aging brain.

In conclusion, we show that *TP73-AS1* levels increase in pathological and natural aging brain and that YY1 directly activates the *TP73-AS1* promoter to induce its expression. These findings provide a plausible explanation for how the expression of *TP73-AS1* is regulated, and an interesting molecular link between aging and GBM.

# Chapter 6

## Conclusion

SIRT6 is highly active in the mammalian brain tissues and protects brain health via several mechanisms, including enhanced DNA repair (Mao et al., 2011; Onn et al., 2020), retrotransposon silencing (Van Meter et al., 2014), telomere maintenance (Michishita et al., 2008) and glucose metabolism regulation (Sebastian et al., 2012). While the reduced activity of SIRT6 is a common signature of both normal and pathological brain aging programs, the interplay between SIRT6 and brain aging, as well as the molecular pathways involved in it, are far from being fully described.

In this thesis, we utilized brain SIRT6-deficient models to study its functions and implications in aging and neurodegeneration through the lens of mitochondrial deregulation. The main obtained results are the following:

- Using multi-omics analysis, we demonstrated that inactivation of SIRT6 results in global transcriptional and metabolic dysregulation in the mouse brain.
- We next showed that changes induced by SIRT6 deficiency in the mouse brain are primarily associated with mitochondrial functions, characterized by decreased expression of genes encoding ETC complexes, abundance alterations of TCA cycle key metabolites, as well as co-reduction of mitochondrial content and average mtDNA gene expression.
- To accomplish regulation of mitochondria-related genes, SIRT6 interacts with two other sirtuins, SIRT3 and SIRT4, that are localized in mitochondria and

were previously shown to promote oxidative phosphorylation, metabolism and mitochondrial translation via interaction networks (Yang et al., 2016).

- Another protein participating in the regulation of mitochondrial activity in a SIRT6-dependent manner is YY1. In addition to being involved in many age-related pathways, it also enhances levels of *TP73-AS1* lncRNA in the normal brain aging as well as in glioblastoma.

This work represents the first systematic study of the SIRT6 regulatory functions in the brain mitochondria. Our results are in good agreement with the previously reported findings on antioxidant and neuroprotective SIRT6 activities (Pan et al., 2016; Kaluski et al., 2017), but provide novel brain-specific mechanisms of its involvement. Our study also connects SIRT6 functions with a progression of a wide range of age-related diseases in the brain, including neurodegenerative diseases (Alzheimer's Disease, Parkinson's Disease, Huntington's Disease) and brain tumors, making it appealing for therapeutic applications.

Taken together, SIRT6 has critical roles in brain health, protecting it from oxidative stress and age-related diseases.

# Bibliography

- (2012). An integrated encyclopedia of dna elements in the human genome. *Nature*, 489(7414):57–74.
- Adibhatla, R. M., Hatcher, J. F., and Dempsey, R. J. (2006). Lipids and lipidomics in brain injury and diseases. *AAPS J.*, 8(2):E314–21.
- Agostini, M., Niklison-Chirou, M. V., Catani, M. V., Knight, R. A., Melino, G., and Rufini, A. (2014). Tap73 promotes anti-senescence-anabolism not proliferation. *Aging (Albany NY)*, 6(11):921–930.
- Agostini, M., Tucci, P., Killick, R., Candi, E., Sayan, B. S., Rivetti di Val Cervo, P., Nicotera, P., McKeon, F., Knight, R. A., Mak, T. W., and Melino, G. (2011). Neuronal differentiation by tap73 is mediated by microrna-34a regulation of synaptic protein targets. *Proc. Natl. Acad. Sci. U. S. A.*, 108(52):21093–21098.
- Aimo, L., Liechti, R., Hyka-Nouspikel, N., Niknejad, A., Gleizes, A., Götz, L., Kuznetsov, D., David, F. P. A., van der Goot, F. G., Riezman, H., Bougueleret, L., Xenarios, I., and Bridge, A. (2015). The swisslipids knowledgebase for lipid biology. *Bioinformatics*, 31(17):2860–2866.
- Albóniga, O. E., González, O., Alonso, R. M., Xu, Y., and Goodacre, R. (2020). Optimization of xcms parameters for lc-ms metabolomics: an assessment of automated versus manual tuning and its effect on the final results. *Metabolomics*, 16(1):14.
- Amelio, I. and Melino, G. (2018). Similar domains for different regulations of p53 family. *Structure*, 26(8):1047–1049.
- Amelio, I., Panatta, E., Niklison-Chirou, M. V., Steinert, J. R., Agostini, M., Morone, N., Knight, R. A., and Melino, G. (2020). The c terminus of p73 is essential for hippocampal development. *Proc. Natl. Acad. Sci. U. S. A.*, 117(27):15694–15701.
- Ansari, A., Rahman, M. S., Saha, S. K., Saikot, F. K., Deep, A., and Kim, K.-H. (2017). Function of the sirt3 mitochondrial deacetylase in cellular physiology, cancer, and neurodegenerative disease. *Aging Cell*, 16(1):4–16.
- Aubry, S., Shin, W., Crary, J. F., Lefort, R., Qureshi, Y. H., Lefebvre, C., Califano, A., and Shelanski, M. L. (2015). Assembly and interrogation of alzheimer’s disease genetic networks reveal novel regulators of progression. *PLoS One*, 10(3):e0120352.

- Barrett, T., Wilhite, S. E., Ledoux, P., Evangelista, C., Kim, I. F., Tomashevsky, M., Marshall, K. A., Phillippy, K. H., Sherman, P. M., Holko, M., Yefanov, A., Lee, H., Zhang, N., Robertson, C. L., Serova, N., Davis, S., and Soboleva, A. (2013). Ncbi geo: archive for functional genomics data sets—update. *Nucleic Acids Res.*, 41(Database issue):D991–5.
- Ben-Zion Berliner, M., Yerushalmi, R., Lavie, I., Benouaich-Amiel, A., Tsoref, D., Hendler, D., Goldvasser, H., Sarfaty, M., Rotem, O., Ulitsky, O., Siegal, T., Neiman, V., and Yust-Katz, S. (2021). Central nervous system metastases in breast cancer: the impact of age on patterns of development and outcome. *Breast Cancer Res. Treat.*, 185(2):423–432.
- Benton, H. P., Want, E. J., and Ebbels, T. M. D. (2010). Correction of mass calibration gaps in liquid chromatography-mass spectrometry metabolomics data. *Bioinformatics*, 26(19):2488–2489.
- Berchtold, N. C., Cribbs, D. H., Coleman, P. D., Rogers, J., Head, E., Kim, R., Beach, T., Miller, C., Troncoso, J., Trojanowski, J. Q., Zielke, H. R., and Cotman, C. W. (2008). Gene expression changes in the course of normal brain aging are sexually dimorphic. *Proc. Natl. Acad. Sci. U. S. A.*, 105(40):15605–15610.
- Bester, A. C., Lee, J. D., Chavez, A., Lee, Y.-R., Nachmani, D., Vora, S., Victor, J., Sauvageau, M., Monteleone, E., Rinn, J. L., Provero, P., Church, G. M., Clohessy, J. G., and Pandolfi, P. P. (2018). An integrated genome-wide crispra approach to functionalize lncrnas in drug resistance. *Cell*, 173(3):649–664.e20.
- Blighe, K. (2018). Enhancedvolcano. DOI: 10.18129/B9.BIOC.ENHANCEDVOLCANO.
- Blinkouskaya, Y., Caçoilo, A., Gollamudi, T., Jalalian, S., and Weickenmeier, J. (2021). Brain aging mechanisms with mechanical manifestations. *Mech. Ageing Dev.*, 200(111575):111575.
- Bolstad, B. M., Irizarry, R. A., Astrand, M., and Speed, T. P. (2003). A comparison of normalization methods for high density oligonucleotide array data based on variance and bias. *Bioinformatics*, 19(2):185–193.
- Boxer, L. D., Renthal, W., Greben, A. W., Whitwam, T., Silberfeld, A., Stroud, H., Li, E., Yang, M. G., Kinde, B., Griffith, E. C., Bonev, B., and Greenberg, M. E. (2020). Mecp2 represses the rate of transcriptional initiation of highly methylated long genes. *Molecular Cell*, 77(2):294–309.e9.
- Bozek, K., Wei, Y., Yan, Z., Liu, X., Xiong, J., Sugimoto, M., Tomita, M., Pääbo, S., Sherwood, C. C., Hof, P. R., Ely, J. J., Li, Y., Steinhauser, D., Willmitzer, L., Giavalisco, P., and Khaitovich, P. (2015). Organization and evolution of brain lipidome revealed by large-scale analysis of human, chimpanzee, macaque, and mouse tissues. *Neuron*, 85(4):695–702.

- Braidy, N., Poljak, A., Grant, R., Jayasena, T., Mansour, H., Chan-Ling, T., Smythe, G., Sachdev, P., and Guillemin, G. J. (2015). Differential expression of sirtuins in the aging rat brain. *Frontiers in Cellular Neuroscience*, 9.
- Brereton, R. G. and Lloyd, G. R. (2014). Partial least squares discriminant analysis: taking the magic away: Pls-da: taking the magic away. *J. Chemom.*, 28(4):213–225.
- Camacho-Pereira, J., Tarragó, M. G., Chini, C. C. S., Nin, V., Escande, C., Warner, G. M., Puranik, A. S., Schoon, R. A., Reid, J. M., Galina, A., and Chini, E. N. (2016). Cd38 dictates age-related nad decline and mitochondrial dysfunction through an sirt3-dependent mechanism. *Cell Metab.*, 23(6):1127–1139.
- Cantó, C. and Auwerx, J. (2009). Pgc-1alpha, sirt1 and ampk, an energy sensing network that controls energy expenditure. *Curr. Opin. Lipidol.*, 20(2):98–105.
- Carithers, L. J., Ardlie, K., Barcus, M., Branton, P. A., Britton, A., Buia, S. A., Compton, C. C., DeLuca, D. S., Peter-Demchok, J., Gelfand, E. T., Guan, P., Korzeniewski, G. E., Lockhart, N. C., Rabiner, C. A., Rao, A. K., Robinson, K. L., Roche, N. V., Sawyer, S. J., Segrè, A. V., Shive, C. E., Smith, A. M., Sobin, L. H., Undale, A. H., Valentino, K. M., Vaught, J., Young, T. R., Moore, H. M., and on behalf of the GTEx Consortium (2015). A novel approach to high-quality postmortem tissue procurement: The gtex project. *Biopreserv. Biobank.*, 13(5):311–319.
- Cha, Y., Kim, T., Jeon, J., Jang, Y., Kim, P. B., Lopes, C., Leblanc, P., Cohen, B. M., and Kim, K.-S. (2021). Sirt2 regulates mitochondrial dynamics and reprogramming via mek1-erk-drp1 and akt1-drp1 axes. *Cell Reports*, 37(13):110155.
- Chabi, B., Ljubcic, V., Menzies, K. J., Huang, J. H., Saleem, A., and Hood, D. A. (2008). Mitochondrial function and apoptotic susceptibility in aging skeletal muscle. *Aging Cell*, 7(1):2–12.
- Chaichana, K. L., Chaichana, K. K., Olivi, A., Weingart, J. D., Bennett, R., Brem, H., and Quiñones-Hinojosa, A. (2011). Surgical outcomes for older patients with glioblastoma multiforme: preoperative factors associated with decreased survival. clinical article: Clinical article. *J. Neurosurg.*, 114(3):587–594.
- Chakrabarti, S., Munshi, S., Banerjee, K., Thakurta, I. G., Sinha, M., and Bagh, M. B. (2011). Mitochondrial dysfunction during brain aging: Role of oxidative stress and modulation by antioxidant supplementation. *Aging Dis.*, 2(3):242–256.
- Chakraborty, M., Hu, S., Visness, E., Del Giudice, M., De Martino, A., Bosia, C., Sharp, P. A., and Garg, S. (2020). Micrnas organize intrinsic variation into stem cell states. *Proceedings of the National Academy of Sciences*, 117(12):6942–6950.
- Chambers, M. C., Maclean, B., Burke, R., Amodei, D., Ruderman, D. L., Neumann, S., Gatto, L., Fischer, B., Pratt, B., Egertson, J., Hoff, K., Kessner, D., Tasman, N., Shulman, N., Frewen, B., Baker, T. A., Brusniak, M.-Y., Paulse, C., Creasy,

- D., Flashner, L., Kani, K., Moulding, C., Seymour, S. L., Nuwaysir, L. M., Lefebvre, B., Kuhlmann, F., Roark, J., Rainer, P., Detlev, S., Hemenway, T., Huhmer, A., Langridge, J., Connolly, B., Chadick, T., Holly, K., Eckels, J., Deutsch, E. W., Moritz, R. L., Katz, J. E., Agus, D. B., MacCoss, M., Tabb, D. L., and Mallick, P. (2012). A cross-platform toolkit for mass spectrometry and proteomics. *Nat. Biotechnol.*, 30(10):918–920.
- Chang, A. R., Ferrer, C. M., and Mostoslavsky, R. (2020). Sirt6, a mammalian deacylase with multitasking abilities. *Physiological Reviews*, 100(1):145–169.
- Chatsirisupachai, K., Lesluyes, T., Paraoan, L., Van Loo, P., and de Magalhães, J. P. (2021). An integrative analysis of the age-associated multi-omic landscape across cancers. *Nat. Commun.*, 12(1):2345.
- Chatterjee, D., Das, P., and Chakrabarti, O. (2022). Mitochondrial epigenetics regulating inflammation in cancer and aging. *Front. Cell Dev. Biol.*, 10:929708.
- Chen, S., Zhou, Y., Chen, Y., and Gu, J. (2018a). fastp: an ultra-fast all-in-one fastq preprocessor. *Bioinformatics*, 34(17):i884–i890.
- Chen, X., Li, D., Gao, Y., Cao, Y., and Hao, B. (2018b). Histone deacetylase sirt6 inhibits glioma cell growth through down-regulating notch3 expression. *Acta Biochimica et Biophysica Sinica*, 50(4):417–424.
- Cheng, M.-Y., Cheng, Y.-W., Yan, J., Hu, X.-Q., Zhang, H., Wang, Z.-R., Yin, Q., and Cheng, W. (2016). Sirt6 suppresses mitochondrial defects and cell death via the nf-b pathway in myocardial hypoxia/reoxygenation induced injury. *Am. J. Transl. Res.*, 8(11):5005–5015.
- Chou, D. M., Adamson, B., Dephoure, N. E., Tan, X., Nottke, A. C., Hurov, K. E., Gygi, S. P., Colaiácovo, M. P., and Elledge, S. J. (2010). A chromatin localization screen reveals poly (adp ribose)-regulated recruitment of the repressive polycomb and nurd complexes to sites of dna damage. *Proc. Natl. Acad. Sci. U. S. A.*, 107(43):18475–18480.
- Colsch, B., Afonso, C., Turpin, J.-C., Portoukalian, J., Tabet, J.-C., and Baumann, N. (2008). Sulfogalactosylceramides in motor and psycho-cognitive adult metachromatic leukodystrophy: relations between clinical, biochemical analysis and molecular aspects. *Biochim. Biophys. Acta*, 1780(3):434–440.
- Cunningham, J. T., Rodgers, J. T., Arlow, D. H., Vazquez, F., Mootha, V. K., and Puigserver, P. (2007). mtor controls mitochondrial oxidative function through a yy1-pgc-1alpha transcriptional complex. *Nature*, 450(7170):736–740.
- Dai, S.-H., Chen, T., Wang, Y.-H., Zhu, J., Luo, P., Rao, W., Yang, Y.-F., Fei, Z., and Jiang, X.-F. (2014). Sirt3 protects cortical neurons against oxidative stress via regulating mitochondrial ca<sup>2+</sup> and mitochondrial biogenesis. *Int. J. Mol. Sci.*, 15(8):14591–14609.

- de Magalhães, J. P. (2013). How ageing processes influence cancer. *Nat. Rev. Cancer*, 13(5):357–365.
- Dimache, A. M., Şalaru, D. L., Sascău, R., and Stătescu, C. (2021). The role of high triglycerides level in predicting cognitive impairment: A review of current evidence. *Nutrients*, 13(6):2118.
- Dobin, A., Davis, C. A., Schlesinger, F., Drenkow, J., Zaleski, C., Jha, S., Batut, P., Chaisson, M., and Gingeras, T. R. (2013). Star: ultrafast universal rna-seq aligner. *Bioinformatics*, 29(1):15–21.
- Dominy, J. E., Lee, Y., Jedrychowski, M. P., Chim, H., Jurczak, M. J., Camporez, J. P., Ruan, H.-B., Feldman, J., Pierce, K., Mostoslavsky, R., Denu, J. M., Clish, C. B., Yang, X., Shulman, G. I., Gygi, S. P., and Puigserver, P. (2012). The deacetylase sirt6 activates the acetyltransferase gcn5 and suppresses hepatic gluconeogenesis. *Molecular Cell*, 48(6):900–913.
- Dong, Z., Zhong, X., Lei, Q., Chen, F., and Cui, H. (2019). Transcriptional activation of sirt6 via fkhrl1/foxo3a inhibits the warburg effect in glioblastoma cells. *Cellular Signalling*, 60:100–113.
- Du, W., Jiang, P., Mancuso, A., Stonestrom, A., Brewer, M. D., Minn, A. J., Mak, T. W., Wu, M., and Yang, X. (2013). Tap73 enhances the pentose phosphate pathway and supports cell proliferation. *Nat. Cell Biol.*, 15(8):991–1000.
- Elhanati, S., Kanfi, Y., Varvak, A., Roichman, A., Carmel-Gross, I., Barth, S., Gibor, G., and Cohen, H. Y. (2013). Multiple regulatory layers of srebp1/2 by sirt6. *Cell Rep.*, 4(5):905–912.
- Etchegaray, J.-P., Chavez, L., Huang, Y., Ross, K. N., Choi, J., Martinez-Pastor, B., Walsh, R. M., Sommer, C. A., Lienhard, M., Gladden, A., Kugel, S., Silberman, D. M., Ramaswamy, S., Mostoslavsky, G., Hochedlinger, K., Goren, A., Rao, A., and Mostoslavsky, R. (2015). The histone deacetylase sirt6 controls embryonic stem cell fate via tet-mediated production of 5-hydroxymethylcytosine. *Nature Cell Biology*, 17(5):545–557.
- Ewels, P., Peltzer, A., Fillinger, S., Patel, H., Alneberg, J., Wilm, A., Ulysse Garcia, M., Di Tommaso, P., and Nahnsen, S. (2022). The nf-core framework for community-curated bioinformatics pipelines. DOI: 10.5281/ZENODO.1400710.
- Fahy, E., Alvarez-Jarreta, J., Brasher, C. J., Nguyen, A., Hawksworth, J. I., Rodrigues, P., Meckelmann, S., Allen, S. M., and O’Donnell, V. B. (2019). Lipidfinder on lipid maps: peak filtering, ms searching and statistical analysis for lipidomics. *Bioinformatics*, 35(4):685–687.
- Fanibunda, S. E., Deb, S., Maniyadath, B., Tiwari, P., Ghai, U., Gupta, S., Figueiredo, D., Weisstaub, N., Gingrich, J. A., Vaidya, A. D. B., Kolthur-Seetharam, U., and Vaidya, V. A. (2019). Serotonin regulates mitochondrial biogenesis and function in rodent cortical neurons via the 5-ht2a receptor and sirt1-pgc-1 axis. *Proc. Natl. Acad. Sci. U. S. A.*, 116(22):11028–11037.

- Feng, J., Yan, P.-F., Zhao, H.-Y., Zhang, F.-C., Zhao, W.-H., and Feng, M. (2015). Sirt6 suppresses glioma cell growth via induction of apoptosis, inhibition of oxidative stress and suppression of jak2/stat3 signaling pathway activation. *Oncology Reports*, 35(3):1395–1402.
- Flores, E. R., Sengupta, S., Miller, J. B., Newman, J. J., Bronson, R., Crowley, D., Yang, A., McKeon, F., and Jacks, T. (2005). Tumor predisposition in mice mutant for p63 and p73: evidence for broader tumor suppressor functions for the p53 family. *Cancer Cell*, 7(4):363–373.
- Gel, B. and Serra, E. (2017). karyoploter: an r/bioconductor package to plot customizable genomes displaying arbitrary data. *Bioinformatics*, 33(19):3088–3090.
- Gromski, P. S., Muhamadali, H., Ellis, D. I., Xu, Y., Correa, E., Turner, M. L., and Goodacre, R. (2015). A tutorial review: Metabolomics and partial least squares-discriminant analysis—a marriage of convenience or a shotgun wedding. *Anal. Chim. Acta*, 879:10–23.
- Gromski, P. S., Xu, Y., Correa, E., Ellis, D. I., Turner, M. L., and Goodacre, R. (2014). A comparative investigation of modern feature selection and classification approaches for the analysis of mass spectrometry data. *Anal. Chim. Acta*, 829:1–8.
- Gu, Z., Eils, R., and Schlesner, M. (2016). Complex heatmaps reveal patterns and correlations in multidimensional genomic data. *Bioinformatics*, 32(18):2847–2849.
- Han, X., M Holtzman, D., McKeel, Jr, D. W., Kelley, J., and Morris, J. C. (2002). Substantial sulfatide deficiency and ceramide elevation in very early alzheimer’s disease: potential role in disease pathogenesis: Sulfatide deficiency and ceramide elevation in ad. *J. Neurochem.*, 82(4):809–818.
- Harman, D. (1956). Aging: a theory based on free radical and radiation chemistry. *J. Gerontol.*, 11(3):298–300.
- Harshfield, E. L., Koulman, A., Ziemek, D., Marney, L., Fauman, E. B., Paul, D. S., Stacey, D., Rasheed, A., Lee, J.-J., Shah, N., Jabeen, S., Imran, A., Abbas, S., Hina, Z., Qamar, N., Mallick, N. H., Yaqoob, Z., Saghir, T., Rizvi, S. N. H., Memon, A., Rasheed, S. Z., Memon, F.-U.-R., Qureshi, I. H., Ishaq, M., Frossard, P., Danesh, J., Saleheen, D., Butterworth, A. S., Wood, A. M., and Griffin, J. L. (2019). An unbiased lipid phenotyping approach to study the genetic determinants of lipids and their association with coronary heart disease risk factors. *J. Proteome Res.*, 18(6):2397–2410.
- Hebert, A. S., Dittenhafer-Reed, K. E., Yu, W., Bailey, D. J., Selen, E. S., Boersma, M. D., Carson, J. J., Tonelli, M., Balloon, A. J., Higbee, A. J., Westphall, M. S., Pagliarini, D. J., Prolla, T. A., Assadi-Porter, F., Roy, S., Denu, J. M., and Coon, J. J. (2013). Calorie restriction and sirt3 trigger global reprogramming of the mitochondrial protein acetylome. *Molecular Cell*, 49(1):186–199.
- Hernandez-Segura, A., Nehme, J., and Demaria, M. (2018). Hallmarks of cellular senescence. *Trends Cell Biol.*, 28(6):436–453.

- Hervé Pagès, Seth Falcon, N. L. M. C. (2017). Annotationdbi. DOI: 10.18129/B9.BIOC.ANNOTATIONDBI.
- Imai, S.-i. and Guarente, L. (2014). Nad<sup>+</sup> and sirtuins in aging and disease. *Trends in Cell Biology*, 24(8):464–471.
- Jassal, B., Matthews, L., Viteri, G., Gong, C., Lorente, P., Fabregat, A., Sidiropoulos, K., Cook, J., Gillespie, M., Haw, R., Loney, F., May, B., Milacic, M., Rothfels, K., Sevilla, C., Shamovsky, V., Shorsler, S., Varusai, T., Weiser, J., Wu, G., Stein, L., Hermjakob, H., and D’Eustachio, P. (2020). The reactome pathway knowledgebase. *Nucleic Acids Res.*, 48(D1):D498–D503.
- Jia, B., Liu, W., Gu, J., Wang, J., Lv, W., Zhang, W., Hao, Q., Pang, Z., Mu, N., Zhang, W., and Guo, Q. (2019). Mir-7-5p suppresses stemness and enhances temozolomide sensitivity of drug-resistant glioblastoma cells by targeting yin yang 1. *Exp. Cell Res.*, 375(1):73–81.
- Jiang, H., Khan, S., Wang, Y., Charron, G., He, B., Sebastian, C., Du, J., Kim, R., Ge, E., Mostoslavsky, R., Hang, H. C., Hao, Q., and Lin, H. (2013). Sirt6 regulates tnf- secretion through hydrolysis of long-chain fatty acyl lysine. *Nature*, 496(7443):110–113.
- Jolliffe, I. T. (2002). *Principal Component Analysis*. Springer, New York, NY, 2 edition. DOI: 10.1007/b98835.
- Jung, E. S., Choi, H., Song, H., Hwang, Y. J., Kim, A., Ryu, H., and Mook-Jung, I. (2016). p53-dependent sirt6 expression protects a42-induced dna damage. *Sci. Rep.*, 6(1).
- Kaluski, S., Portillo, M., Besnard, A., Stein, D., Einav, M., Zhong, L., Ueberham, U., Arendt, T., Mostoslavsky, R., Sahay, A., and Toiber, D. (2017). Neuroprotective functions for the histone deacetylase sirt6. *Cell Reports*, 18(13):3052–3062.
- Kanehisa, M. (2019). Toward understanding the origin and evolution of cellular organisms. *Protein Sci.*, 28(11):1947–1951.
- Kanehisa, M. and Goto, S. (2000). Kegg: kyoto encyclopedia of genes and genomes. *Nucleic Acids Res.*, 28(1):27–30.
- Kawamura, K., Higuchi, T., and Fujiwara, S. (2021). Yaf2-mediated yy1-sirtuin6 interactions responsible for mitochondrial downregulation in aging tunicates. *Mol. Cell. Biol.*, 41(7):e0004721.
- Kessner, D., Chambers, M., Burke, R., Agus, D., and Mallick, P. (2008). Proteowizard: open source software for rapid proteomics tools development. *Bioinformatics*, 24(21):2534–2536.
- Khan, R. I., Nirzhor, S. S. R., and Akter, R. (2018). A review of the recent advances made with sirt6 and its implications on aging related processes, major human diseases, and possible therapeutic targets. *Biomolecules*, 8(3):44.

- Kim, H.-S., Xiao, C., Wang, R.-H., Lahusen, T., Xu, X., Vassilopoulos, A., Vazquez-Ortiz, G., Jeong, W.-I., Park, O., Ki, S. H., Gao, B., and Deng, C.-X. (2010). Hepatic-specific disruption of sirt6 in mice results in fatty liver formation due to enhanced glycolysis and triglyceride synthesis. *Cell Metab.*, 12(3):224–236.
- Kincaid, B. and Bossy-Wetzel, E. (2013). Forever young: Sirt3 a shield against mitochondrial meltdown, aging, and neurodegeneration. *Front. Aging Neurosci.*, 5.
- Kjeldahl, K. and Bro, R. (2010). Some common misunderstandings in chemometrics. *J. Chemom.*, 24(7-8):558–564.
- Klar, A. J. S., Fogel, S., and Macleod, K. (1979). Mar1—a regulator of the hm a and hm loci in *saccharomyces cerevisiae*. *Genetics*, 93(1):37–50.
- Korotkov, A., Seluanov, A., and Gorbunova, V. (2021). Sirtuin 6: linking longevity with genome and epigenome stability. *Trends Cell Biol.*, 31(12):994–1006.
- Ladomersky, E., Scholtens, D. M., Kocherginsky, M., Hibler, E. A., Bartom, E. T., Otto-Meyer, S., Zhai, L., Lauing, K. L., Choi, J., Sosman, J. A., Wu, J. D., Zhang, B., Lukas, R. V., and Wainwright, D. A. (2019). The coincidence between increasing age, immunosuppression, and the incidence of patients with glioblastoma. *Front. Pharmacol.*, 10:200.
- Ladomersky, E., Zhai, L., Gritsina, G., Genet, M., Lauing, K. L., Wu, M., James, C. D., and Wainwright, D. A. (2016). Advanced age negatively impacts survival in an experimental brain tumor model. *Neurosci. Lett.*, 630:203–208.
- Lapidot-Cohen, T., Rosental, L., and Brotman, Y. (2020). Liquid chromatography–mass spectrometry (lc-ms)-based analysis for lipophilic compound profiling in plants. *Current Protocols in Plant Biology*, 5(2).
- Laurent, G., German, N. J., Saha, A. K., de Boer, V. C. J., Davies, M., Koves, T. R., Dephoure, N., Fischer, F., Boanca, G., Vaitheesvaran, B., Lovitch, S. B., Sharpe, A. H., Kurland, I. J., Steegborn, C., Gygi, S. P., Muoio, D. M., Ruderman, N. B., and Haigis, M. C. (2013). Sirt4 coordinates the balance between lipid synthesis and catabolism by repressing malonyl coa decarboxylase. *Mol. Cell*, 50(5):686–698.
- Lee, O.-H., Kim, J., Kim, J.-M., Lee, H., Kim, E. H., Bae, S.-K., Choi, Y., Nam, H. S., and Heo, J. H. (2013). Decreased expression of sirtuin 6 is associated with release of high mobility group box-1 after cerebral ischemia. *Biochemical and Biophysical Research Communications*, 438(2):388–394.
- Lee, S.-H., Hong, S.-H., Tang, C.-H., Ling, Y. S., Chen, K.-H., Liang, H.-J., and Lin, C.-Y. (2018). Mass spectrometry-based lipidomics to explore the biochemical effects of naphthalene toxicity or tolerance in a mouse model. *PLoS One*, 13(10):e0204829.

- Lee, S. Y. (2016). Temozolomide resistance in glioblastoma multiforme. *Genes Dis.*, 3(3):198–210.
- Li, X., Liu, L., Li, T., Liu, M., Wang, Y., Ma, H., Mu, N., and Wang, H. (2021). Sirt6 in senescence and aging-related cardiovascular diseases. *Front. Cell Dev. Biol.*, 9:641315.
- Liang, W. S., Dunkley, T., Beach, T. G., Grover, A., Mastroeni, D., Walker, D. G., Caselli, R. J., Kukull, W. A., McKeel, D., Morris, J. C., Hulette, C., Schmechel, D., Alexander, G. E., Reiman, E. M., Rogers, J., and Stephan, D. A. (2007). Gene expression profiles in anatomically and functionally distinct regions of the normal aged human brain. *Physiol. Genomics*, 28(3):311–322.
- Libiseller, G., Dvorzak, M., Kleb, U., Gander, E., Eisenberg, T., Madeo, F., Neumann, S., Trausinger, G., Sinner, F., Pieber, T., and Magnes, C. (2015). Ipo: a tool for automated optimization of xcms parameters. *BMC Bioinformatics*, 16(1):118.
- Liebisch, G., Vizcaíno, J. A., Köfeler, H., Trötz Müller, M., Griffiths, W. J., Schmitz, G., Spener, F., and Wakelam, M. J. O. (2013). Shorthand notation for lipid structures derived from mass spectrometry. *J. Lipid Res.*, 54(6):1523–1530.
- Lin, W.-J., Shen, P.-C., Liu, H.-C., Cho, Y.-C., Hsu, M.-K., Lin, I.-C., Chen, F.-H., Yang, J.-C., Ma, W.-L., and Cheng, W.-C. (2021). Lipidsig: a web-based tool for lipidomic data analysis. *Nucleic Acids Research*, 49(W1):W336–W345.
- Liszczak, G., Diehl, K. L., Dann, G. P., and Muir, T. W. (2018). Acetylation blocks dna damage-induced chromatin adp-ribosylation. *Nat. Chem. Biol.*, 14(9):837–840.
- Liu, W., Guo, Q., and Zhao, H. (2018). Oxidative stress-elicited yy1 potentiates antioxidative response via enhancement of nrf2-driven transcriptional activity: A potential neuronal defensive mechanism against ischemia/reperfusion cerebral injury. *Biomed. Pharmacother.*, 108:698–706.
- Lomb, D. J., Laurent, G., and Haigis, M. C. (2010). Sirtuins regulate key aspects of lipid metabolism. *Biochim. Biophys. Acta*, 1804(8):1652–1657.
- Lopriore, P., Capitanio, N., Panatta, E., Di Daniele, N., Gambacurta, A., Melino, G., and Amelio, I. (2018). Tap73 regulates atp7a: possible implications for ageing-related diseases. *Aging (Albany NY)*, 10(12):3745–3760.
- Love, M. I., Huber, W., and Anders, S. (2014). Moderated estimation of fold change and dispersion for rna-seq data with deseq2. *Genome Biol.*, 15(12):550.
- Luo, Y.-X., Tang, X., An, X.-Z., Xie, X.-M., Chen, X.-F., Zhao, X., Hao, D.-L., Chen, H.-Z., and Liu, D.-P. (2016). Sirt4 accelerates ang ii-induced pathological cardiac hypertrophy by inhibiting manganese superoxide dismutase activity. *Eur. Heart J.*, page ehw138.

- Lê Cao, K.-A., Boitard, S., and Besse, P. (2011). Sparse pls discriminant analysis: biologically relevant feature selection and graphical displays for multiclass problems. *BMC Bioinformatics*, 12(1):253.
- López-Otín, C., Blasco, M. A., Partridge, L., Serrano, M., and Kroemer, G. (2013). The hallmarks of aging. *Cell*, 153(6):1194–1217.
- Mao, Z., Hine, C., Tian, X., Van Meter, M., Au, M., Vaidya, A., Seluanov, A., and Gorbunova, V. (2011). Sirt6 promotes dna repair under stress by activating parp1. *Science*, 332(6036):1443–1446.
- Marine, J.-C., Dawson, S.-J., and Dawson, M. A. (2020). Non-genetic mechanisms of therapeutic resistance in cancer. *Nat. Rev. Cancer*, 20(12):743–756.
- Marini, A., Rotblat, B., Sbarrato, T., Niklison-Chirou, M. V., Knight, J. R. P., Dudek, K., Jones, C., Bushell, M., Knight, R. A., Amelio, I., Willis, A. E., and Melino, G. (2018). Tap73 contributes to the oxidative stress response by regulating protein synthesis. *Proc. Natl. Acad. Sci. U. S. A.*, 115(24):6219–6224.
- Mariottini, C., Scartabelli, T., Bongers, G., Arrigucci, S., Nosi, D., Leurs, R., Chiarugi, A., Blandina, P., Pellegrini-Giampietro, D. E., and Passani, M. B. (2009). Activation of the histaminergic h3 receptor induces phosphorylation of the akt/gsk-3 beta pathway in cultured cortical neurons and protects against neurotoxic insults. *J. Neurochem.*, 110(5):1469–1478.
- Mattson, M. P. and Arumugam, T. V. (2018). Hallmarks of brain aging: Adaptive and pathological modification by metabolic states. *Cell Metab.*, 27(6):1176–1199.
- Mazor, G., Levin, L., Picard, D., Ahmadov, U., Carén, H., Borkhardt, A., Reifemberger, G., Leprivier, G., Remke, M., and Rotblat, B. (2019). The lncrna tp73-as1 is linked to aggressiveness in glioblastoma and promotes temozolomide resistance in glioblastoma cancer stem cells. *Cell Death Dis.*, 10(3):246.
- Mecocci, P., MacGarvey, U., Kaufman, A. E., Koontz, D., Shoffner, J. M., Wallace, D. C., and Beal, M. F. (1993). Oxidative damage to mitochondrial dna shows marked age-dependent increases in human brain. *Ann. Neurol.*, 34(4):609–616.
- Michishita, E., McCord, R. A., Berber, E., Kioi, M., Padilla-Nash, H., Damian, M., Cheung, P., Kusumoto, R., Kawahara, T. L. A., Barrett, J. C., Chang, H. Y., Bohr, V. A., Ried, T., Gozani, O., and Chua, K. F. (2008). Sirt6 is a histone h3 lysine 9 deacetylase that modulates telomeric chromatin. *Nature*, 452(7186):492–496.
- Min, Z., Gao, J., and Yu, Y. (2018). The roles of mitochondrial sirt4 in cellular metabolism. *Front. Endocrinol. (Lausanne)*, 9:783.
- Mohamed, A., Molendijk, J., and Hill, M. M. (2020). lipidr: A software tool for data mining and analysis of lipidomics datasets. *Journal of Proteome Research*, 19(7):2890–2897.

- Mostoslavsky, R., Chua, K. F., Lombard, D. B., Pang, W. W., Fischer, M. R., Gellon, L., Liu, P., Mostoslavsky, G., Franco, S., Murphy, M. M., Mills, K. D., Patel, P., Hsu, J. T., Hong, A. L., Ford, E., Cheng, H.-L., Kennedy, C., Nunez, N., Bronson, R., Frendewey, D., Auerbach, W., Valenzuela, D., Karow, M., Hottiger, M. O., Hursting, S., Barrett, J. C., Guarente, L., Mulligan, R., Demple, B., Yancopoulos, G. D., and Alt, F. W. (2006). Genomic instability and aging-like phenotype in the absence of mammalian sirt6. *Cell*, 124(2):315–329.
- Motori, E., Atanassov, I., Kochan, S. M. V., Folz-Donahue, K., Sakthivelu, V., Givalisco, P., Toni, N., Puyal, J., and Larsson, N.-G. (2020). Neuronal metabolic rewiring promotes resilience to neurodegeneration caused by mitochondrial dysfunction. *Sci. Adv.*, 6(35):eaba8271.
- Mouchiroud, L., Houtkooper, R. H., Moullan, N., Katsyuba, E., Ryu, D., Cantó, C., Mottis, A., Jo, Y.-S., Viswanathan, M., Schoonjans, K., Guarente, L., and Auwerx, J. (2013). The nad<sup>+</sup>/sirtuin pathway modulates longevity through activation of mitochondrial upr and foxo signaling. *Cell*, 154(2):430–441.
- Naiman, S., Huynh, F. K., Gil, R., Glick, Y., Shahar, Y., Touitou, N., Nahum, L., Avivi, M. Y., Roichman, A., Kanfi, Y., Gertler, A. A., Doniger, T., Ilkayeva, O. R., Abramovich, I., Yaron, O., Lerrer, B., Gottlieb, E., Harris, R. A., Gerber, D., Hirschev, M. D., and Cohen, H. Y. (2019). Sirt6 promotes hepatic beta-oxidation via activation of ppar. *Cell Reports*, 29(12):4127–4143.e8.
- Oberdoerffer, P., Michan, S., McVay, M., Mostoslavsky, R., Vann, J., Park, S.-K., Hartlerode, A., Stegmuller, J., Hafner, A., Loerch, P., Wright, S. M., Mills, K. D., Bonni, A., Yankner, B. A., Scully, R., Prolla, T. A., Alt, F. W., and Sinclair, D. A. (2008). Sirt1 redistribution on chromatin promotes genomic stability but alters gene expression during aging. *Cell*, 135(5):907–918.
- Oki, S., Ohta, T., Shioi, G., Hatanaka, H., Ogasawara, O., Okuda, Y., Kawaji, H., Nakaki, R., Sese, J., and Meno, C. (2018). Chip-atlas: a data-mining suite powered by full integration of public chip-seq data. *EMBO Rep.*, 19(12):e46255.
- Onn, L., Portillo, M., Ilic, S., Cleitman, G., Stein, D., Kaluski, S., Shirat, I., Slobodnik, Z., Einav, M., Erdel, F., Akabayov, B., and Toiber, D. (2020). Sirt6 is a dna double-strand break sensor. *Elife*, 9.
- Pal, R., Tiwari, P. C., Nath, R., and Pant, K. K. (2016). Role of neuroinflammation and latent transcription factors in pathogenesis of parkinson’s disease. *Neurol. Res.*, 38(12):1111–1122.
- Pan, H., Guan, D., Liu, X., Li, J., Wang, L., Wu, J., Zhou, J., Zhang, W., Ren, R., Zhang, W., Li, Y., Yang, J., Hao, Y., Yuan, T., Yuan, G., Wang, H., Ju, Z., Mao, Z., Li, J., Qu, J., Tang, F., and Liu, G.-H. (2016). SIRT6 safeguards human mesenchymal stem cells from oxidative stress by coactivating NRF2. *Cell Research*, 26(2):190–205.

- Pang, J. C.-S., Li, K. K.-W., Lau, K.-M., Ng, Y. L., Wong, J., Chung, N. Y.-F., Li, H.-M., Chui, Y.-L., Lui, V. W. Y., Chen, Z.-P., Chan, D. T.-M., Poon, W. S., Wang, Y., Mao, Y., Zhou, L., and Ng, H.-K. (2010). Kiaa0495/pdam is frequently downregulated in oligodendroglial tumors and its knockdown by sirna induces cisplatin resistance in glioma cells: Pdam downregulation in oligodendroglial tumors. *Brain Pathol.*, 20(6):1021–1032.
- Pang, Z., Chong, J., Zhou, G., de Lima Morais, D. A., Chang, L., Barrette, M., Gauthier, C., Jacques, P.-, Li, S., and Xia, J. (2021). Metaboanalyst 5.0: narrowing the gap between raw spectra and functional insights. *Nucleic Acids Res.*, 49(W1):W388–W396.
- Park, C. B. and Larsson, N.-G. (2011). Mitochondrial dna mutations in disease and aging. *J. Cell Biol.*, 193(5):809–818.
- Patil, I. (2021). Visualizations with statistical details: The 'ggstatsplot' approach. *J. Open Source Softw.*, 6(61):3167.
- Patro, R., Duggal, G., Love, M. I., Irizarry, R. A., and Kingsford, C. (2017). Salmon provides fast and bias-aware quantification of transcript expression. *Nat. Methods*, 14(4):417–419.
- Patti, G. J., Tautenhahn, R., and Siuzdak, G. (2012). Meta-analysis of untargeted metabolomic data from multiple profiling experiments. *Nat. Protoc.*, 7(3):508–516.
- Peters, R. (2006). Ageing and the brain. *Postgrad. Med. J.*, 82(964):84–88.
- Pillai, V. B., Samant, S., Hund, S., Gupta, M., and Gupta, M. P. (2021). The nuclear sirtuin sirt6 protects the heart from developing aging-associated myocyte senescence and cardiac hypertrophy. *Aging (Albany NY)*, 13(9):12334–12358.
- Portillo, M., Eremenko, E., Kaluski, S., Garcia-Venzor, A., Onn, L., Stein, D., Slobodnik, Z., Zaretsky, A., Ueberham, U., Einav, M., Brückner, M. K., Arendt, T., and Toiber, D. (2021). Sirt6-cbp-dependent nuclear tau accumulation and its role in protein synthesis. *Cell Rep.*, 35(4):109035.
- Prince, J. T. and Marcotte, E. M. (2006). Chromatographic alignment of esi-lcms proteomics data sets by ordered bijective interpolated warping. *Anal. Chem.*, 78(17):6140–6152.
- Raichle, M. E. and Gusnard, D. A. (2002). Appraising the brain's energy budget. *Proc. Natl. Acad. Sci. U. S. A.*, 99(16):10237–10239.
- Rainer, J. (2017). Ensdb.mmusculus.v79. DOI: 10.18129/B9.BIOC.ENSDB.MMUSCULUS.V79.
- Rath, S., Sharma, R., Gupta, R., Ast, T., Chan, C., Durham, T. J., Goodman, R. P., Grabarek, Z., Haas, M. E., Hung, W. H. W., Joshi, P. R., Jourdain, A. A., Kim, S. H., Kotrys, A. V., Lam, S. S., McCoy, J. G., Meisel, J. D., Miranda, M.,

- Panda, A., Patgiri, A., Rogers, R., Sadre, S., Shah, H., Skinner, O. S., To, T.-L., Walker, M. A., Wang, H., Ward, P. S., Wengrod, J., Yuan, C.-C., Calvo, S. E., and Mootha, V. K. (2021). Mitocarta3.0: an updated mitochondrial proteome now with sub-organelle localization and pathway annotations. *Nucleic Acids Res.*, 49(D1):D1541–D1547.
- Raz, N., Lindenberger, U., Rodrigue, K. M., Kennedy, K. M., Head, D., Williamson, A., Dahle, C., Gerstorf, D., and Acker, J. D. (2005). Regional brain changes in aging healthy adults: general trends, individual differences and modifiers. *Cereb. Cortex*, 15(11):1676–1689.
- Reifenberger, G., Wirsching, H.-G., Knobbe-Thomsen, C. B., and Weller, M. (2017). Advances in the molecular genetics of gliomas - implications for classification and therapy. *Nat. Rev. Clin. Oncol.*, 14(7):434–452.
- Rine, J., Strathern, J. N., Hicks, J. B., and Herskowitz, I. (1979). A suppressor of mating-type locus mutations in *saccharomyces cerevisiae*: evidence for and identification of cryptic mating-type loci. *Genetics*, 93(4):877–901.
- Rizzo, A., Iachettini, S., Salvati, E., Zizza, P., Maresca, C., D’Angelo, C., Benarroch-Popivker, D., Capolupo, A., del Gaudio, F., Cosconati, S., Di Maro, S., Merlino, F., Novellino, E., Amoreo, C. A., Mottolese, M., Sperduti, I., Gilson, E., and Biroccio, A. (2017). Sirt6 interacts with trf2 and promotes its degradation in response to dna damage. *Nucleic Acids Res.*, 45(4):1820–1834.
- Rohart, F., Gautier, B., Singh, A., and Lê Cao, K.-A. (2017). mixomics: An r package for ’omics feature selection and multiple data integration. *PLoS Comput. Biol.*, 13(11):e1005752.
- Roichman, A., Elhanati, S., Aon, M. A., Abramovich, I., Di Francesco, A., Shahar, Y., Avivi, M. Y., Shurgi, M., Rubinstein, A., Wiesner, Y., Shuchami, A., Petrover, Z., Lebenthal-Loinger, I., Yaron, O., Lyashkov, A., Ubaida-Mohien, C., Kanfi, Y., Lerrer, B., Fernández-Marcos, P. J., Serrano, M., Gottlieb, E., de Cabo, R., and Cohen, H. Y. (2021). Restoration of energy homeostasis by sirt6 extends healthy lifespan. *Nature Communications*, 12(1):3208.
- Rotblat, B., Agostini, M., Niklison-Chirou, M. V., Amelio, I., Willis, A. E., and Melino, G. (2018). Sustained protein synthesis and reduced eef2k levels in tap73<sup>-/-</sup> mice brain: a possible compensatory mechanism. *Cell Cycle*, 17(23):2637–2643.
- Rufini, A., Niklison-Chirou, M. V., Inoue, S., Tomasini, R., Harris, I. S., Marino, A., Federici, M., Dinsdale, D., Knight, R. A., Melino, G., and Mak, T. W. (2012). Tap73 depletion accelerates aging through metabolic dysregulation. *Genes Dev.*, 26(18):2009–2014.
- Ruiz-Perez, D., Guan, H., Madhivanan, P., Mathee, K., and Narasimhan, G. (2020). So you think you can pls-da? *BMC Bioinformatics*, 21(Suppl 1):2.

- Ryu, D., Jo, Y. S., Lo Sasso, G., Stein, S., Zhang, H., Perino, A., Lee, J. U., Zeviani, M., Romand, R., Hottiger, M. O., Schoonjans, K., and Auwerx, J. (2014). A sirt7-dependent acetylation switch of gabp1 controls mitochondrial function. *Cell Metab.*, 20(5):856–869.
- Sahin, E. and DePinho, R. A. (2012). Axis of ageing: telomeres, p53 and mitochondria. *Nat. Rev. Mol. Cell Biol.*, 13(6):397–404.
- Sarvagalla, S., Kolapalli, S. P., and Vallabhapurapu, S. (2019). The two sides of yy1 in cancer: A friend and a foe. *Front. Oncol.*, 9:1230.
- Schiffman, C., Petrick, L., Perttula, K., Yano, Y., Carlsson, H., Whitehead, T., Metayer, C., Hayes, J., Rappaport, S., and Dudoit, S. (2019). Filtering procedures for untargeted lc-ms metabolomics data. *BMC Bioinformatics*, 20(1):334.
- Sebastian, C., Zhong, L., Silberman, M., Toiber, D., Martinez, B., Etchegaray, J.-P., Cosentino, C., Giacosa, S., and Mostoslavsky, R. (2012). The histone deacetylase SIRT6, a critical modulator of metabolism and tumorigenesis. *BMC Proceedings*, 6(S3).
- Shannon, P., Markiel, A., Ozier, O., Baliga, N. S., Wang, J. T., Ramage, D., Amin, N., Schwikowski, B., and Ideker, T. (2003). Cytoscape: a software environment for integrated models of biomolecular interaction networks. *Genome Res.*, 13(11):2498–2504.
- Shao, J., Yang, X., Liu, T., Zhang, T., Xie, Q. R., and Xia, W. (2016). Autophagy induction by sirt6 is involved in oxidative stress-induced neuronal damage. *Protein Cell*, 7(4):281–290.
- Shih, J., Liu, L., Mason, A., Higashimori, H., and Donmez, G. (2014). Loss of sirt4 decreases glt-1-dependent glutamate uptake and increases sensitivity to kainic acid. *J. Neurochem.*, 131(5):573–581.
- Simon, M., Van Meter, M., Ablueva, J., Ke, Z., Gonzalez, R. S., Taguchi, T., De Cecco, M., Leonova, K. I., Kogan, V., Helfand, S. L., Neretti, N., Roichman, A., Cohen, H. Y., Meer, M. V., Gladyshev, V. N., Antoch, M. P., Gudkov, A. V., Sedivy, J. M., Seluanov, A., and Gorbunova, V. (2019). Line1 derepression in aged wild-type and sirt6-deficient mice drives inflammation. *Cell Metabolism*, 29(4):871–885.e5.
- Simons, K. and Toomre, D. (2000). Lipid rafts and signal transduction. *Nat. Rev. Mol. Cell Biol.*, 1(1):31–39.
- Slanzi, A., Iannoto, G., Rossi, B., Zenaro, E., and Constantin, G. (2020). In vitro models of neurodegenerative diseases. *Frontiers in Cell and Developmental Biology*, 8.
- Smith, C. A., Want, E. J., O’Maille, G., Abagyan, R., and Siuzdak, G. (2006). Xcms: processing mass spectrometry data for metabolite profiling using nonlinear peak alignment, matching, and identification. *Anal. Chem.*, 78(3):779–787.

- Song, D., Yang, Q., Jiang, X., Shan, A., Nan, J., Lei, Y., Ji, H., Di, W., Yang, T., Wang, T., Wang, W., Ning, G., and Cao, Y. (2020). Yy1 deficiency in  $\beta$ -cells leads to mitochondrial dysfunction and diabetes in mice. *Metabolism*, 112:154353.
- Stein, D., Mizrahi, A., Golova, A., Saretzky, A., Venzor, A. G., Slobodnik, Z., Kaluski, S., Einav, M., Khrameeva, E., and Toiber, D. (2021). Aging and pathological aging signatures of the brain: through the focusing lens of sirt6. *Aging (Albany NY)*, 13(5):6420–6441.
- Storozhuk, M. V., Ivanova, S. Y., Balaban, P. M., and Kostyuk, P. G. (2005). Possible role of mitochondria in posttetanic potentiation of gabaergic synaptic transmission in rat neocortical cell cultures. *Synapse*, 58(1):45–52.
- Stupp, R., Mason, W. P., van den Bent, M. J., Weller, M., Fisher, B., Taphoorn, M. J. B., Belanger, K., Brandes, A. A., Marosi, C., Bogdahn, U., Curschmann, J., Janzer, R. C., Ludwin, S. K., Gorlia, T., Allgeier, A., Lacombe, D., Cairncross, J. G., Eisenhauer, E., Mirimanoff, R. O., for Research, E. O., of Cancer Brain Tumor, T., Groups, R., and of Canada Clinical Trials Group, N. C. I. (2005). Radiotherapy plus concomitant and adjuvant temozolomide for glioblastoma. *N. Engl. J. Med.*, 352(10):987–996.
- Subramanian, I., Verma, S., Kumar, S., Jere, A., and Anamika, K. (2020). Multi-omics data integration, interpretation, and its application. *Bioinform. Biol. Insights*, 14:1177932219899051.
- Sumner, L. W., Amberg, A., Barrett, D., Beale, M. H., Beger, R., Daykin, C. A., Fan, T. W.-M., Fiehn, O., Goodacre, R., Griffin, J. L., Hankemeier, T., Hardy, N., Harnly, J., Higashi, R., Kopka, J., Lane, A. N., Lindon, J. C., Marriott, P., Nicholls, A. W., Reilly, M. D., Thaden, J. J., and Viant, M. R. (2007). Proposed minimum reporting standards for chemical analysis chemical analysis working group (cawg) metabolomics standards initiative (msi): Chemical analysis working group (cawg) metabolomics standards initiative (msi). *Metabolomics*, 3(3):211–221.
- Sunkin, S. M., Ng, L., Lau, C., Dolbeare, T., Gilbert, T. L., Thompson, C. L., Hawrylycz, M., and Dang, C. (2013). Allen brain atlas: an integrated spatio-temporal portal for exploring the central nervous system. *Nucleic Acids Res.*, 41(Database issue):D996–D1008.
- Sysi-Aho, M., Katajamaa, M., Yetukuri, L., and Oresic, M. (2007). Normalization method for metabolomics data using optimal selection of multiple internal standards. *BMC Bioinformatics*, 8(1):93.
- Tanner, K. G., Landry, J., Sternglanz, R., and Denu, J. M. (2000). Silent information regulator 2 family of nad<sup>+</sup>-dependent histone/protein deacetylases generates a unique product, 1-o-acetyl-adp-ribose. *Proc. Natl. Acad. Sci. U. S. A.*, 97(26):14178–14182.

- Tasselli, L., Xi, Y., Zheng, W., Tennen, R. I., Odrowaz, Z., Simeoni, F., Li, W., and Chua, K. F. (2016). Sirt6 deacetylates h3k18ac at pericentric chromatin to prevent mitotic errors and cellular senescence. *Nat. Struct. Mol. Biol.*, 23(5):434–440.
- Tautenhahn, R., Böttcher, C., and Neumann, S. (2008). Highly sensitive feature detection for high resolution lc/ms. *BMC Bioinformatics*, 9(1):504.
- Thul, P. J., Åkesson, L., Wiking, M., Mahdessian, D., Geladaki, A., Ait Blal, H., Alm, T., Asplund, A., Björk, L., Breckels, L. M., Bäckström, A., Danielsson, F., Fagerberg, L., Fall, J., Gatto, L., Gnann, C., Hober, S., Hjelmare, M., Johansson, F., Lee, S., Lindskog, C., Mulder, J., Mulvey, C. M., Nilsson, P., Oksvold, P., Rockberg, J., Schutten, R., Schwenk, J. M., Sivertsson, , Sjöstedt, E., Skogs, M., Stadler, C., Sullivan, D. P., Tegel, H., Winsnes, C., Zhang, C., Zwahlen, M., Mardinoglu, A., Pontén, F., von Feilitzen, K., Lilley, K. S., Uhlén, M., and Lundberg, E. (2017). A subcellular map of the human proteome. *Science*, 356(6340).
- Toiber, D., Erdel, F., Bouazoune, K., Silberman, D. M., Zhong, L., Mulligan, P., Sebastian, C., Cosentino, C., Martinez-Pastor, B., Giacosa, S., D’Urso, A., Näär, A. M., Kingston, R., Rippe, K., and Mostoslavsky, R. (2013). Sirt6 recruits snf2h to dna break sites, preventing genomic instability through chromatin remodeling. *Mol. Cell*, 51(4):454–468.
- Toiber, D., Leprivier, G., and Rotblat, B. (2017). Erratum: Long noncoding rna: noncoding and not coded. *Cell Death Discov.*, 3(1):17035.
- Tomasini, R., Tsuchihara, K., Wilhelm, M., Fujitani, M., Rufini, A., Cheung, C. C., Khan, F., Itie-Youten, A., Wakeham, A., Tsao, M.-S., Iovanna, J. L., Squire, J., Jurisica, I., Kaplan, D., Melino, G., Jurisicova, A., and Mak, T. W. (2008). Tap73 knockout shows genomic instability with infertility and tumor suppressor functions. *Genes Dev.*, 22(19):2677–2691.
- van de Ven, R. A., Santos, D., and Haigis, M. C. (2017). Mitochondrial sirtuins and molecular mechanisms of aging. *Trends in Molecular Medicine*, 23(4):320–331.
- Van Meter, M., Kashyap, M., Rezazadeh, S., Geneva, A. J., Morello, T. D., Seluanov, A., and Gorbunova, V. (2014). Sirt6 represses line1 retrotransposons by ribosylating kap1 but this repression fails with stress and age. *Nat. Commun.*, 5(1):5011.
- Varon, M., Levy, T., Mazor, G., Ben David, H., Marciano, R., Krelin, Y., Prasad, M., Elkabets, M., Pauck, D., Ahmadov, U., Picard, D., Qin, N., Borkhardt, A., Reifemberger, G., Leprivier, G., Remke, M., and Rotblat, B. (2019). The long noncoding rna tp73-as1 promotes tumorigenicity of medulloblastoma cells. *Int. J. Cancer*, 145(12):3402–3413.
- Verheul, T. C. J., van Hijfte, L., Perenthaler, E., and Barakat, T. S. (2020). The why of yy1: Mechanisms of transcriptional regulation by yin yang 1. *Front. Cell Dev. Biol.*, 8:592164.

- Viswanathan, M. and Tissenbaum, H. A. (2013). *C. elegans Sirtuins*, page 39–56. Humana Press.
- Wallace, D. C. (2005). A mitochondrial paradigm of metabolic and degenerative diseases, aging, and cancer: a dawn for evolutionary medicine. *Annu. Rev. Genet.*, 39(1):359–407.
- Wang, X., Patel, N. D., Hui, D., Pal, R., Hafez, M. M., Sayed-Ahmed, M. M., Al-Yahya, A. A., and Michaelis, E. K. (2014). Gene expression patterns in the hippocampus during the development and aging of *glud1* (glutamate dehydrogenase 1) transgenic and wild type mice. *BMC Neurosci.*, 15(1):37.
- Want, E. J. (2018). Lc-ms untargeted analysis. *Methods Mol. Biol.*, 1738:99–116.
- Wehrens, R., Hageman, J. A., van Eeuwijk, F., Kooke, R., Flood, P. J., Wijnker, E., Keurentjes, J. J. B., Lommen, A., van Eekelen, H. D. L. M., Hall, R. D., Mumm, R., and de Vos, R. C. H. (2016). Improved batch correction in untargeted ms-based metabolomics. *Metabolomics*, 12(5):88.
- Weintraub, A. S., Li, C. H., Zamudio, A. V., Sigova, A. A., Hannett, N. M., Day, D. S., Abraham, B. J., Cohen, M. A., Nabet, B., Buckley, D. L., Guo, Y. E., Hnisz, D., Jaenisch, R., Bradner, J. E., Gray, N. S., and Young, R. A. (2017). Yy1 is a structural regulator of enhancer-promoter loops. *Cell*, 171(7):1573–1588.e28.
- Wheeler, D. A., Takebe, N., Hinoue, T., Hoadley, K. A., Cardenas, M. F., Hamilton, A. M., Laird, P. W., Wang, L., Johnson, A., Dewal, N., Miller, V., Piñeyro, D., Castro de Moura, M., Esteller, M., Shen, H., Zenklusen, J. C., Tarnuzzer, R., McShane, L. M., Tricoli, J. V., Williams, P. M., Lubensky, I., O’Sullivan-Coyne, G., Kohn, E. C., Little, R. F., White, J., Malik, S., Harris, L., Weil, C., Chen, A. P., Karlovich, C., Rodgers, B., Shankar, L., Jacobs, P., Nolan, T., Hu, J., Muzny, D. M., Doddapaneni, H., Korchina, V., Gastier-Foster, J., Bowen, J., Leraas, K., Edmondson, E. F., Doroshow, J. H., Conley, B. A., Ivy, S. P., and Staudt, L. M. (2021). Molecular features of cancers exhibiting exceptional responses to treatment. *Cancer Cell*, 39(1):38–53.e7.
- Wood, J. G., Schwer, B., Wickremesinghe, P. C., Hartnett, D. A., Burhenn, L., Garcia, M., Li, M., Verdin, E., and Helfand, S. L. (2018). Sirt4 is a mitochondrial regulator of metabolism and lifespan in drosophila melanogaster. *Proc. Natl. Acad. Sci. U. S. A.*, 115(7):1564–1569.
- Wu, X., Zhu, J.-C., Zhang, Y., Li, W.-M., Rong, X.-L., and Feng, Y.-F. (2016). Lipidomics study of plasma phospholipid metabolism in early type 2 diabetes rats with ancient prescription huang-qi-san intervention by uplc/q-tof-ms and correlation coefficient. *Chem. Biol. Interact.*, 256:71–84.
- Xia, Y., Li, K., Li, J., Wang, T., Gu, L., and Xun, L. (2018). T5 exonuclease-dependent assembly offers a low-cost method for efficient cloning and site-directed mutagenesis. *Nucleic Acids Research*, 47(3):e15–e15.

- Xicota, L., Ichou, F., Lejeune, F.-X., Colsch, B., Tenenhaus, A., Leroy, I., Fontaine, G., Lhomme, M., Bertin, H., Habert, M.-O., Epelbaum, S., Dubois, B., Mochel, F., Potier, M.-C., and study group, I. (2019). Multi-omics signature of brain amyloid deposition in asymptomatic individuals at-risk for alzheimer's disease: The insight-pread study. *EBioMedicine*, 47:518–528.
- Xu, Z., Zhang, L., Zhang, W., Meng, D., Zhang, H., Jiang, Y., Xu, X., Van Meter, M., Seluanov, A., Gorbunova, V., and Mao, Z. (2015). Sirt6 rescues the age related decline in base excision repair in a parp1-dependent manner. *Cell Cycle*, 14(2):269–276.
- Yang, A., Walker, N., Bronson, R., Kaghad, M., Oosterwegel, M., Bonnin, J., Vagner, C., Bonnet, H., Dikkes, P., Sharpe, A., McKeon, F., and Caput, D. (2000). P73-deficient mice have neurological, pheromonal and inflammatory defects but lack spontaneous tumours. *Nature*, 404(6773):99–103.
- Yang, W., Nagasawa, K., Münch, C., Xu, Y., Satterstrom, K., Jeong, S., Hayes, S. D., Jedrychowski, M. P., Vyas, F. S., Zaganjor, E., Guarani, V., Ringel, A. E., Gygi, S. P., Harper, J. W., and Haigis, M. C. (2016). Mitochondrial sirtuin network reveals dynamic sirt3-dependent deacetylation in response to membrane depolarization. *Cell*, 167(4):985–1000.e21.
- Yang, X., Feng, J., Liang, W., Zhu, Z., Chen, Z., Hu, J., Yang, D., and Ding, G. (2021). Roles of sirt6 in kidney disease: a novel therapeutic target. *Cellular and Molecular Life Sciences*, 79(1).
- Yoshizawa, T., Sato, Y., Sobuz, S. U., Mizumoto, T., Tsuyama, T., Karim, M. F., Miyata, K., Tasaki, M., Yamazaki, M., Kariba, Y., Araki, N., Araki, E., Kajimura, S., Oike, Y., Braun, T., Bober, E., Auwerx, J., and Yamagata, K. (2022). Sirt7 suppresses energy expenditure and thermogenesis by regulating brown adipose tissue functions in mice. *Nat. Commun.*, 13(1):7439.
- Yu, G. (2018). enrichplot. DOI: 10.18129/B9.BIOC.ENRICHPLOT.
- Yu, G., Wang, L.-G., Han, Y., and He, Q.-Y. (2012). clusterprofiler: an r package for comparing biological themes among gene clusters. *OMICS*, 16(5):284–287.
- Yu, G., Wang, L.-G., and He, Q.-Y. (2015). Chipseeker: an r/bioconductor package for chip peak annotation, comparison and visualization. *Bioinformatics*, 31(14):2382–2383.
- Zhang, B., Li, Q., Wu, B., Zhang, S., Li, L., Jin, K., Li, S., Li, K., Wang, Z., Lu, Y., Xia, L., and Sun, C. (2021). Long non-coding rna tp73-as1 is a potential immune related prognostic biomarker for glioma. *Aging (Albany NY)*, 13(4):5638–5649.
- Zhang, J., Bajari, R., Andric, D., Gerthoffert, F., Lepsa, A., Nahal-Bose, H., Stein, L. D., and Ferretti, V. (2019). The international cancer genome consortium data portal. *Nat. Biotechnol.*, 37(4):367–369.

- Zhang, J., Li, N., Fu, J., and Zhou, W. (2020a). Long noncoding rna hotair promotes medulloblastoma growth, migration and invasion by sponging mir-1/mir-206 and targeting yy1. *Biomed. Pharmacother.*, 124(109887):109887.
- Zhang, P., Tu, B., Wang, H., Cao, Z., Tang, M., Zhang, C., Gu, B., Li, Z., Wang, L., Yang, Y., Zhao, Y., Wang, H., Luo, J., Deng, C.-X., Gao, B., Roeder, R. G., and Zhu, W.-G. (2014a). Tumor suppressor p53 cooperates with sirt6 to regulate gluconeogenesis by promoting foxo1 nuclear exclusion. *Proceedings of the National Academy of Sciences*, 111(29):10684–10689.
- Zhang, X., Liu, W., Zan, J., Wu, C., and Tan, W. (2020b). Untargeted lipidomics reveals progression of early alzheimer’s disease in app/ps1 transgenic mice. *Sci. Rep.*, 10(1):14509.
- Zhang, Y., Chen, K., Sloan, S. A., Bennett, M. L., Scholze, A. R., O’Keeffe, S., Phatnani, H. P., Guarnieri, P., Caneda, C., Ruderisch, N., Deng, S., Liddelow, S. A., Zhang, C., Daneman, R., Maniatis, T., Barres, B. A., and Wu, J. Q. (2014b). An rna-sequencing transcriptome and splicing database of glia, neurons, and vascular cells of the cerebral cortex. *J. Neurosci.*, 34(36):11929–11947.
- Zhong, L., D’Urso, A., Toiber, D., Sebastian, C., Henry, R. E., Vadysirisack, D. D., Guimaraes, A., Marinelli, B., Wikstrom, J. D., Nir, T., Clish, C. B., Vaitheesvaran, B., Iliopoulos, O., Kurland, I., Dor, Y., Weissleder, R., Shirihai, O. S., Ellisen, L. W., Espinosa, J. M., and Mostoslavsky, R. (2010). The histone deacetylase sirt6 regulates glucose homeostasis via hif1alpha. *Cell*, 140(2):280–293.
- Zottel, A., Šamec, N., Videtič Paska, A., and Jovčevska, I. (2020). Coding of glioblastoma progression and therapy resistance through long noncoding rnas. *Cancers (Basel)*, 12(7):1842.

# Supplementary materials for Chapter 3: A novel pipeline for untargeted lipidomics data analysis

## Supplementary tables

Table S.1: A non-comprehensive list of tools suitable for the analysis of LC-MS data

<b>Tool</b>	<b>Implementation</b>	<b>Last update</b>	<b>Description</b>
XCMS	Web, R	2021 (R version)	Performs all preprocessing steps for untargeted LC-MS data from data input to statistical testing and visualization.

LipidFinder	WEB, Python	2021	Identifies lipid features from pre-aligned data using information from LIPID MAPS (COMP_DB and LMSD databases). Additionally performs statistical analysis on identified lipids. Part of the LIPID MAPS web interface.
MZmine 2	Java	2019	Provides modules for raw data filtering, peak calling, peak processing and downstream analysis. Along with XCMS, MZmine 2 is the most widely used program for LC-MS data analysis.
MetaboAnalyst 5.0	Web, R	2021	Incorporates a large number of functions for downstream analysis, including statistical testing methods, enrichment and pathway analyses. Requires XCMS functionality for raw LC-MS spectra processing.
Galaxy-M	R, Python, MATLAB	2016	A pipeline for LC-MS metabolomics working in the Galaxy environment.

LipidXplorer	Windows executable	2019	Implements functionality for peaks alignment and subsequent lipid identification based on Molecular Fragmentation Query Language (MFQL) approach.
OpenMS	Linux, Windows, macOS executable	2021	“All-in-one” solution for the lipidomics data analysis. Includes ThermoRawFileParser data conversion.
Lipid Data Analyzer (LDA)	Java	2021	A tool for lipid species interpretation. It is also able to detect novel features.
LipidHunter 2	Python	2020	Identifies phospholipids, glycerolipids, and lysophospholipids. Supports multiple instrument vendors.
MetAlign 3	Windows executable	2018	Provides a large number of functions for MS data preprocessing (e.g., for baseline correction, peak picking, annotation)

LipidMatch	R	2020	Performs rule-based lipid identification within LC-HRMS/MS data.
LipidMS	R	2021	An R package developed for lipid annotation in LC-DIA-MS data.
LipidSearch (Thermo Scientific)	-	-	A commercial software suitable for raw LC-MS data processing and lipid identification using an internal library of ion masses.
MSClust	Windows executable	2012	Reduces the number of redundant peaks using the subtractive fuzzy clustering approach.
LipidBlast	-	2014	Provides a comprehensive database for peak annotation.
MS-DIAL 4	Linux, Windows, macOS executable	2020	Provides a graphical interface for peak identification within untargeted metabolomics data. Also holds modules for normalization and multivariate analysis. Supports multiple instruments, including LC-MS.

LIQUID	Windows executable, .Net	ex-C#	2021	Similar to MS-DIAL, it allows peak identification through a graphical interface, but is focused on lipids in LS-MS/MS data.
lipidr	R		2021	Provides a set of functions for downstream analysis of LC-MS lipidomics data.
lipyd	Python		2020	Provides workflow for lipidomics data analysis. Requires OpenMS for the data preprocessing step.
LipiDex	Java		2018	Allows gaussian peak modeling based lipid identification and result filtering.
LION	Web		2020	Provides functionality for the enrichment analysis of lipids using a GO database containing information about lipid classification, subcellular localization, and biophysical properties.

LICRE 1.0	MATLAB	2017	Reduces the number of redundant features in lipidomic data by identification and pruning of groups of highly correlated lipids.
LipidSig	Web	2021	Implements a web-based workflow for downstream analysis of lipidomics data.
LipidLynxX	Windows executable, Web	2020	Provides resources for lipid annotation and ID conversion. Part of the LIPID MAPS web interface.
LPPtiger	Windows executable	2017	Performs detection of oxidized phospholipids.
Cytoscape 3	Cross-platform	2021	Allows network analysis and visualization of omics datasets, including lipidomics profiles.
LIPEA	Web	2018	Performs Over Representation analysis of lipid features using KEGG pathways.

Supplementary materials for Chapter  
4: Effect of SIRT6 deficiency on  
transcriptome and metabolome levels  
during normal and pathological aging

Supplementary figures

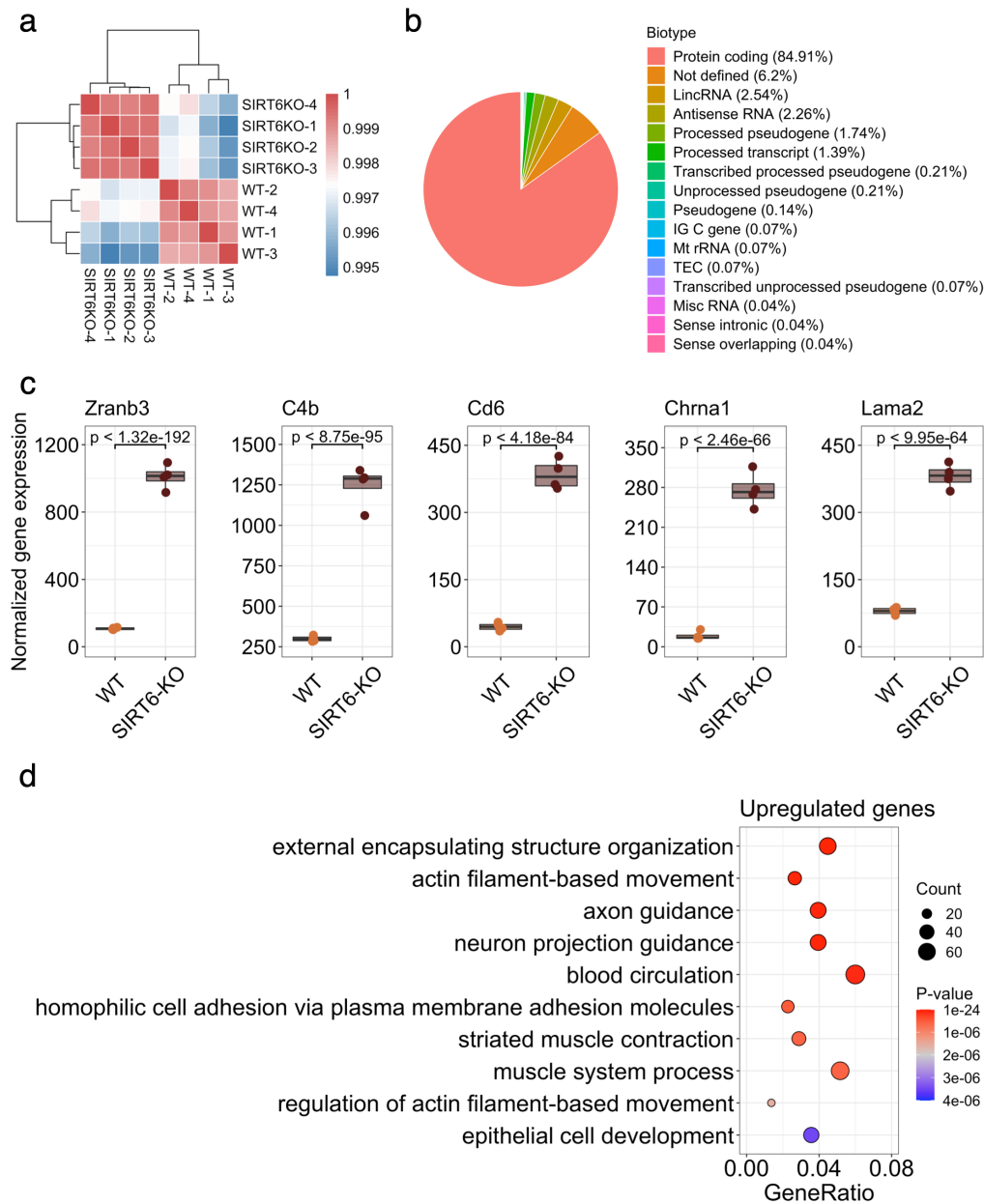


Figure S-1: Analysis of WT and brSIRT6-KO gene expression data. (a) Heatmap illustrating Pearson's correlation between experimental samples. (b) Pie plot representing proportion of biotype annotations among DE genes. 'IG C gene' annotation denotes constant chain immunoglobulin genes, 'TEC' annotation describes predicted genes that require experimental validation. (c) Boxplots of the top 5 most differentially expressed genes in the analysis. Expression of WT samples are shown by orange points and expression of brSIRT6 are shown by brown points. (d) GO analysis showing top 10 enriched biological processes for upregulated genes. Each circle corresponds to the enriched GO term and varies in size according to the number of significant genes belonging to this term. Gene ratio represents the number of DE genes belonging to the enrichment categories divided by the total number of genes per category.

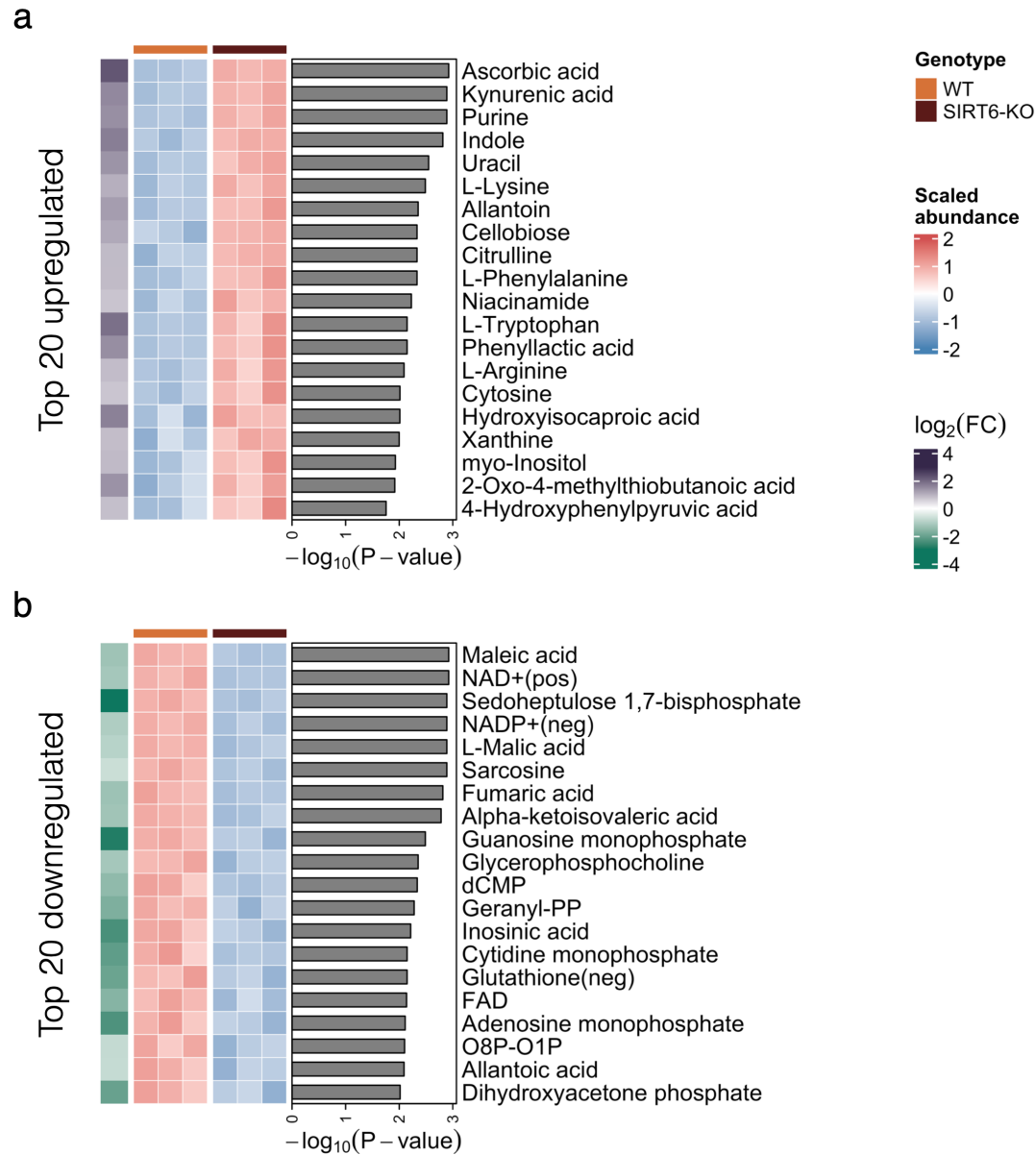


Figure S-2: mESC metabolomics. (a,b) Heatmaps showing abundances of the top 20 most significantly upregulated (panel a) and downregulated (panel b) in SIRT6-KO (brown) compared to WT (orange) metabolites. Row annotations on the left of the heatmaps represent  $\log_2(\text{Fold Change})$  values corresponding to the metabolites. Barplots on the right side of the heatmaps represent  $-\log_{10}$  transformed FDR p-value of the metabolites.

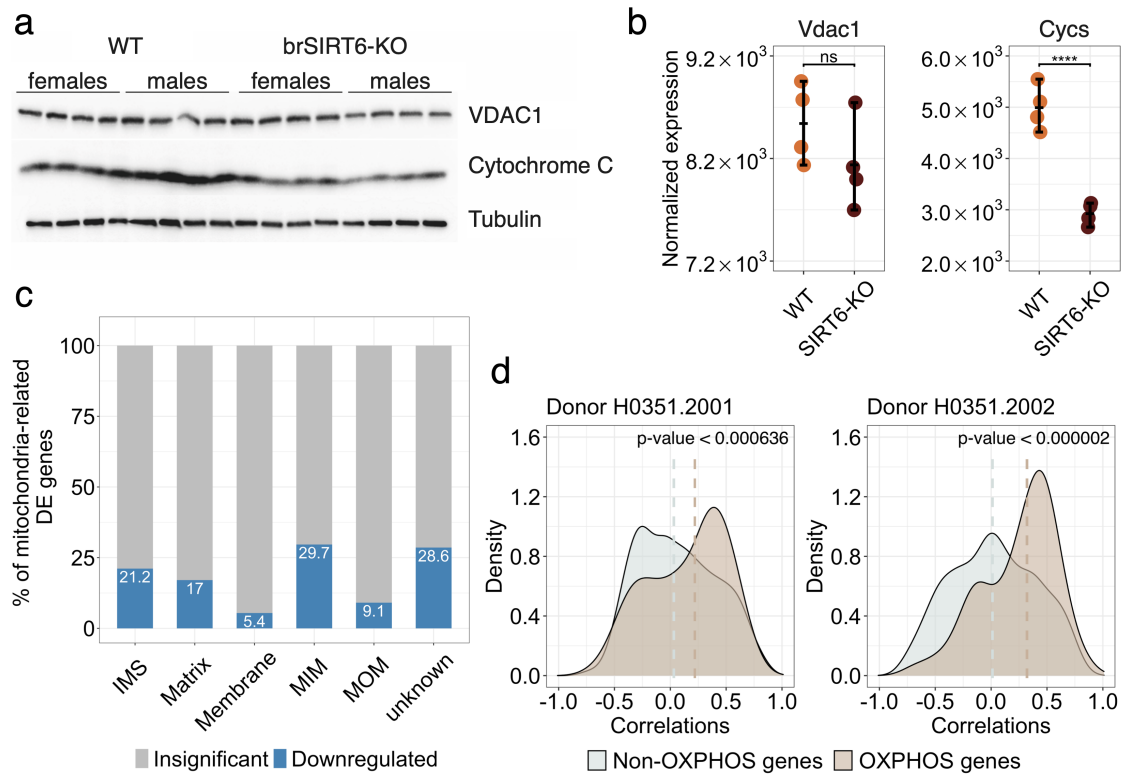


Figure S-3: SIRT6 regulates OXPPOS-related genes. (a) Western blot analysis of total brain extracts from W.T. (n=8) and brSIRT6-KO brains (n=8). The total brain fraction was prepared as described in Methods (Chapter 4). Membrane blots were incubated with antibodies against Cytochrome C, Tubulin and VDAC. (b) Vdac1 and Cycc expression levels in WT and SIRT6-KO RNA-seq profiles. (c) The percentage of significant (blue bars) and insignificant (gray bars) genes across mitochondrial compartments. 'IMS' denotes intermembrane space, 'MIM' denotes mitochondrial inner membrane, and 'MOM' corresponds to the mitochondrial outer membrane. (d) Spearman's correlation value distributions for SIRT6 with OXPPOS-related (brown shapes) and other mitochondria-related genes (blue shapes) in the Allen Brain Atlas RNA-seq datasets of two donors (H0351.2001, H0351.2002). Brown and blue dashed lines correspond to medians of correlation distributions for OXPPOS and non-OXPPOS genes, respectively. Statistical significance for SIRT6 correlation with OXPPOS-related genes is calculated via permutation test.

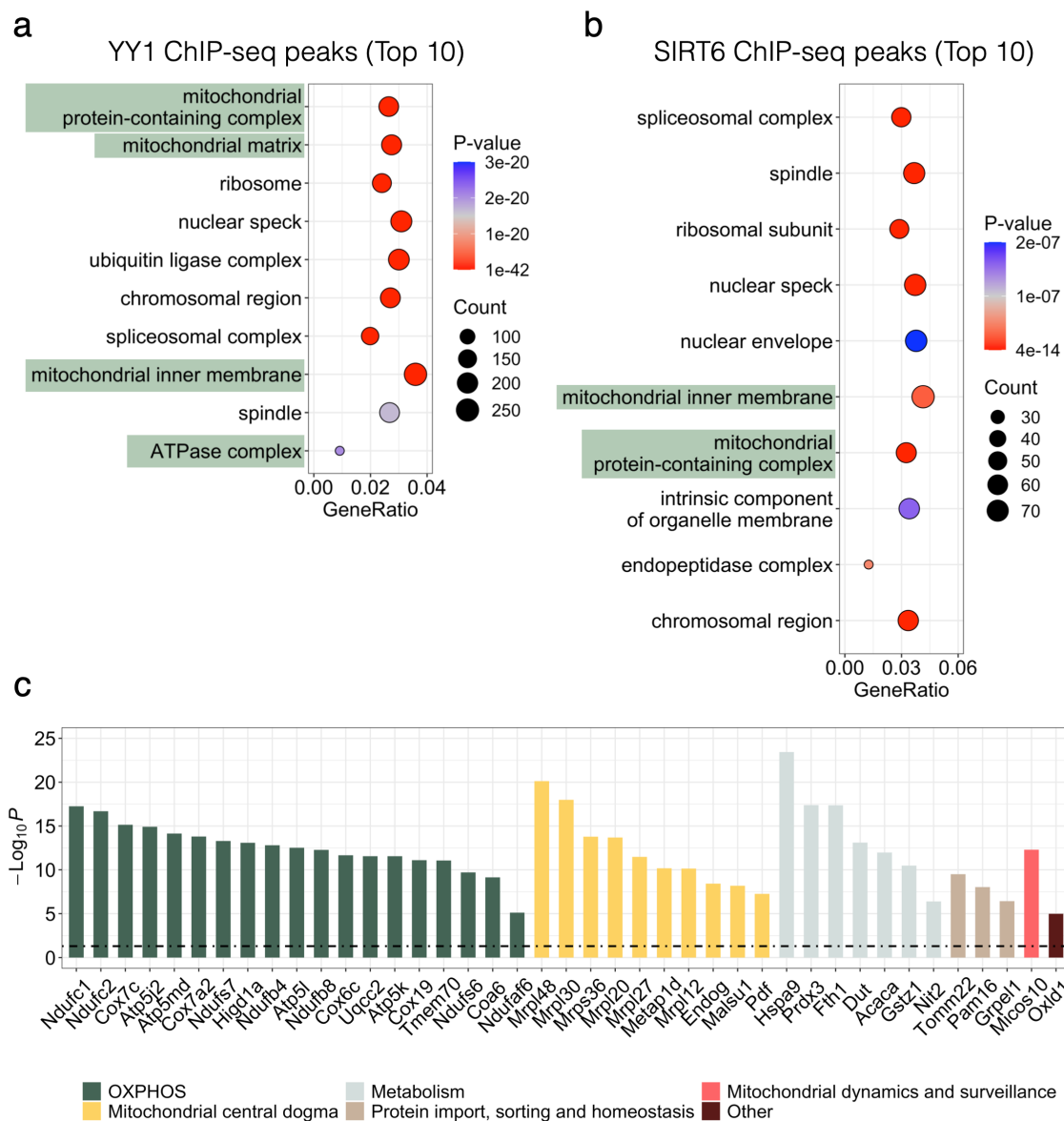


Figure S-4: Analysis of public YY1 and SIRT6 ChIP-seq datasets. (a-b) Top 10 significant cellular component terms from GO ontology analysis of genes associated with YY1 (panel a) and SIRT6 (panel b) peaks. Mitochondria-related cell compartments are marked by green. (c) Barplot showing the expression change magnitudes of genes overlapped between all the datasets presented in Figure 4-5d. Bars are colored according to the cellular function of corresponding genes. Black dashed denotes significance cut off for  $-\log_{10}$  FDR p-value.

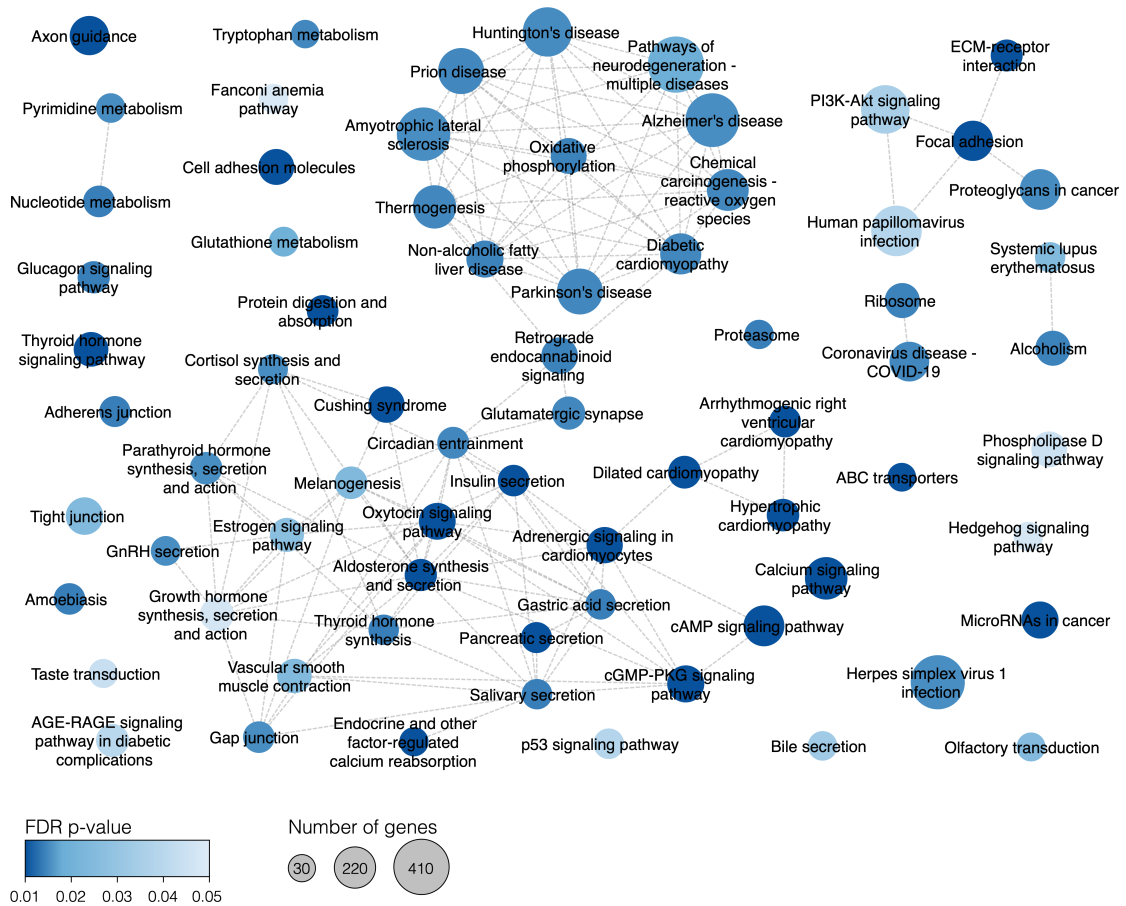


Figure S-5: Full network of enriched KEGG pathways. Each circle represents an enriched pathway in GSEA analysis and is colored according to the FDR p-value. The size of the circles corresponds to the number of detected genes related to the particular pathway.

# Supplementary materials for Chapter 5: The role of SIRT6' co-partner YY1 in aging and brain tumors

## Supplementary figures

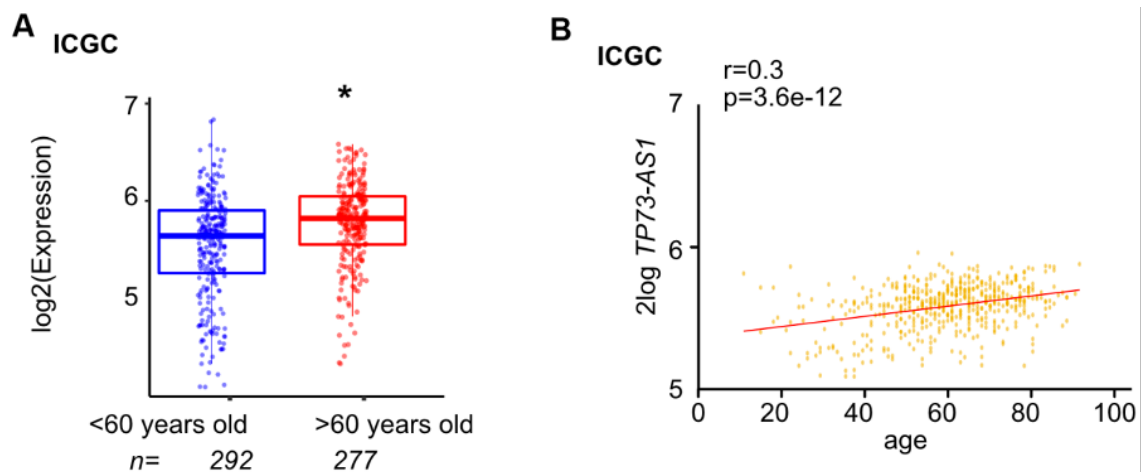


Figure S-6: *TP73-AS1* is highly expressed in GBM tumors of aged patients. (A) The levels of *TP73-AS1* in GBM tumors obtained from the old vs. young patients are shown. Data were obtained from GBM-US donors (a total of 595 donors) from ICGC database. (B) The correlation between the expression of *TP73-AS1* and age in the tumors of GBM patients. Data were obtained from GBM-US donors (a total of 595 donors) from ICGC database

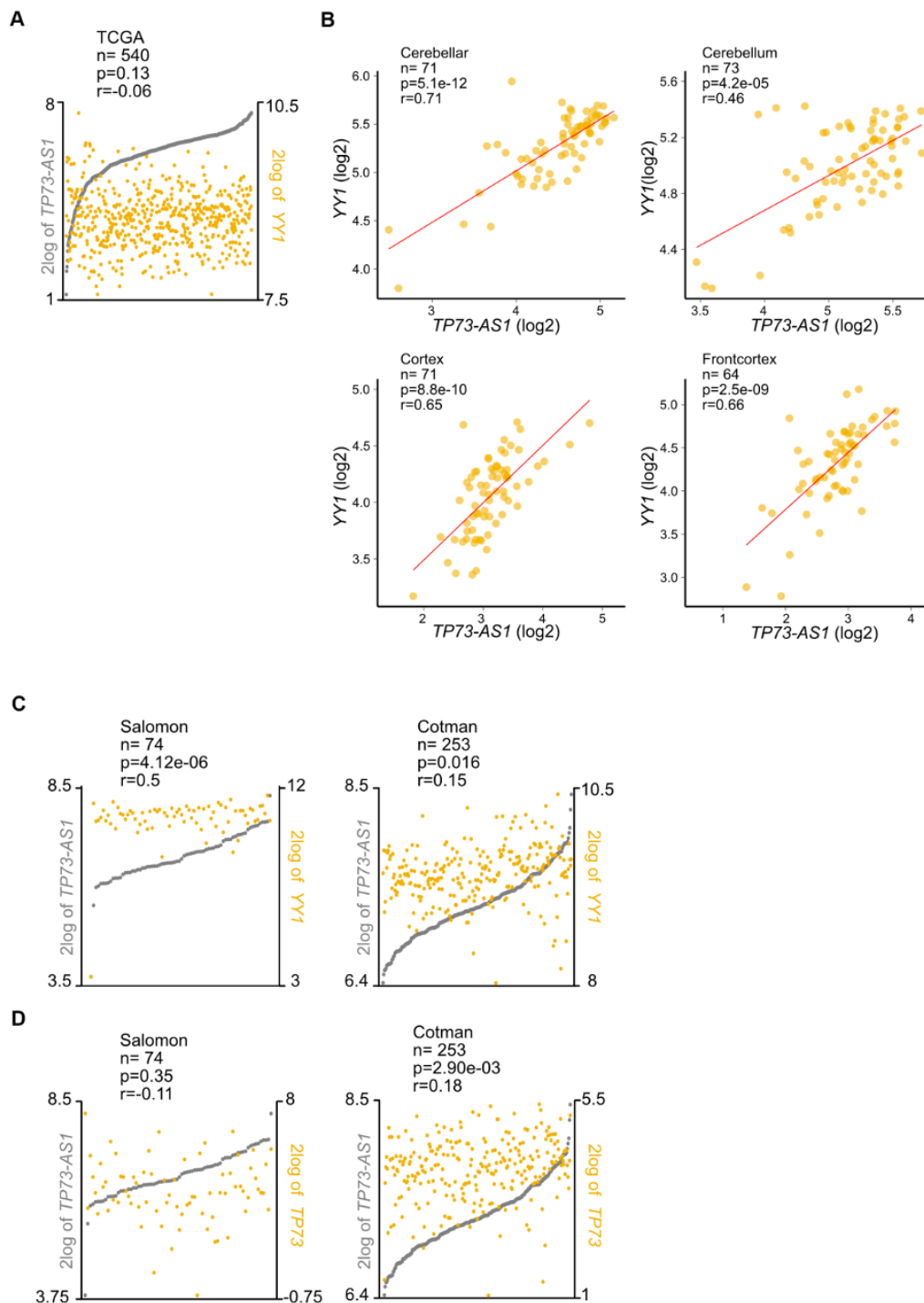


Figure S-7: *YY1* and *TP73-AS1* are co-expressed in GBM and aging brain. (A) The correlation between the expression of *TP73-AS1* and *YY1* in the GBM were determined using R2 and TCGA dataset. (B) The correlation between the expression of *TP73-AS1* and *YY1* across different brain parts in the GTEx dataset. (C) The correlation between the expression of *TP73-AS1* and *YY1* in aging brain were determined using R2 and the indicated datasets. (D) The correlation between the expression of *TP73-AS1* and *p73* in the aging were determined using R2 and indicated dataset.